Simulation of precipitation and discharge extremes
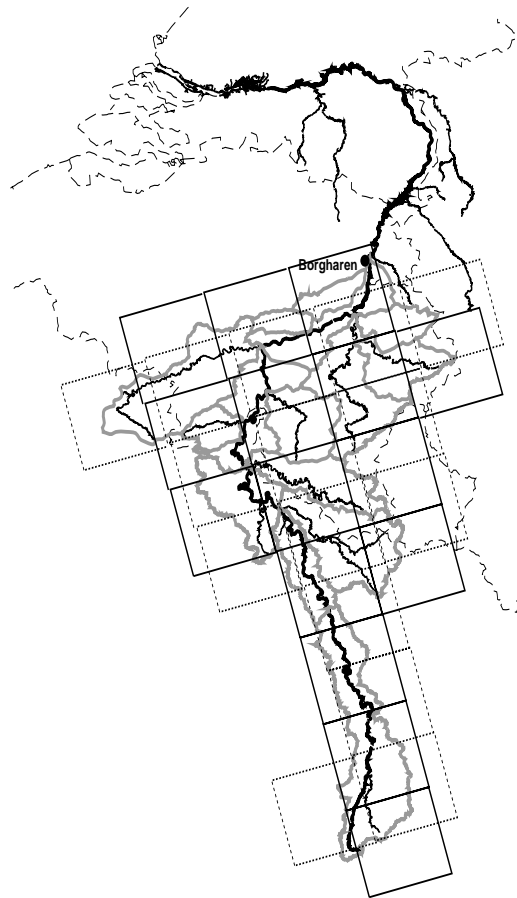# of the river Meuse
in current and future climate

Robert Leander

Simulation of precipitation and discharge extremes of the river Meuse in current and future climate

De simulatie van neerslag- en afvoerextremen van de Maas
in huidig en toekomstig klimaat
(met een samenvatting in het Nederlands)

Proefschrift

ter verkrijging van de graad van doctor aan de Universiteit Utrecht
op gezag van de rector magnificus, prof. dr. J.C. Stoof,
ingevolge het besluit van het college voor promoties
in het openbaar te verdedigen op
donderdag 7 mei 2009 des middags te 4.15 uur

door

Robert Leander

geboren op 1 november 1973 te Woerden

Promotor: Prof. dr. B.J.J.M. van den Hurk

Co-promotor: Dr. T.A. Buishand

Aan mijn ouders

Abstract

The river Meuse is the second largest river in the Netherlands and is characterized by strong variations in its discharge. From a government point of view there is a particular interest in discharge levels with return periods in the order of 1000 years, far beyond the length of the observed discharge record (several decades). Traditionally, these extreme quantiles are estimated by fitting extreme value distributions to observed maxima, which are then extrapolated upto the return period of interest. However, such strong extrapolation induces a large uncertainty in the estimated quantile. Moreover, the discharge record might be inhomogeneous due to changes in the river basin. As an alternative, a methodology has been developed which is based on the resampling of meteorological data for the basin in combination with hydrological modelling.

The resampling algorithm is used to synthesize long-year sequences of spatially varying daily precipitation and temperature for the river basin and is based on the concept of "nearest-neighbours". It is capable of reproducing several characteristics of the data crucial for the simulation of extreme multi-day precipitation events, such as spatial correlation of daily precipitation and temperature, persistence and variance as well as the correlation between precipitation and temperature. One of the major advantages of this algorithm is that it is entirely "data-driven" and does not rely upon assumptions about the underlying distribution or correlation structure of the data. Since the generated sequences consist of values from the original data only and therefore cannot exceed the highest data value, something which is sometimes seen as a somewhat unrealistic limitation. To examine to what extent this limitation affects the simulation of discharge extremes, a modified resampling algorithm was tested on the Ourthe subbasin using historical meteorological data. The modified algorithm is based on nearest-neighbour regression and allows for the exceedance of the largest historical daily precipitation in a simulation by recombining a conditional expectation and a sampled residual. Though the algorithm produces daily amounts well outside the range of historical values, the effect on the distribution of simulated discharge extremes on the Ourthe was very small.

To assess the changes of these discharge quantiles related to climate change, this methodology was applied to the output of regional climate models (RCMs) for the control climate (1961-1990) and the SRES-scenario A2 (2071-2100). To compensate for systematic differences in the mean and variance between the RCM run for the control climate and observations in the Meuse basin, the synthesized sequences were subjected to a nonlinear bias correction. This type of bias correction allows for the mean and variability of daily precipitation to be adjusted simultaneously, which turned out to be indispensable for the realistic simulation of extreme discharge events. It was observed that the changes in the extreme quantiles of multi-day precipitation and discharge in the winter half-year (i.e. the flooding season) are to a large extent determined by the global climate model (GCM) which drives the RCM at its lateral boundaries. One of the two used GCMs leads to a decrease in the relative variability of the modelled winter precipitation. This decrease largely compensates the effect of the increasing mean precipitation on the extremes. As a result, the RCM simulations driven by this GCM show a slight decrease of the quantiles at intermediate return periods and only a slight increase of those at long return periods. In the simulations driven by the other GCM the relative variability of precipitation hardly changes and the extreme quantiles roughly increase proportionally with the mean precipitation.

Resampling data from RCMs combined with hydrological modelling proves to be a suitable instrument to obtain more insight in the changes of rare discharge extremes of rivers like the Meuse. The biases in the mean and variability of RCM precipitation and their correction deserve careful consideration. In particular for the study to extreme precipitation events, changes in precipitation variability are as important as changes in the mean. In the flooding season these changes are primarily determined by the driving GCM. The model uncertainty in the changes of such extreme events is therefore best represented by an ensemble of modelruns, driven by different GCMs.

Contents

R. Leander and T.A. Buishand, 2007,
Journal of Hydrology, **332**, 487–496

R. Leander, T.A. Buishand, B.J.J.M van den Hurk and M.J.M. de Wit, 2008,
Journal of Hydrology, **351**, 331–343

Chapter **1**

Introduction

For the Netherlands, being situated on the North Sea coast and for a large part lying below sea-level, the threat of flooding has always been an important issue. However, danger of flooding not only comes from the sea; a substantial part of the country belongs to the delta of the rivers Rhine and Meuse. The areas alongside these rivers have always experienced occasional flooding. Therefore, it is evident that protection from river flooding is an issue of high priority for the Netherlands government. Nation-wide river management in the Netherlands exists since 1798 (van Bennekom and Parmet, 1998). In the early days heightening of the dikes usually was part of the restoration process after a flood and the heights were simply adapted to the maximum height of the flood, increased by a safety margin. The Delta Committee, installed in the aftermath of the North Sea flood of January 1953, defined levels of acceptable flood risk as a standard for flood protection. The risk is here defined as the probability of flooding in an arbitrary year. Its inverse is generally referred to as the return period, i.e. the mean time interval in years between floods. For the embanked section of the main rivers the acceptable return period for flooding was initially set to 3000 years. Measures required to meet this standard and their effect on the landscape were heavily debated by the public. In 1977 the Becht Committee (Commissie Becht, 1977) proposed a reduction of the standard to allow for exceedances once in 1250 years for the embanked areas along the rivers. The 3000-year level was maintained for the part of the rivers influenced by the tide in the transition zone to the North Sea coast. Also a method was presented for the estimation of the 1250-year discharge level by extrapolating an exponential distribution fitted to a record of peak discharges (flood peaks). This particular level defines the design discharge used for the dimensioning of flood-protection works. Therefore, the determination of this level requires careful consideration. While it is obvious that an underestimation of the design discharge results in an unacceptable flood risk, an overestimation leads to overdimensioned structures and unnecessary costs, not to mention the impact on landscape and environment.

1.1   Flood events of the river Meuse

The vulnerability of populated areas in the Netherlands to river flooding was demonstrated in December 1993 and January 1995, when large floods of the river Meuse hit north-eastern Belgium and the province of Limburg in the south of the Netherlands. Those floods are fairly well documented, from a hydrological (de Wit et al., 2007) as well as a meteorological point-of-view (van Meijgaard, 1995; van Meijgaard and Jilderda, 1996). Figure 1.1 displays the daily basin-average precipitation and the river discharge at Borgharen, located near the point where the river enters the Netherlands. Though both floods have in common that they were preceded by a wet period leading to a saturated soil, there are some differences regarding the meteorological conditions. The flood of December 1993 was characterized by a single, narrow discharge peak of 3120 m^3s^{-1}, which was primarily due to intense precipitation on the 19th and 20th of December (van Meijgaard, 1995). On the 19th most precipitation was recorded in the French part of the basin. The precipitation of the 20th, most of which fell in Belgium, originated from an atmospheric disturbance following a more northerly track than the one on the day before. This precipitation coincided with the traveling high-water wave from France, leading to a higher peak discharge at Borgharen than expected from the total amount of precipitation on the two days.

The flood of January 1995 can be ascribed to a prolonged period of heavy precipitation. Snowmelt in the higher areas of the Belgian Ardennes contributed to saturate the already wet soil. Though the maximum discharge in January 1995 was lower (2860 m^3s^{-1}), the total discharge volume was larger, filling the entire river bed downstream of Borgharen. Therefore, the propagating flood wave was hardly attenuated (Heylen, 1998). At gauging points more than 50 km downstream of Borgharen the measured flood peak exceeded the flood peak of 1993. Apart from a high flood peak, persistent excessive discharge and high water levels may cause structural damage to flood-protection works. Therefore, both the duration and the total volume of the flood are of importance to safety. Because in 1995 the area of precipitation also covered the northern part of the Rhine basin, the discharge of the river Rhine in the Netherlands was also rising rapidly at that time. This led to a threatening situation in the centre of the Netherlands, where both rivers are close to each other. Owing to the flood of 1993, though, local authorities were better prepared to take evasive action this time.

The hydrographs in Fig. 1.1 of both cases furthermore illustrate that, even though large isolated daily precipitation amounts caused rapid increases of the discharge, excessive discharges mainly depend on the long-term history of precipitation, because the antecedent soil moisture conditions also play an important role.
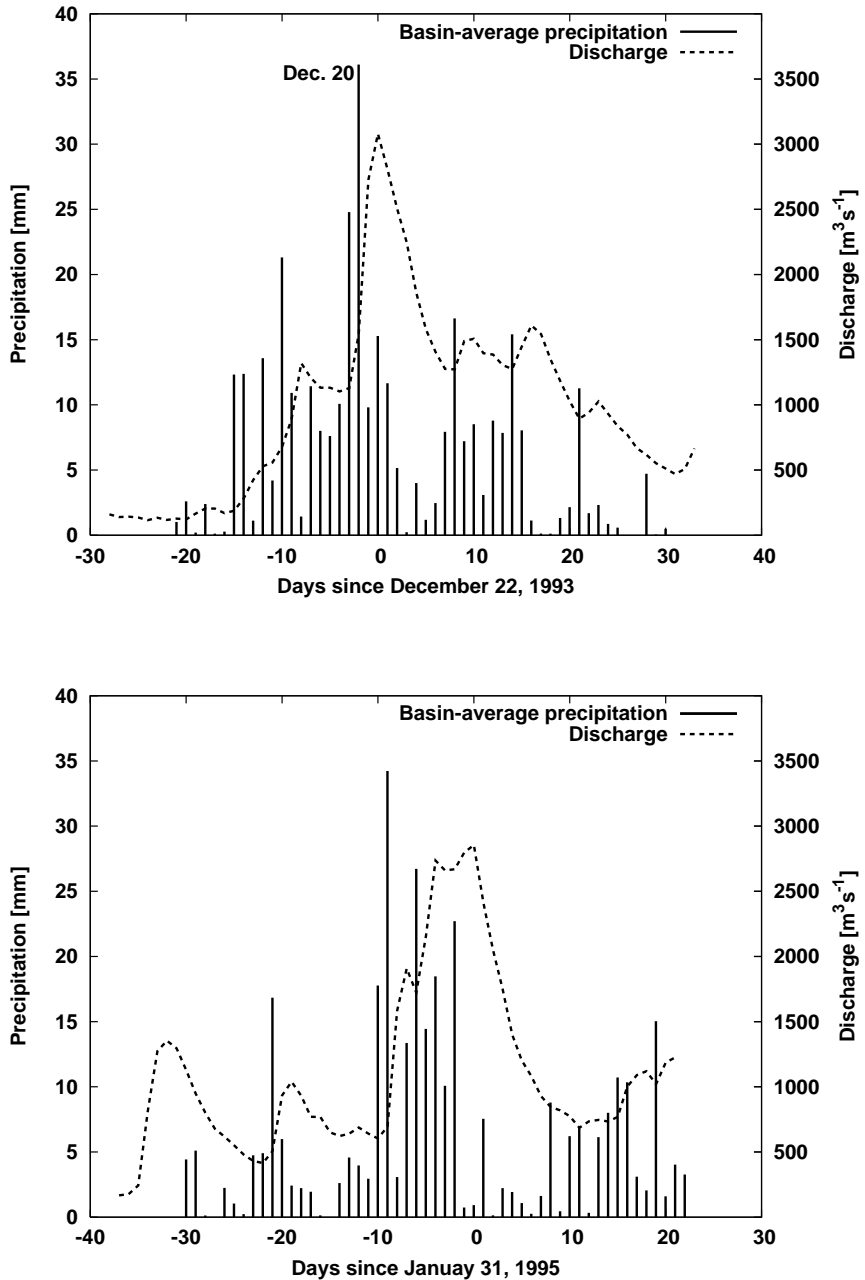
Figure 1.1: *Daily precipitation and discharge of the river Meuse at Borgharen during the flood events of December 1993 (top) and January-February 1995 (bottom). Day 0 corresponds with the recorded discharge maximum (1993, December 22 and 1995, January 31).*

1.2   The Flood Protection Act and the design discharge

In 1992 the Boertien-I Committee was given the task to re-evaluate the recommendations of the Becht Committee of 1977. The goal was to unite the demand for safety with environmental targets. This committee more or less confirmed the findings of 1977 and refined the estimation of the design discharge (Commissie Boertien I, 1993). The most important modification to the procedure was to consider a set of distribution functions, instead of just the exponential distribution. The committee primarily considered the river Rhine. After the Meuse flood of 1993 the Boertien-II Committee was formed to advise on flood-protection measures for the river Meuse. In 1996 the Flood Protection Act was established, prescribing a five-year cycle of determining the design discharge and the hydraulic safety standards (the so-called hydraulic boundary conditions) for testing flood-protection works.

The current method used to determine the design discharge is still based on the frequency analysis of historical flood peaks. The flood-peak record for the Meuse at Borgharen goes back to 1911. The procedure is described in one of the technical reports that are part of the Boertien-II report (Commissie Boertien II, 1994). In the first step of the procedure the record of flood peaks is corrected and homogenized, because the frequency analysis assumes the record to be representative of the current situation of the basin and river bed. This step therefore requires additional information, for instance on the history of river works. In the analysis of the design discharge for the Hydraulic Boundary Conditions 2001 (Parmet et al., 2001) the years 1993 through 1998 were added to the homogenized 1911-1992 record used in the investigation for the Boertien-II Committee. In addition, a record was constructed in which the flood peaks of the years 1984-1987 were recalculated using an adapted stage-discharge relation (referred to as Variant 2, as opposed to Variant 1 in which these flood peaks were not corrected). The modified relation decreases the flood peaks of those years considerably (13% for the flood peak of 1984).

In the second step the exponential distribution is fitted to the partial series of peaks exceeding a threshold of 1300 m^3s^{-1}. In addition a set of distributions, namely the three-parameter log-normal, three-parameter gamma and Gumbel distributions (left-censored at 1000 m^3s^{-1}), are fitted to the annual discharge maxima through a modified maximum-likelihood method. The flood quantile at a given return period is then derived as the (arithmetic) average of the flood quantiles for this return period from the fitted distributions.

An additional variant (Variant 3) is produced by assigning weights to the distributions using a kind of Bayesian approach. The distributions showing the best fit to the data receive the highest weigths. Furthermore, the Rayleigh distribution was added to the set of distributions because of its ability to describe the flood peaks. Based on the Bayesian analysis, this distribution receives the highest weight (van Noortwijk et al., 2004).

Table 1.1: *Estimated design discharges through the years. 'HBC' refers to the value used for the Hydraulic Boundary Conditions.*

Source		Design discharge
Commissie Becht (1977)		3600 m^3s^{-1}
Commissie Boertien I (1993)		3650
Commissie Boertien II (1994)		3800
Parmet et al. (2001)	Variant 1	3850
	Variant 2	3805
	Variant 3	3690
Ministerie van Verkeer en Waterstaat (2001)	HBC 2001	3800
Diermanse (2004)		3965
Ministerie van Verkeer en Waterstaat (2007)	HBC 2006	3800

The procedure described by Parmet et al. (2001) results in three estimates of the design discharge, the first and second only differing in the used data, whereas the third is based on the Bayesian approach. Although Bayesian methods increase in popularity, the authors present the outcomes of the three variants without giving prior preference to any of them. The design discharge eventually used as a basis for the hydraulic boundary conditions is rounded to hundreds of m^3s^{-1} to avoid the false suggestion of unrealistic accuracy and to reduce the influence of individual flood peaks. For the Hydraulic Boundary Conditions 2001 the value of 3800 m^3s^{-1} from Boertien II was maintained, which is supported by variants 1 and 2 after rounding off (see also van de Langemheen and Berger, 2001). The same value was used for the Hydraulic Boundary Conditions 2006, even though a new estimate was presented by Diermanse (2004). Table 1.1 shows different estimates of the design discharge of the river Meuse and the year in which they were issued. In particular, a jump in the design discharge is seen between Boertien I and Boertien II. This increase should be ascribed to the influence of the floods of 1993 and 1995 on the latter. There is also a strong difference between the methodology of the Becht and Boertien-I committees: whereas for the former only a single distribution was fitted to the discharge maxima, the latter was based on four distributions. The fact that the third variant of Parmet et al. (2001) turns out to be much lower than the other two variants could be ascribed to the short upper tail of the Rayleigh distribution.

The estimated quantiles thus are sensitive to the recorded floodpeaks and the choice of the distribution. In particular, extrapolating from a *short* historical record generally induces a large uncertainty in the outcome. On the other hand, due to changes in the river basin and climate, a *long* historical record of flood peaks can not be considered as a stationary sequence (assumed in the analysis), despite the homogenization of the flood-peak record mentioned earlier. In the Boertien-I report it is recommended to make use of the knowledge of the physical mechanism behind flood generation by means

of a hydrological/hydraulical model. In conjunction with a statistical method for the generation of synthetic meteorological spatial data for the river basin, such a model could reduce the uncertainties inherent to the extrapolation of flood-frequency distributions. (Buishand and Brandsma, 1996). For the river Rhine such an approach has already been explored (Buishand and Brandsma, 2001) and applied to studies of flooding in North-Rhine-Westphalia in Germany and an adjacent region in the east of the Netherlands (Lammersen, 2004). This thesis is focussed on the development and application of a similar instrument for the river Meuse.

1.3   Discharge extremes in a changing climate

It is widely accepted that the effects of global warming ascribed to greenhouse gas emissions influence the hydrological cycle. Rising temperatures have a direct positive effect on the amount of water that can evaporate into the atmosphere and are therefore at midlatitudes associated with an increase in precipitation and river discharge. It is far less clear how flood extremes respond to these changes. The influence of climate change on river discharges was also mentioned as a potential threat in the Boertien-I report in 1993. The report states that General Circulation Models (GCMs), which form the basis of climate change projections, are too coarse to provide useful quantitative information on the changes of the discharge of the rivers Rhine and Meuse.

For the river Meuse it has been assumed that the relative increase in peak discharges is roughly equal to the relative increase in extreme 10-day winter precipitation (Parmet and Burgdorfer, 1995). According to the WB21 climate-change scenarios (Kors et al., 2000) that have been used in the Netherlands until 2006 (van den Hurk and Co-authors, 2006), extreme 10-day winter precipitation increases by 10% per ^{o}C. Combined with an expected temperature rise of 2°C, this results in an increase of the design discharge of 20%, i.e., a change from 3800 m^{3}s^{-1} to 4600 m^{3}s^{-1} (de Wit et al., 2008).

Recently there has been a rapid development in high-resolution regional climate models (RCMs) within co-operative projects such as PRUDENCE (Prediction of Regional scenarios and Uncertainties for Defining EuropeaN Climate change risks and Effects), (Christensen and Christensen, 2007). These RCMs are driven by GCMs at the lateral boundaries of their domains and translate the climate of the GCM to smaller scales. RCM runs driven by respectively a GCM control run (i.e. under current climate conditions) and a GCM run for a possible future climate ('scenario') give insight into the induced changes at the regional scale. A complication is that no climate model perfectly represents the real climate (as verified by comparing the control run with observations). One way around this shortcoming is the use of some bias correction that, if applied to the control simulation of the RCM, leads to the correct values of a set of characteristics (mean, variance etc.) of the meteorological variables relevant to extreme river discharge. It is then silently assumed that the application of the same bias correction to scenario

simulations yields a realistic representation of a future climate in terms of these characteristics. The corrected output of both runs can be fed into a rainfall-runoff model to study the impact of climate change on (extreme) discharges. This is the 'direct' approach followed in this thesis. A different path is to extract changes in certain characteristics from a comparison between the control simulation and the scenario simulation and to modify observed data to reflect these changes, a 'delta' approach. The modified observations are used as input to the rainfall-runoff model.

Both approaches, schematically illustrated in Fig. 1.2, will generally not lead to identical changes in discharge extremes. If the direct approach is followed, the bias in a limited set of characteristics of the RCM data is corrected (left branch of the circle). On the other hand, the perturbed observations in the delta approach will only incorporate a fraction of the changes imposed by the scenario (right branch). These paths will lead to the same result if in the direct approach the bias correction adjusts all characteristics relevant to the simulation of discharge extremes *and* in the delta approach the changes of all relevant characteristics are imposed on the observed data. Both approaches rely on the assumptions that biases of the climate model are the same in the control and scenario simulations, which for the latter cannot be verified. There are, however, some decisive arguments favouring the direct approach. A scenario run of an RCM incorporates changes of more characteristics (in other words, encompasses a more complete picture of climate change) than can be represented by a delta approach. Examples are the change in spatial and temporal precipitation patterns which can be of major importance to the simulation of extreme river flows. Furthermore, the realism of climate models is expected to improve as knowledge of the fundamental processes of climate (e.g., the influence of feedbacks) and the capacity of computational resources increases. Procedures taking advantage of the direct output of RCMs anticipate these improvements.

1.4 Objectives, methodology and structure of this thesis

The central objectives of this study are the estimation of flood quantiles in the current climate as well as a future climate. The aim is to investigate a methodology that can do both, thereby answering the central questions:

- **How large are flood quantiles at long return periods (in particular the design discharge) under current climate conditions?**

- **How should the output of regional climate models be processed to be useful for the determination of flood quantiles?**

- **How do these quantiles change in a future climate scenario simulated by a regional climate model ?**

The key-components of this methodology are a stochastic weather generator and a semi-distributed conceptual rainfall-runoff model for the Meuse basin upstream of Borgharen. The stochastic weather generator, based on a nearest-neighbour resampling algorithm, is driven by daily data from either historical records or the output of RCM runs. Its purpose is to generate long (order 1000 years) synthetic time series of daily precipitation and temperature. Because this weather generator is non-parametric, no explicit information is required on the statistical properties of the meteorological variables. The rainfall-runoff model converts the generated time series into an equally long series of daily river discharge of which the extremes are analyzed. Though both components are indispensable to the methodology, the preparation of the synthetic time series for the rainfall-runoff model receives most attention. The methodology is expected to result in more accurate estimates of flood quantiles than the extrapolation of a distribution fitted to a short sequence of flood peaks.

Direct methods   **RCM Output**   **Delta methods**

bias correction   **change in**
mean   **mean**

bias correction   **change in**
mean + variability   **mean + variability**

???   **???**

change in discharge extremes
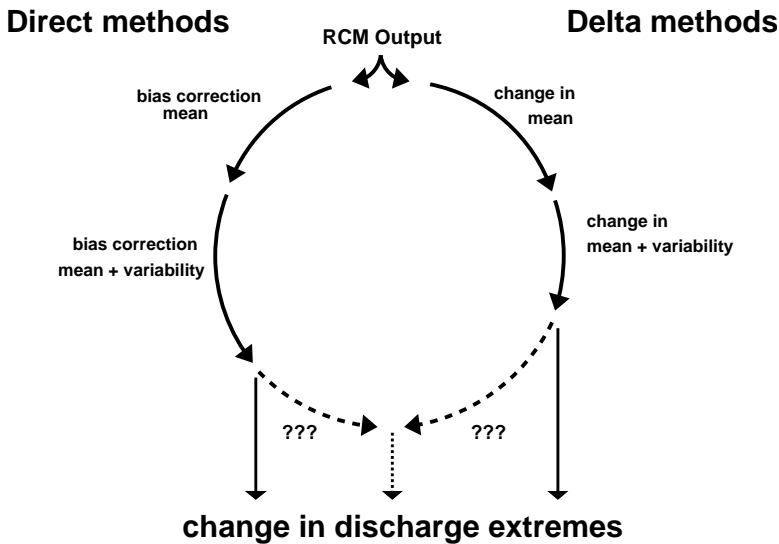
Figure 1.2: *Different routes towards future discharge, starting from regional climate model data from a control simulation and a scenario simulation: direct methods versus delta methods. Arrows along the circle symbolize subsequential steps taken towards the outcome, such as different levels of bias correction in the direct methods and different levels of transformation of the observations in the delta methods (courtesy to J.J. Beersma).*

By driving the weather generator with the output of RCM runs it is also possible to investigate the *change* of flood quantiles by comparing the simulated discharge extremes from the control run and a scenario run. As explained in Section 1.3, it is necessary to investigate the discrepancies between the control run and observational data (bias) and to devise a means of correction.

The chapters of this thesis are set up as follows. In Chapter 2 the weather generator developed for the Rhine basin is applied to observed daily precipitation and temperature for the Meuse basin. Attention is given to the combined use of long station records and shorter records of area-averaged precipitation. The rainfall-runoff model HBV (Lindström et al., 1997) is introduced and its performance is evaluated. HBV is then used to obtain long-duration series of daily discharge at Borgharen from which the extremes are analyzed.

Chapter 3 discusses a modification of the resampling algorithm that enables the simulation of daily precipitation and temperature beyond the range of the values used for resampling. This is achieved by first estimating the expected precipitation amount and temperature from the values simulated for the previous days. For precipitation the expected amount is then multiplied by a random residual, whereas for temperature a random residual is added to the expected value. The concept is tested on the precipitation and temperature records for the basin of the river Ourthe, a tributary of the river Meuse. The effect of the higher daily precipitation amounts on the simulated discharge extremes for this basin is studied.

Chapters 4 and 5 describe the application of nearest-neighbour resampling to the output of regional climate models. In Chapter 4 two runs of the RACMO model of the Royal Netherlands Meteorological Institute (KNMI) (respectively driven by the control simulation of the global model HadAM3H from the Hadley Centre and the ERA40 reanalysis from the European Centre for Medium-range Weather Forecasting, ECMWF) are discussed. The focus in this chapter is primarily on the model bias, its correction and its consequences for the simulation of extreme discharges. The importance of the correction of the relative variability of multi-day precipitation is emphasized. A nonlinear bias-correction method is tested on the resampled sequences of model output. In Chapter 5 the methodology presented in Chapter 4 is employed to investigate the change of flood quantiles in three different RCM experiments. In these experiments two different GCMs are combined with two RCMs. The bias correction introduced in Chapter 4 is slightly modified where necessary.

Chapter 6 briefly summarizes the work done in Chapters 2 through 5 and presents the major conclusions of this study. The methods used are evaluated and the three central questions are again addressed.

Simulation of extreme floods

Abstract

A stochastic weather generator has been developed to simulate long daily sequences of areal precipitation and station temperature for the Belgian and French subbasins of the river Meuse. The weather generator is based on the principle of nearest-neighbour resampling. In this method precipitation and temperature data are sampled simultaneously from multiple historical records with replacement such that the temporal and spatial correlations are well preserved. Particular emphasis is given to the use of a small number of long station records in the resampling algorithm. The distribution of the 10-day winter maxima of basin-average precipitation is quite well reproduced. The generated sequences were used as input for discharge simulations with the semi-distributed HBV rainfall-runoff model. Though this model is capable of reproducing the flood peaks of December 1993 and January 1995, it tends to underestimate the less extreme daily peak discharges. This underestimation does not show up in the 10-day average discharges. The discharge simulations with the generated daily precipitation and temperature data reproduce the distribution of the winter maxima of the 10-day average discharges well. Resampling based on long station records leads to lower precipitation and discharge extremes than resampling from the data over a shorter period for which areal precipitation was available.

2.1   Introduction

The Meuse is one of the largest rivers in northwest Europe. Its basin covers an area of more than 30 000 km^2, including parts of France, Belgium, Germany and The Netherlands. Protection against flooding is a matter of continuous concern. In The Netherlands

the design discharge for flood protection works is based on the extrapolation of the distribution of historical annual discharge maxima at Borgharen, where the river enters the country. Disadvantages of this method are that strong extrapolation is required, and that discharge records are potentially inhomogeneous. Furthermore, considering annual discharge maxima gives no insight into the shape and duration of the flood peaks. As an alternative, the simulation of long-duration discharge sequences by running a rainfall-ruonoff model with generated sequences of precipitation and temperature has been suggested (Parmet et al., 2001).

A weather generator based on nearest-neighbour resampling has been developed to provide long daily sequences of precipitation and temperature for the Meuse basin. This weather generator is similar to that in Buishand and Brandsma (2001) for the contiguous Rhine basin, except that in this study areal precipitation of the subbasins is simulated rather than station precipitation. A particular problem is to make use of a number of station records of daily precipitation that were longer than those of the available areal precipitation. It is desirable to take advantage of these long records to reduce the influence of recent years. In this chapter the simulation of both extreme multi-day precipitation and river discharges are addressed. The weather generator is described first. Then rainfall-runoff modelling and the simulation of extreme discharges using the generated precipitation and temperature data are discussed. The chapter ends with a presentation of the conclusions.

2.2   Weather generator

2.2.1   Nearest-neighbour resampling

In nearest-neighbour resampling, daily weather variables are sampled with replacement from the historical data to generate long daily sequences. The most important advantage of nearest-neighbour resampling, compared to other stochastic weather generators, is that it automatically preserves the correlation between variables on the same day. Furthermore, due to the conditioning of new daily values on the preceding days, the autocorrelation of those variables can also be well preserved, though there is a random influence in the selection process. The reproduction of the autocorrelation of daily precipitation is in particular crucial for the Meuse basin, because large river flows are generally induced by persistent precipitation over a multi-day period. The method requires no assumptions concerning statistical distributions and relationships and is completely data-driven.

In the resampling process, both in the generated sequence and the historical data, each day is characterized by a feature vector, which summarizes the weather conditions for the region of interest. The extent to which two days t and u differ is quantified by the weighted squared Euclidean distance $\delta^2(\mathbf{D}_u, \mathbf{D}_t)$ between their feature vectors $\mathbf{D}_u$ and

$\mathbf{D}_t$, i.e.

$$\delta^2\left(\mathbf{D}_u, \mathbf{D}_t\right) = \sum_{j=1}^{p} w_j\left(D_{tj} - D_{uj}\right)^2 \ , \tag{2.1}$$

where the index j refers to the jth of the p elements of the feature vector and w_j is the weight of this element. In each cycle of the algorithm one of the k closest historical days ('nearest neighbours') of the latest simulated day is selected at random. The weather variables of the historical successor to the selected nearest neighbour are then added to the sequence. Following a suggestion of Lall and Sharma (1996), a decreasing kernel is used to select one of the k nearest neighbours. This kernel gives more weight to closer neighbours. The probability of selecting the jth closest neighbour is given by

$$p_j \;=\; \frac{1/j}{\sum\limits_{i=1}^{k} 1/i} \ . \tag{2.2}$$

In order to account for the seasonal variation in the data and to prevent that typical winter and summer days are mixed up in the simulation, the search for nearest neighbours is usually restricted to a window of W calendar days, centred on the last simulated day. A more elaborate discussion on the nearest-neighbour resampling of daily weather variables can be found in Rajagopalan and Lall (1999) and Buishand and Brandsma (2001).

2.2.2 The Meuse basin and available data

Figure 2.1 shows the Meuse basin upstream of Borgharen (20 830 km^2), which is partly situated in France (45%) and partly in Belgium (55%). The Meuse is dominated by a precipitation-evaporation regime that produces low flows during summer and high flows during winter. For Borgharen a daily discharge record was available beginning in 1911. The record was corrected for the influence of the Albert Canal, Zuid-Willemsvaart and Juliana Canal, branching off just upstream of the gauging station. Fifteen subbasins were defined for rainfall-runoff modelling. One of these, the Sambre subbasin, was further subdivided into a French (9F) and a Belgian (9B) part. For all subbasins, daily areal precipitation was available for the period 1961-1998. The areal precipitation for the Belgian part was based on the Thiessen method and was obtained from the Belgian Meteorological Institute. For the French part, the areal precipitation was calculated from the data of 63 stations using squared inverse distance interpolation on a 5km grid.

Apart from the daily areal precipitation amounts of the 15 subbasins, daily point precipitation data from a number of stations in and around the Meuse basin were available for this study. The locations of these stations are shown in Fig. 2.1. In Table 2.1 the average totals are listed for the winter half-year (October-March) and the summer half-year (April-September) for all precipitation stations. The differences between the winter and summer averages are small. The wettest stations in France (Neufchâteau and Le Chesne) and southern Belgium (Chiny) have relatively large precipitation amounts in

Figure 2.1: *Locations of stations in and around the Meuse basin and the definition of the subbasins. Stations providing temperature data are indicated by [T].*

winter. The average precipitation amounts in Table 2.1 refer to the period 1961-1998 for which areal precipitation is also available. Seven stations have homogeneous records over the longer period 1930-1998. The year 1940 is missing in most of these records. Daily temperature records were available for the stations Langres (1949-1998), Reims (1949-1998), Uccle (1930-1998) and Aachen (1930-1998). Additional daily temperature data for the period 1968-1998 were obtained for six stations in Belgium and one in The Netherlands (not shown in Fig. 2.1).

2.2.3 Resampling of subbasin precipitation amounts and station temperatures

In the current study, nearest-neighbour resampling is applied to jointly simulate daily sequences of areal precipitation for each of the 15 subbasins in Fig. 2.1 and daily temperature at 11 locations in the basin. Simulations based on historical data for the period 1961-1998 (hereinafter referred to as Sim61) were performed, as well as simulations

based on the period 1930-1998 (Sim30), each with a length of 3000 years. Daily data from temperature and precipitation stations with complete records for the entire base period were used to form the feature vector in the resampling algorithm. For day t this vector consists of three elements:

- The average daily temperature $\widetilde{T}_t$ at two stations (Sim30) or four stations (Sim61). The temperature records were standardized with the calendar-day mean and standard deviation before averaging.

- The average daily precipitation $\widetilde{P}_t$ at seven stations. The rainfall records were standardized with the (seasonally varying) mean wet-day amount.

- The average of standardized precipitation for the four preceding days, i.e. $\left(\widetilde{P}_{t-1} + \widetilde{P}_{t-2} + \widetilde{P}_{t-3} + \widetilde{P}_{t-4}\right)/4$.

The third element was included to improve the reproduction of the autocorrelation of daily precipitation and the standard deviation of monthly totals (Harrold et al., 2003a and 2003b). For Sim61, $\widetilde{T}_t$ was derived from the daily temperature at Langres, Reims, Uccle and Aachen, and $\widetilde{P}_t$ from the daily precipitation at Le Chesne, Langres, Rochefort, Stavelot, Uccle, Chiny and Neufchâteau. The selected precipitation stations were judged to be the most representative of the basin because of their location and their mean annual precipitation. In Sim30, $\widetilde{T}_t$ was based on the temperature records from Uccle and Aachen, and $\widetilde{P}_t$ on the seven long-term daily precipitation records indicated in Table 2.1.

Table 2.1: *Average winter and summer precipitation totals for the stations in Fig. 2.1 for the period 1961-1998.*

Country	Station name	Altitude (m)	Winter (mm)	Summer (mm)
France	St. Quentin*	95	358	344
	Nancy*	212	374	378
	Vouziers*	96	380	363
	Chaumont*	317	474	432
	Langres	467	455	423
	Neufchâteau	286	515	428
	Le Chesne	174	536	425
Belgium	Uccle*	100	417	405
	Chiny*	299	728	529
	Stavelot	298	572	520
	Rochefort	193	406	422
Germany	Aachen*	202	388	423

*Homogeneous records available from 1930 (Leander & Buishand, 2004).

In contrast to the earlier study of nearest-neighbour resampling for the Rhine basin (Buishand and Brandsma, 2001), the areal precipitation of the 15 subbasins of the historical successor to the selected nearest neighbour was resampled, rather than the daily precipitation amounts for the seven stations used for the feature vector. This is straightforward in the case of Sim61 for which the records of subbasin precipitation cover the base period. For Sim30 an additional step in the algorithm is needed, because the subbasin data are incomplete over the period 1930-1960. Whenever a day from before 1961 is selected in Sim30, the closest neighbour of that day is sought among the days in or after 1961 to serve as an alternative from which the subbasin precipitation is resampled. For this new search, two-dimensional feature vectors were used, containing only $\widetilde{P}_t$ and $\widetilde{T}_t$. Though the areal values in the resampled sequence correspond to days within the period 1961-1998, the sampling of these days is based on station data for the entire period 1930-1998. Thus, if 1930-1960 is relatively dry, the algorithm will resample more intensely from the drier days in 1961-1998.

For temperature a similar additional nearest-neighbour search was performed to obtain temperature data for 11 locations, instead of two (Sim30) or four (Sim61), using data from the seven additional stations for the period 1968-1998. Since temperature plays only a minor role in the simulation of extreme floods, only the results for precipitation are presented in this chapter.

Besides the composition of the feature vector, a few additional settings are required. The number of nearest neighbours k was set equal to 10. Buishand and Brandsma (2001) show that loops could occur in the simulation in which certain historical days are repeatedly sampled if k is not sufficiently large. On the other hand, the reproduction of the autocorrelation of the generated sequences worsens if k is too large. Buishand and Brandsma (2001) obtained good results with $k = 5$, but in a later study for the Rhine basin (Beersma, 2002), $k = 10$ was used to be better protected against loops. For the width of the moving window, $W = 61$ was used, in accordance with Buishand and Brandsma (2001). A rather broad window can be chosen because the feature vector was formed from standardized precipitation and temperature data. The areal precipitation data were standardized in the same way as the point rainfall data. The weights w_j in the Euclidean distance were determined globally for each of the feature vector elements as the inverse of their sample variance over the entire series, resulting in a constant set of weights for all days in the year. The use of local (i.e. seasonally varying) weights was also considered. This had little effect because the seasonal variation of the weights turned out to be small, due to the standardization of the individual station records in an earlier stage.

The nearest-neighbour resampling algorithm can briefly be summarized as follows:

1. Randomly select a historical day within the moving window centred on 1 January as the first simulated day.

2. Compose a feature vector of average standardized station precipitation and temperature for the latest simulated day.

3. Find the k nearest neighbours of the latest simulated day within a W-day window centred on this day.

4. Select one of these nearest neighbours at random, using the decreasing kernel, given by Eqn. 2.2. Denote the date of the selected nearest neighbour by i and that of its historical successor by $i+1$.

5. For each of the simulated variables (areal precipitation or station temperature), check whether data for this variable exist for day $i+1$. If so, add the standardized historical data to the generated sequence for this variable. If not, form a feature vector of the standardized station data for day $i+1$, find the nearest neighbour of day $i+1$ among the days for which the data for the considered variable do exist and add the standardized data of this nearest neighbour to the generated sequence. The search is restricted to a W-day window centred on day $i+1$.

6. Repeat steps 2-5 for each simulated day.

7. Transform the resampled standardized variables back to their original scale.

2.3 Analysis of the generated precipitation sequences

The analysis of the generated areal precipitation sequences was focused on the reproduction of the autocorrelation of daily precipitation and the extreme-value distribution of the 10-day precipitation amounts. Large multi-day rainfall amounts in the winter half-year are known to induce high discharges. Figure 2.2 shows the basin-average autocorrelation coefficients (i.e. an area-weighted average of the coefficients for each individual subbasin) in the winter half-year for the historical records as well as two 3000-year simulations based on the data for 1961-1998 (Sim61), one with and one without the use of the 4-day memory element in the feature vector. It is seen that the memory element enhances the third- and higher-order autocorrelation coefficients. This leads to a reduction of the bias in the standard deviation of the monthly totals (in winter) from 7.4% to 1.6%.
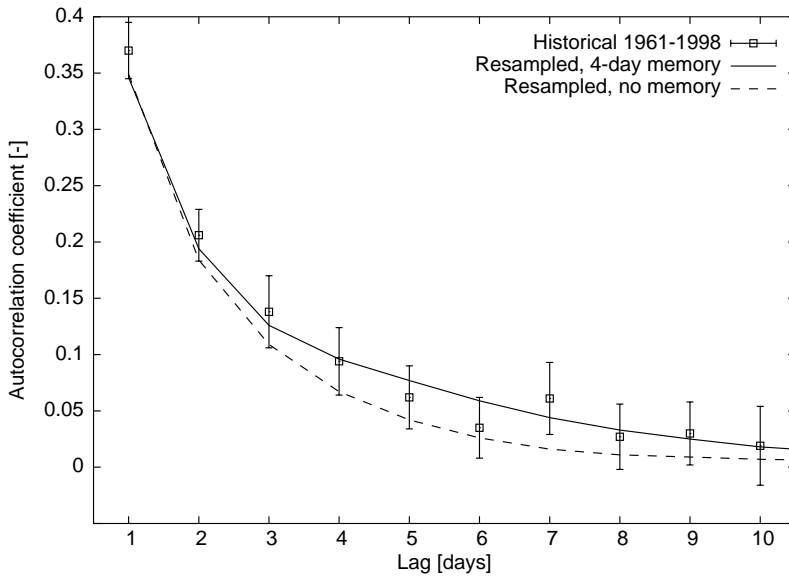
Figure 2.2: *Basin-average autocorrelation coefficients for the winter half-year of one 3000- year simulation with and one without the 4-day memory element in the feature vector, compared with those of the historical data. Both simulations are based on daily data for the period 1961-1998 (Sim61). The bars correspond to the $2\times se$-intervals. The standard errors se were calculated using a jackknife technique (Buishand and Beersma, 1993).*
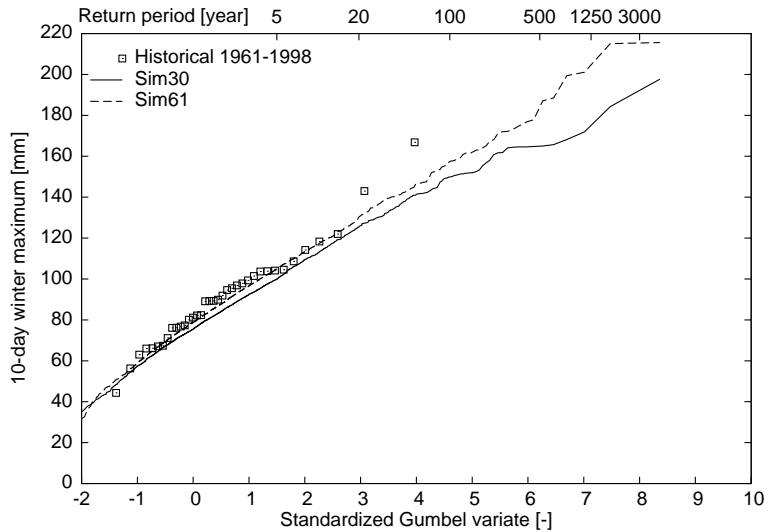
Figure 2.3: *Winter maxima of 10-day basin-average precipitation from 15 subbasin records for the period 1961-1998 and from the simulations Sim30 and Sim61.*
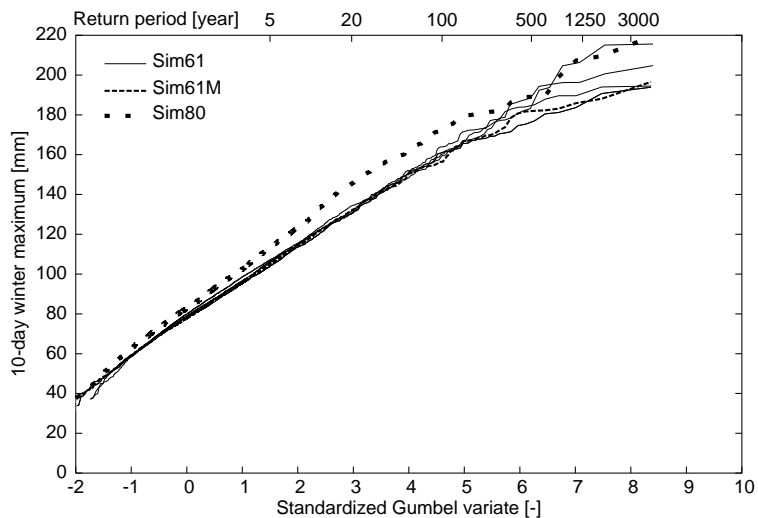

Figure 2.4: *Winter maxima of 10-day basin-average precipitation for Sim61M (dashed), Sim80 (big dots) and four runs of Sim61 with different random number seeds.*

Figure 2.3 compares the 10-day winter maxima of basin-average precipitation from the historical data and two 3000-year simulations (one Sim30 and one Sim61). There is a good agreement between the plot of Sim61 and that of the historical maxima. However, the two largest historical extremes lie clearly above the plot of Sim61. These extremes correspond to the Meuse floods of December 1993 and January 1995 (Parmet and Burgdorfer, 1995; van Meijgaard, 1995; van Meijgaard and Jilderda, 1996). To investigate whether the events of 1993 and 1995 deviate significantly from the simulated maxima, Sim61 was split into 78 segments of the same length as the historical record (38 years). It turned out that the maximum of 164 mm in 1995 was exceeded by about 20% of the 38-year segments of Sim61. The observed deviation between the plots of the simulated and historical maxima is therefore not considered to be significant. The plot of Sim30 is somewhat below that of Sim61. This can be ascribed to the fact that the winter half-year is on average drier for the period 1930-1960 than for the years 1961-1998. The effect of the additional nearest-neighbour step was assessed with a modified version of Sim61, Sim61M. This simulation was also based on the period 1961-1998, but the historical areal precipitation data for the period 1961-1979 were discarded. The additional nearest-neighbour step was used to obtain areal precipitation when a day before 1980 was sampled. Figure 2.4 compares the Gumbel plot of the 10-day winter maxima of Sim61M with those of four runs of Sim61 with different random number seeds and a simulation based on the period 1980-1998 (Sim80). It can be seen that the plot of Sim80 does not fall within the spread of those of the four Sim61 runs. On the other hand, Sim61M cannot clearly be distinguished from these four runs, even though the areal precipitation data of this simulation are sampled from the same period as those of Sim80. This indicates that the areal precipitation of Sim61M is representative of the period 1961-1998, just like the areal precipitation of Sim61. Figure 2.5 compares the 10-day precipitation extremes for the Semois subbasin (5 in Fig. 2.1). The correspondence between the simulated and historical maxima is similar to that in Fig. 2.3 From this it can be concluded that the method described here also works for a smaller area, even though only basin-average weather characteristics were used in the resampling algorithm.

2.4   The rainfall-runoff model

In this study the HBV model has been used for rainfall-runoff modelling of each subbasin. HBV is a conceptual model, developed at the Swedish Meteorological and Hydrological Institute (Lindström et al., 1997). The calculation within HBV is organized into several routines. The snow routine represents snow accumulation and snowmelt; the soil moisture routine controls which part of precipitation and melt water forms excess water and how much is evaporated or stored in the soil; and the runoff generation routine consists of an upper, nonlinear reservoir representing fast runoff components and a lower, linear reservoir representing base flow. Flood routing processes are simulated with a simplified Muskingum approach. Precipitation, temperature and potential evapotranspiration (PET) are required as input for the model. The temperature for each subbasin was
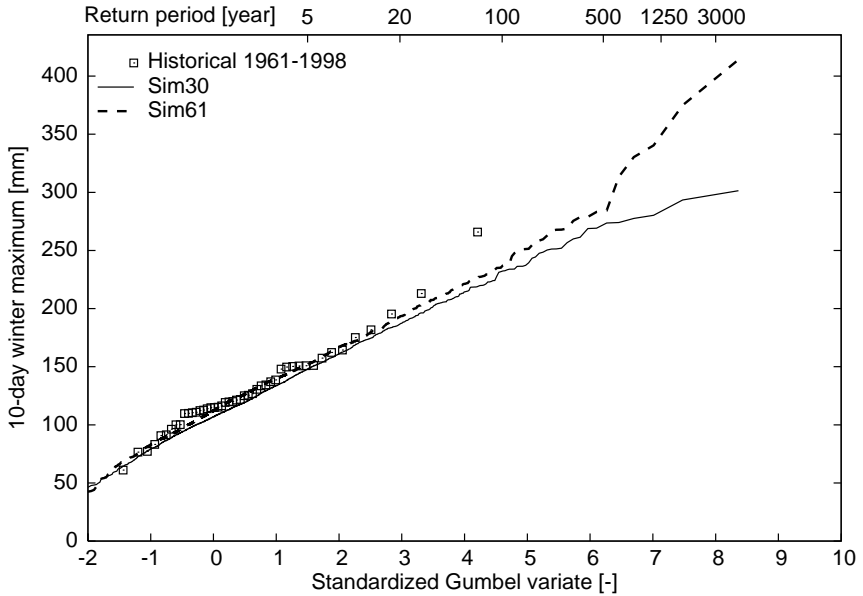
Figure 2.5: *Winter maxima of 10-day precipitation for the Semois subbasin from the historical record for the period 1961-1998 and from Sim30 and Sim61.*

set equal to the average of the four nearest stations using an altitude correction of 6^oC km^{-1}. For the Belgian subbasins, sequences of daily PET have been made available for the period 1967-1998 by the Belgian Meteorological Institute. For the calibration of HBV in the French part of the basin, PET was set equal to the average PET of the Belgian part. In the 3000-year simulations PET was obtained from the simulated daily temperature T as:

$$\mathrm{PET} = \left[1 + \alpha\left(T - \overline{T}\right)\right] \overline{\mathrm{PET}} \, , \qquad (2.3)$$

with $\overline{T}$ (^oC) and PET (mm day^{-1}) being the mean daily temperature and mean monthly PET for the period 1967-1998 and α a constant factor. Van der Wal (2002) found for α a value of 0.17^oC^{-1}. In the following chapters an improved estimate of α is used, which varies seasonally.

2.4.1 Calibration and validation

The original calibration of HBV for the Meuse was carried out by Booij (2005). He observed that the most influential parameters were three parameters in the soil moisture routine and three parameters in the fast flow routine. These parameters were optimized for the Lesse, the Ourthe, the Amblève and the Vesdre (respectively subbasins 8, 12, 13

Table 2.2: *Mean, maximum, standard deviation and the mean annual maximum of the simulated and observed daily discharges (*m^{3}s^{-1}*) for the river Meuse (period 1968-1998).*

	Mean	Maximum	Standard deviation	Mean annual max
Recorded discharge	267	3080	269	1474
HBV simulation	277	2976	286	1288

and 14 in Fig. 2.1). For the other subbasins, for which he had no discharge data, the values of these parameters were derived from river basin characteristics, such as slope, area and soil porosity. Default values were taken for the remaining parameters. In the framework of this study, recalibration took place with more detailed meteorological input and additional discharge records for the Semois (subbasin 5) and a gauging station along the main branch of the river at the French Belgian border (Chooz, Fig. 2.1). For the discharge at Borgharen this resulted in a Nash-Sutcliffe efficiency of 0.91 for the calibration period 1969-1984 and 0.93 for the validation period 1985-1998.

Table 2.2 shows that the mean, the standard deviation and the maximum of the daily discharges from the HBV simulation resemble those of the observed data. However, the mean of the annual maximum discharges is underestimated considerably. An underestimation of the mean annual maximum discharge is in line with the results in Eberle et al. (2002) for the major subbasins of the river Rhine. Figure 2.6 compares the observed and simulated discharges for four historical extreme events. The two highest peaks, in December 1993 (panel C) and January 1995 (panel D), are well reproduced by the HBV model. The peaks of February 1984 (panel A) and January 1993 (panel B) are too low in the simulation. The simulated hydrograph is smoother than the observed hydrograph, in particular for January 1993. The total volume of this event, however, is well preserved. The underestimation of the February 1984 peak is partly due to an inappropriate stage-discharge curve, which was used during 1984-1987 (Parmet et al., 2001). The operation of weirs, sluices and small reservoirs upstream of Borgharen may be another source of bias in peak flows. The regulation of those reservoirs is not included in the HBV modelling.

2.4.2   Simulated extreme discharges

Two 3000-year generated sequences (one Sim30 and one Sim61) of areal precipitation and station temperature were used to simulate the daily discharge at Borgharen with the HBV model. Figure 2.7 shows the highest peak discharge for Sim61 and the corresponding basin-average precipitation amounts, illustrating that high discharge is the result of long periods of persistent precipitation, rather than large rainfall amounts on a single day. This is related to the integrating effect of a large river basin.
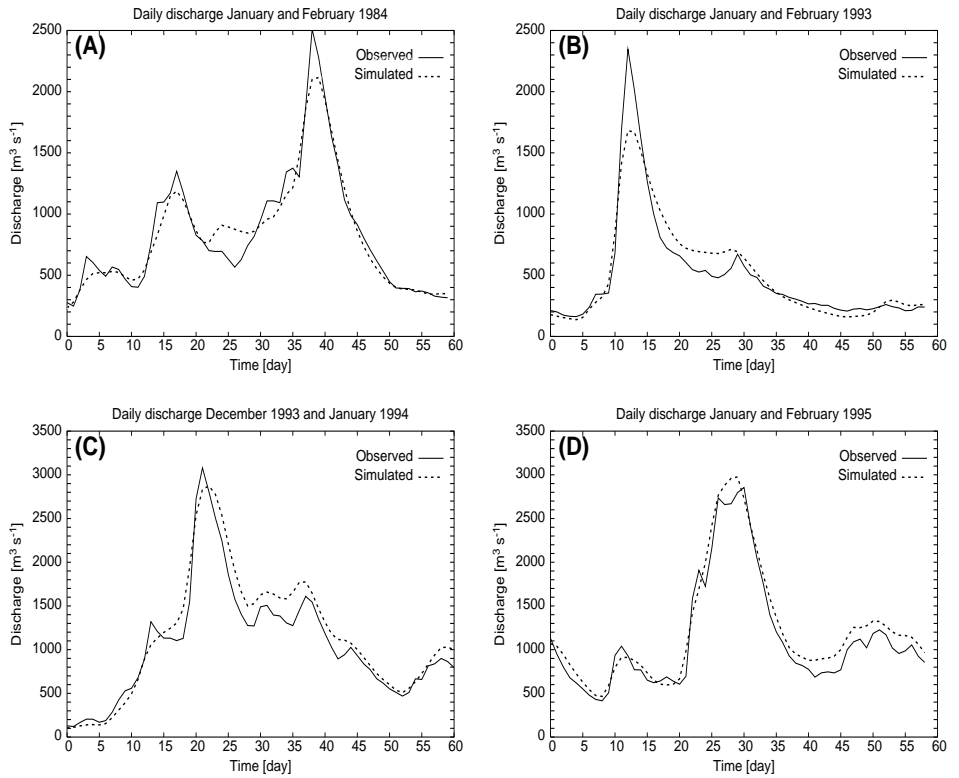
Figure 2.6: *Observed (solid) and simulated (dashed) daily discharge at Borgharen around the winter maxima of (A) 1984, (B) 1993, (C) 1994 and (D) 1995.*

Figure 2.7:   *The daily discharge (dashed curve) around the highest discharge maximum*
(4464 m^{3}s^{-1}*) in the HBV simulation driven by Sim61 and the corresponding daily pre-*
cipitation (bars).

Figure 2.8:   *Winter maxima of the observed daily discharge at Borgharen (1968-1998)*
and the simulated daily discharge based on the historical meteorological data for 1968-
1998, Sim30 and Sim61.

Figure 2.8 shows a Gumbel plot of the winter maxima of the observed daily discharge record at Borgharen, the simulated discharge based on historical meteorological data and the simulated discharge b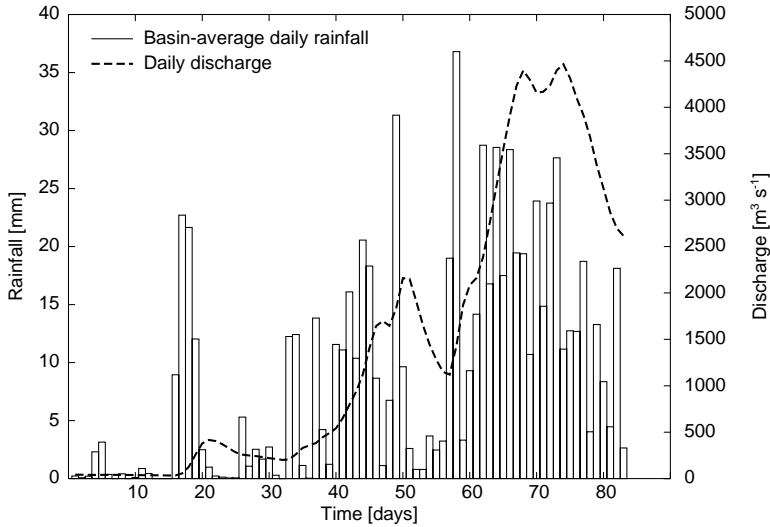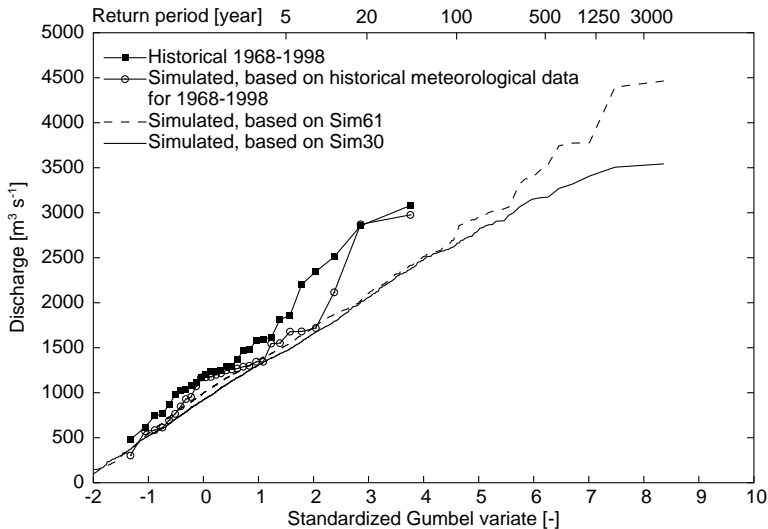ased on Sim30 and Sim61. The HBV simulation using the Sim61 data shows a good correspondence with the simulation using historical meteorological data. However, the simulated maxima for December 1993 and January 1995 are far above the plot of the extremes from the Sim61 data. This deviation is more apparent for the discharges than for the 10-day precipitation amounts shown in Fig. 2.3. It is rather accidental that two such floods occurred in the relatively short period 1968-1998. These floods are among the three largest daily discharges in the 93-year record. There is only one flood of comparable magnitude within the period 1911-1967 (January 1926). The difference between the results for the two 3000-year simulations is small. As expected, the plot of Sim30 is somewhat below that of Sim61. A point of concern is the systematic difference between the plot of the observed discharges and the plots of the simulations at short and moderate return periods due to a systematic underestimation of the flood peaks by the HBV model in this frequency range. This systematic difference is not apparent in the extreme 10-day average discharges, as is shown in Fig. 2.9.

The largest historical 10-day average discharge occurred in 1995. Although the peak discharge of the 1995 event was somewhat below that of the 1993 event, its volume was much larger, due to the relatively long duration of discharges exceeding 2500 m^{3}s^{-1}. The attenuation of the flood wave was therefore less in 1995, which resulted in higher water levels downstream of Borgharen. It should be noted that in the 3000-year simulations much larger 10-day average discharges are found than the historical 1995 maximum.

It is unclear how well HBV can describe flood peaks outside the range for which it was calibrated. The model does not consider the possibility of inundations upstream of Borgharen, which may limit the amount of water that can reach The Netherlands.

2.5 Conclusion

A stochastic weather generator for the Meuse basin upstream of Borgharen based on nearest-neighbour resampling has been developed. Daily sequences of areal precipitation for 15 subbasins and station temperatures were simultaneously generated using nearest-neighbour resampling. Several 3000-year simulations were performed, driven by the historical precipitation and temperature for the periods 1961-1998 and 1930-1998. An additional nearest-neighbour step was applied to resample from records which did not completely cover the base period. The generated precipitation and temperature sequences were used to perform 3000-year simulations of the daily discharge at Borgharen with the HBV rainfall-runoff model.

The weather generator reproduces the distribution of the extreme 10-day precipitation quite well both for individual subbasins and the entire basin. The choice of base period
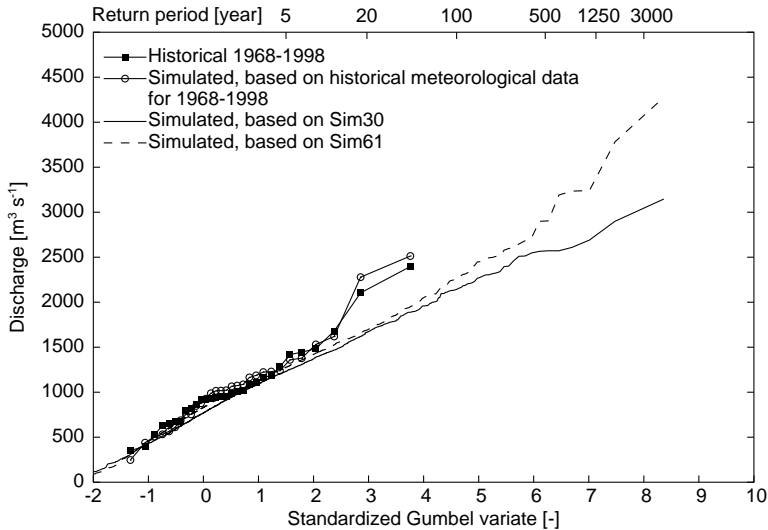
Figure 2.9:   *Winter maxima of the observed 10-day average discharge at Borgharen (1968-1998) and those simulated using respectively historical meteorological data and data from Sim30 and Sim61.*

1930-1998 leads to somewhat lower extreme 10-day winter precipitation because of the drier winters that occurred during 1930-1960. The distributions of the discharge winter maxima from the 3000-year simulations resemble those from the HBV simulations with historical meteorological data. The influence of the base period for resampling turns out to be small. For the daily discharges there are significant differences between the extreme-value distributions from the observed and simulated data because of the tendency of HBV to underestimate flood peaks. Improvement requires more detailed modelling (a finer temporal resolution, inclusion of the reservoir regulation and coupling with a hydraulic model for flood routing) for which not all required data are readily available. However, the major floods of December 1993 and January 1995 are already adequately reproduced by the current HBV model. Moreover, the discrepancies between the observed and simulated extreme-value distributions disappear if the 10-day average discharges are considered. This indicates that the weather generator is able to provide reliable estimates of the volumes and durations of extreme floods.

Acknowledgements

A two-stage resampling algorithm

Abstract

A two-stage time series resampling algorithm is presented that is capable of generating daily values of weather variables outside their historical ranges. In this algorithm the simulated daily values are composed of an expected value and a sampled historical residual. The residuals broaden the range of the simulated daily values. Both the estimation of the expected value and the sampling of the residuals are based on the nearest-neighbours concept. In particular the influence of the neighbourhood sizes in both nearest-neighbour searches was studied. The algorithm was tested with data generated by two theoretical time-series models. Using observed precipitation and temperature data, a 12 000-year series of precipitation and temperature for the Ourthe catchment (Belgium) are simulated and used as input for the HBV rainfall-runoff model to produce a long synthetic sequence of daily discharge. The two-stage algorithm correctly reproduces the mean, standard deviation and lag 1 autocorrelation of daily precipitation. The simulated distributions of 4-day and 10-day precipitation maxima in winter also show good correspondence with those observed, while the largest daily amounts substantially exceed those in the original data. However, the widened range of daily precipitation amounts has no discernible effect on the simulated discharge maxima in winter.

3.1 Introduction

The stochastic generation of weather variables relevant to hydrologic simulation has long been of interest. This is reflected by the variety of papers on this topic, in particular on the generation of daily precipitation sequences (the oldest dating from the

1970s). Initially parametric models were used. Quite often the occurrence of precipita-
tion was described by a two-state Markov chain or an alternating renewal process and
the amount of precipitation on a wet day by a positively skewed distribution (gamma or
mixed exponential), see Woolhiser (1992) for a review. Transformations of the multivari-
ate normal distribution have been considered for multi-site simulation (e.g., Richardson,
1977; Bárdossy and Plate, 1992; Wilks, 1998). Nonhomogeneous hidden Markov chains
have been developed for the conditional simulation of daily precipitation on large-scale
weather variables (e.g., Hughes and Guttorp, 1994; Charles et al., 1999). Parametric
models require rather restrictive assumptions regarding the probability distributions and
the correlation structure. Nonparametric models avoid this difficulty and are therefore
gaining in popularity. Examples of this approach are nearest-neighbour resampling (e.g.,
Young, 1994; Rajagopalan and Lall, 1999; Lall and Sharma, 1996) and methods involv-
ing kernel-density estimation techniques (e.g., Harrold et al., 2003a and 2003b). An
advantage of nearest-neighbour resampling is that it can easily be extended to multi-site
simulation (Buishand and Brandsma, 2001). A significant disadvantage of the algorithm
presented in Chapter 2 is, however, the fact that it cannot produce amounts beyond
those present in the sequences used as base material. This limitation may not hamper
applications relying mainly on extreme multi-day precipitation. However, in some ap-
plications it might be desirable to allow for daily amounts beyond the maximum found
in the historical record.

In this chapter an extension of the nearest-neighbour resampling algorithm is explored
that is capable of generating larger daily precipitation amounts than those observed. This
is achieved by a two-stage resampling scheme. In the first stage the expected amount
is determined, using a nearest-neighbour regression. In the second stage the expected
amount is multiplied by a randomly selected residual factor, which is also based on a
nearest-neighbour search. The general concept is first tested for two univariate cases
using simulated data from theoretical time-series models. Subsequently, this idea is used
to generate sequences of daily precipitation and temperature of a river catchment in the
Ardennes, Belgium. The properties of the resampled precipitation are studied in detail.
A 12 000-year synthetic series of daily precipitation and temperature serves as input
for simulations with the semi-distributed rainfall-runoff model HBV (Lindström et al.,
1997). The results for extreme floods are compared with the results of a traditional
single-stage algorithm. Additionally, a series resampled with the single-stage algorithm
is considered in which the largest daily precipitation amounts are perturbed.

3.2   Method

The simulation procedure is based on the decomposition of the variable X into an ex-
pected value M conditional on prior values of X and a non-negative residual factor e
with unit mean, i.e.

$$X = M\,e\;. \tag{3.1}$$

Simulating a value X_j^* for a certain day j proceeds in two stages, the estimation of its expected value M_j from the simulated values for previous days and the generation of a residual e_j^*. This requires information on the distribution of e to be extracted from the historical record.

Prior to the simulation, for each day i in the historical sequence the expected value M_i of X_i is estimated by a nearest-neighbour regression. 'Nearest-neighbour' (Lall and Sharma, 1996) here refers to a day $l \neq i-1$ that is similar to day $i-1$ in terms of $\delta_{l,i-1} = |X_l - X_{i-1}|$ (or the weighted Euclidean distance in the case of multiple variables characterizing day $i-1$, see Eqn. 2.1). The estimate $\widehat{M_i}$ of M_i can be expressed as a linear combination of the successors of the sorted k_M nearest neighbours of day $i-1$ with coefficients λ_k:

$$\widehat{M_i} = \sum_{k=1}^{k_M} \lambda_k \ X_{\mathrm{nnb}(k,i-1)+1} \ , \tag{3.2}$$

where $\mathrm{nnb}(k, i-1)$ refers to the k-th closest neighbour of X_{i-1}. The residual $\widehat{e_i}$ of day i then equals the historical value X_i divided by $\widehat{M_i}$.

The simulation of daily values proceeds in an analogous way. For each new day j in the simulation, an estimate $\widetilde{M_j}$ of the expected value is calculated from the historical successors of the nearest neighbours of the last simulated value X_{j-1}^* as:

$$\widetilde{M_j} = \sum_{k=1}^{k_M} \lambda_k \ X_{\mathrm{nnb}(k,j-1)+1} \ . \tag{3.3}$$

From the k_e historical days of which $\widehat{M_i}$ is closest to $\widetilde{M_j}$, one of the residuals $\widehat{e_i}$ is randomly selected as the simulated residual e_j^*, using the decreasing $\frac{1}{\mathbf{k}}$-kernel introduced by Lall and Sharma (1996):

$$\alpha_k = \frac{1/k}{\sum\limits_{k=1}^{k_e} 1/k} \qquad 1 \leq k \leq k_e \tag{3.4}$$

with α_k the probability of selecting the residual of the k-th closest neighbour. From the expected value and the residual factor the simulated value for day j then becomes:

$$X_j^* = \widetilde{M_j} \ e_j^* \ . \tag{3.5}$$

Based on a suggestion of Lall and Sharma (1996), Prairie et al. (2006) followed an analoguous approach to simulate values beyond the observed range. They used an additive algorithm instead of a multiplicative algorithm. In particular with a view to simulating precipitation, the latter has the advantage that the generation of negative values is avoided. Another difference with the algorithm discussed here is that in their algorithm

the residual was sampled from the successor of one of the nearest neighbours used for estimating M.

The decomposition of the historical value X_i into an expected value $\widehat{M}_i$ and a residual $\widehat{e}_i$ can be summarized as follows:

1. Find and sort the k_M nearest neighbours of the historical day $i - 1$.

2. Determine the expected value $\widehat{M}_i$ from the historical successors of these nearest neighbours (Eqn. 3.2).

3. Obtain the residual as $\widehat{e}_i = X_i/\widehat{M}_i$.

The simulation is then initialized by selecting a historical day at random and values at subsequent days j are simulated:

1. Find and sort the k_M nearest neighbours of the last simulated day $j - 1$.

2. Determine the expected value $\widetilde{M}_j$ of the new day j as a weighted average of the historical successors of these nearest neighbours (Eqn. 3.3).

3. Find and sort the k_e historical days of which $\widehat{M}$ is nearest to $\widetilde{M}_j$.

4. Sample the residual $\widehat{e}$ of one of these days as e_j^* using the $\frac{1}{k}$-kernel (Eqn. 3.4).

5. Multiply $\widetilde{M}_j$ and e_j^* to simulate the value X_j^* for day j.

For the hydrological application in this study this algorithm has been extended in order to generate daily precipitation and temperature simultaneously.

3.3   Theoretical models

The algorithm described above was first tested with data from theoretical time-series models which both generate only positive values. The advantage of considering a theoretical model lies in the fact that its statistical properties can usually be derived exactly from the model formulation. Two first-order autoregressive (AR1) models were considered, a lognormal AR1 model and an exponential AR1 model. The lognormal model was chosen because it is multiplicative, similar to the algorithm. The exponential model is useful to detect possible effects of non-multiplicativity on the algorithm. Both models have commonly been used within a hydrologic context, usually for the stochastic simulation of streamflows.

The lognormal AR1 model

A sequence $\{X_i\}$ of correlated standard lognormal variables can be generated by transforming the values $\{Y_i\}$ of a normal AR1 process:

$$Y_i = \rho Y_{i-1} + \varepsilon_i \sqrt{1 - \rho^2} \ . \tag{3.6}$$

$$X_i = \exp(Y_i) = \exp\left[\rho \log\left(X_{i-1}\right) + \varepsilon_i \sqrt{1 - \rho^2}\right]$$

$$= X_{i-1}^\rho \exp\left(\varepsilon_i \sqrt{1 - \rho^2}\right) \ , \tag{3.7}$$

where the $\{\varepsilon_i\}$ are independent standard normal variables. The $\{X_i\}$ have mean $\sqrt{e} \approx 1.65$ and standard deviation $\sqrt{e(e-1)} \approx 2.16$. The lag 1 autocorrelation coefficient ϱ_1 of the lognormal process $\{X_i\}$ can be derived from the lag 1 autocorrelation coefficient ρ of the underlying AR1 process $\{Y_i\}$ using (Mejía and Rodríguez-Iturbe, 1974):

$$\varrho_1 = \frac{\exp\left(\rho\right) - 1}{e - 1} \ . \tag{3.8}$$

The expectation M_i follows from Eqn. 3.7:

$$M_i = E\left(X_i | X_{i-1}\right) = X_{i-1}^\rho \exp\left[\frac{1}{2}\left(1 - \rho^2\right)\right]$$

$$= \exp\left[\rho \log X_{i-1} + \frac{1}{2}\left(1 - \rho^2\right)\right] \ . \tag{3.9}$$

Note that M_i is nonlinear in X_{i-1}. For this AR1 process the residuals

$$e_i = \frac{\exp\left(\varepsilon_i \sqrt{1 - \rho^2}\right)}{\exp\left(\frac{1}{2} - \frac{1}{2}\rho^2\right)} \tag{3.10}$$

have a lognormal distribution with

$$E(e_i) = 1 \qquad\qquad \mathrm{Var}(e_i) = \exp\left(1 - \rho^2\right) - 1 \ . \tag{3.11}$$

Since the distribution of $\log X_{i-1}$ in Eqn. 3.9 is standard normal, the distribution of M_i is lognormal with mean and variance

$$E(M_i) = \exp\left(\frac{1}{2}\right) \approx 1.65 \qquad \mathrm{Var}(M_i) = \exp\left[\exp\left(\rho^2\right) - 1\right] \ . \tag{3.12}$$

Here $\rho = 0.5$ was chosen, for which $\mathrm{Var}(M_i) \approx 0.77$, $\mathrm{Var}(e_i) \approx 1.12$ and $\varrho_1 \approx 0.378$. Furthermore, M_i and e_i are independent, because X_{i-1} and ε_i are independent.

The exponential AR1 model

An exponential AR1 model (EAR1) was presented by Gaver and Lewis (1980). Here this model is used to generate a sequence $\{X_i\}$ of correlated standard exponential variables. The EAR1 process has the same additive form as a normal AR1 process:

$$X_i = \rho X_{i-1} + \varepsilon_i \ . \tag{3.13}$$

The innovation ε_i equals zero with probability ρ and is positive with probability $1 - \rho$, in which case it is sampled from the standard exponential distribution, i.e. $\Pr(\varepsilon_i > x) = (1 - \rho) \exp(-x)$. A generalization of this process to gamma-distributed random variables (Gaver and Lewis, 1980; Lawrance, 1980) is related to the shot-noise models of Weiss (1977) for the generation of daily streamflow data. If the innovations ε_i are zero, the X_i decay exponentially, resembling streamflow recessions during dry periods. The autocorrelation structure is the same as that of a normal AR1 process, i.e. the lag j autocorrelation coefficient ϱ_j equals ρ^j. A value of $\rho = 0.5$ was chosen. Though a nonlinear multiplicative first-order exponential autoregressive process is known in the literature (McKenzie, 1982; Fernandez and Salas, 1986), the EAR1 process is considered here to detect possible limitations of non-multiplicativity to the resampling procedure.

The conditional means $\{M_i\}$ and the corresponding residuals $\{e_i\}$ for this model are given by

$$M_i = \rho X_{i-1} + (1 - \rho) \quad \text{and} \quad e_i = \frac{X_i}{M_i} = 1 + \frac{\varepsilon_i - (1 - \rho)}{M_i} \ . \tag{3.14}$$

The means of M and e are both equal to one and the variance of M equals ρ^2. Contrary to the lognormal model, the variance of e_i depends on M_i:

$$\text{Var}\ (e_i|M_i) = \frac{1}{M_i^2}\text{Var}\ (\varepsilon_i) = \frac{1 - \rho^2}{M_i^2} \ . \tag{3.15}$$

This dependence may put a restriction on k_e in the second step of the resampling algorithm. The $\{M_i\}$ follow a shifted exponential distribution with location parameter $1 - \rho$ and scale parameter ρ, i.e.

$$\Pr(M \leq x) = 1 - \exp\left[-\frac{x - (1 - \rho)}{\rho}\right] \ , \qquad\qquad x \geq 1 - \rho \tag{3.16}$$

Simulation results

With both AR1 models a sequence of 2000 values was generated (from here on referred to as 'data'). From these sequences, simulations with a length of 20 000 values were obtained by applying the two-stage resampling algorithm. For the coefficients λ_k in Eqns 3.2 and 3.3 the $1/k$-kernel in Eqn. 3.4 was used, but with k_M instead of k_e. The neighbourhood sizes k_M and k_e were expected to influence the statistical properties of

the simulated series. Table 3.1 lists the mean, the standard deviation s_d and the lag 1 autocorrelation r_1 of resampled sequences from the data of the lognormal model (left) and the exponential model (right) with various settings of k_M and k_e. For each model the theoretical values and the empirical estimates derived from the data are given in the first two rows.

The theoretical mean and standard deviation of both models are reasonably well reproduced by most simulations and seem insensitive to the choice of k_M and k_e. Both parameters are slightly overestimated in most simulations. In both cases (lognormal as well as exponential) r_1 is underestimated for all combinations of k_M and k_e. Since persistence is introduced into the simulation through M, its estimation from the nearest neighbours has been investigated in some detail. Figure 3.1 compares the values of $\widehat{M_i}$ from the exponential data, using $k_M = 400$ (dots) with the theoretical value from Eqn. 3.14 (solid straight line). The values of $\widehat{M_i}$ are considerably scattered. This scatter was suspected to be the source of the negative bias in r_1. To reduce the scatter, the LOESS smoother (Cleveland, 1979) was studied as an alternative for the estimation of M_i. In this method a polynomial is fitted to the successors of the nearest neighbours by means of weighted least-squares with weights

Table 3.1: *Sensitivity of the mean, standard deviation s_d and lag 1 autocorrelation coefficient to the neighbourhood sizes k_M and k_e for resampling from lognormal data (left) and exponential data (right). The theoretical values, those extracted from the data (2000 values) and those of several resampling simulations (20 000 values) are listed.*

k_M	k_e	Lognormal			Exponential		
		Mean	s_d	r_1	Mean	s_d	r_1
Theory		1.65	2.16	0.378	1.00	1.00	0.500
Data		1.69	2.22	0.376	1.02	1.01	0.500
50	100	1.69	2.24	0.281	1.04	1.02	0.406
100	100	1.66	2.23	0.288	1.03	1.01	0.422
200	100	1.71	2.29	0.298	1.03	1.01	0.440
400	100	1.68	2.23	0.329	1.02	1.02	0.458
800	100	1.69	2.25	0.308	1.02	1.00	0.454
400	50	1.67	2.16	0.321	1.04	1.01	0.440
400	200	1.70	2.26	0.309	1.05	1.02	0.441
400	400	1.70	2.25	0.315	1.03	1.02	0.439
400	800	1.72	2.33	0.323	1.02	1.03	0.439
400	1600	1.67	2.28	0.315	1.01	1.08	0.412

$$w_k = \left[1 - \left(\frac{\delta_k}{\delta_{k_M}} \right)^3 \right]^3 , \tag{3.17}$$

where δ_k is the distance between X_{i-1} and its k-th nearest neighbour and δ_{k_M} the largest distance within the neighbourhood. The estimate of M_i is calculated as the value of the fitted polynomial at X_{i-1}. The LOESS smoothers of degree zero L_0 (local constant) and degree one L_1 (local linear relation) are considered. In both cases the estimate of M_i can be written as a linear combination of the successors of the nearest neighbours, as in

Table 3.2:   *Same as Table 3.1, but now for two modifications of the original algorithm with respect to the estimation of M, respectively based on the zeroth-order (L_0) and first-order (L_1) LOESS smoother.*

k_M	k_e	Lognormal			Exponential			
		Mean	s_d	r_1	Mean	s_d	r_1	
Theory		1.65	2.16	0.378	1.00	1.00	0.500	
Data		1.69	2.23	0.377	1.02	1.01	0.500	
50	100	1.68	2.23	0.335	1.00	0.98	0.460	
100	100	1.69	2.20	0.345	1.01	0.97	0.481	
200	100	1.65	1.99	0.359	0.98	0.98	0.497	
400	100	1.70	2.17	0.387	0.95	0.95	0.508	
800	100	1.69	2.22	0.359	1.00	0.99	0.489	
								L_0
400	50	1.70	2.25	0.340	0.97	0.97	0.503	
400	200	1.70	2.17	0.373	0.95	0.96	0.510	
400	400	1.66	2.11	0.356	0.97	0.99	0.497	
400	800	1.68	2.19	0.339	0.98	0.98	0.482	
400	1600	1.71	2.23	0.359	0.97	1.00	0.462	
50	100	1.68	2.19	0.332	1.04	0.98	0.462	
100	100	1.73	2.27	0.368	1.01	0.97	0.478	
200	100	1.75	2.24	0.338	1.03	0.97	0.481	
400	100	1.67	2.15	0.348	0.97	0.99	0.510	
800	100	1.73	2.33	0.350	1.00	0.99	0.494	
								L_1
400	50	1.67	2.14	0.366	0.98	0.97	0.494	
400	200	1.68	2.17	0.373	1.00	1.00	0.503	
400	400	1.73	2.35	0.356	0.97	0.98	0.509	
400	800	1.70	2.26	0.359	0.99	1.00	0.508	
400	1600	1.64	2.12	0.357	0.98	1.05	0.505	

Eqn. 3.2. For L_0 the weights λ_k reduce to $w_k / \sum w_k$. For L_1 the expression of λ_k is more complex. As is seen in Fig. 3.1, the use of L_0 considerably reduces the scatter of $\widehat{M}_i$. However, it is also seen that $\widehat{M}_i$ based on the $^1\!/_{\mathbf{k}}$-kernel and L_0 falls below the theoretical line for $X_{i-1} > 3$. Method L_1, on the contrary, does not underestimate M_i at large X_{i-1}. The mean, s_d and r_1 for methods L_0 and L_1 are listed in Table 3.2. Especially the reproduction of r_1 improves substantially, compared to the values in Table 3.1 for the $^1\!/_{\mathbf{k}}$-kernel. The best results are found for $k_M > 100$. This could be related to the scatter of $\widehat{M}_i$, which decreases with k_M. In the case of the lognormal data a negative bias in r_1 still remains in most simulations, probably induced by the long tail of the distribution. Furthermore, the standard error of the estimated lag 1 autocorrelation is much larger in the lognormal case than in the exponential case, due to the influence of fourth order moments (Bartlett, 1946).

The upper panels of Fig. 3.2 show probability plots of X_j^*, resulting from resampling the lognormal data (left) and the exponential data (right) with method L_1 using different values of k_M and $k_e = 100$. The lower panels show the corresponding distributions of the
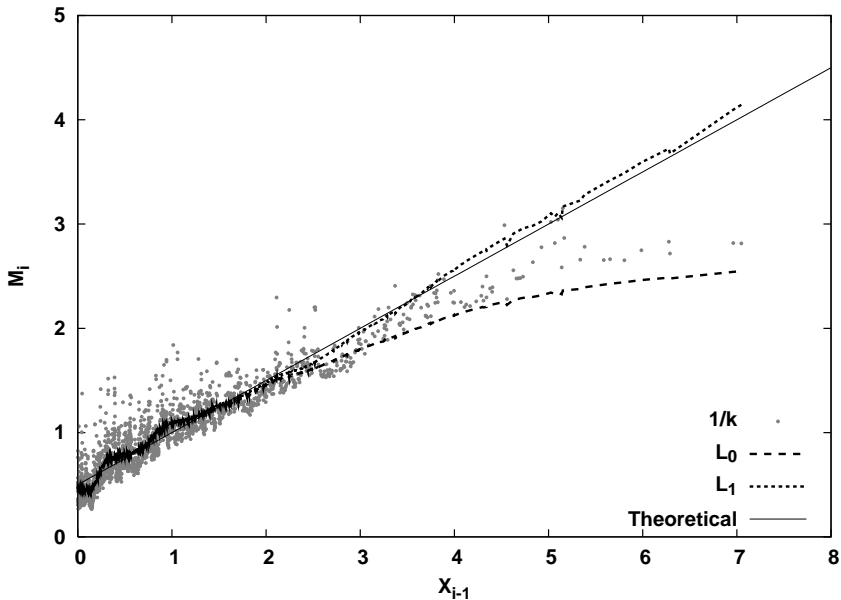

Figure 3.1: *Expected values $\widehat{M}_i$ versus the 'historical' predecessor X_{i-1} for the 2000 values from the exponential model, estimated as a weighted average with $^1\!/_{\mathbf{k}}$-weights and by the zeroth- and first-order LOESS smoother (L_0 and L_1) with $k_M = 400$. The straight line represents the theoretical value from Eqn. 3.14 with $\rho = 0.5$.*

simulated means $\widetilde{M}_j$. In the simulations with the lognormal data, the values hardly exceed the highest value in the data, irrespective of the choice of k_M. These simulations are also unable to reproduce the upper 0.5% of the distribution of M. For the exponential data in the upper right panel the tail of the distribution of X^* shows a better agreement with the theoretical distribution when k_M increases. This can solely be ascribed to the fact that in this case the reproduction of the distribution of M is improved by increasing k_M. The difference between the results for both models may be due to the long tail of the lognormal distribution.

For the simulations in Fig. 3.2 a relatively small value of k_e was used. The $(\widetilde{M}_j, e_j^*)$-pairs will then generally be close to those in the data. Increasing the value of k_e enhances the simulation of new combinations of M and e and therefore leads to higher simulated values, which is demonstrated in Fig. 3.3. For large k_e the upper tail of the simulated distribution approaches that of the underlying distribution. However, in the case of the exponential data the distribution for $k_e = 1600$ clearly overshoots the theoretical distribution. This effect should be ascribed to variance heterogeneity: if k_e is too large, the residuals associated with the set of k_e nearest neighbours can no longer be considered as identically distributed random variables, due to the dependence of the variance of e on M (Eqn. 3.15). The effect of variance heterogeneity becomes more pronounced if a uniform kernel is used instead of the $\mathbf{1/k}$-kernel.

From the foregoing results it is concluded that k_M should be chosen sufficiently large in order to avoid an underestimation of r_1 in the simulations. The value of k_e has a direct influence on the range of simulated values, in particular the highest value. To simulate values that are substantially larger than those in the data, k_e should be chosen sufficiently large. However, too large values of k_e should be avoided, because of possible dependence of the distribution of e on M, which causes the reproduction of the distribution to deteriorate. The optimum choice of these parameters depends on the characteristics of the underlying data.
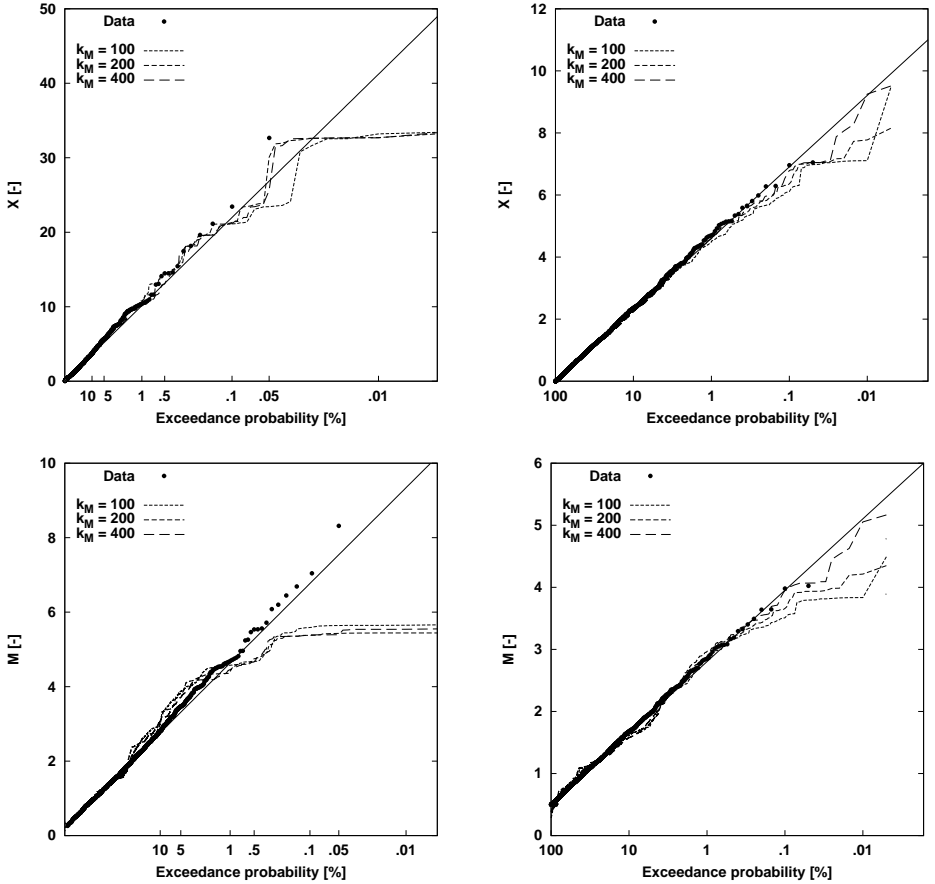
Figure 3.2: *Probability plots of resampled data X^* and simulated means $\widetilde{M}$ for different values of k_M and $k_e = 100$. The upper panels show the probability plots of the data (2000 values, dots) from the lognormal model (left) and the exponential model (right) and the series resampled from these data with method L_1 (20 000 values, curves). The lower panels display the corresponding probability plots of $\widetilde{M}$ and those of the empirical distributions (2000 values, dots) calculated from the data through Eqns 3.9 and 3.14 with $\rho = 0.5$. The straight lines represent the theoretical distributions of X in the upper panels and M in the lower panels.*
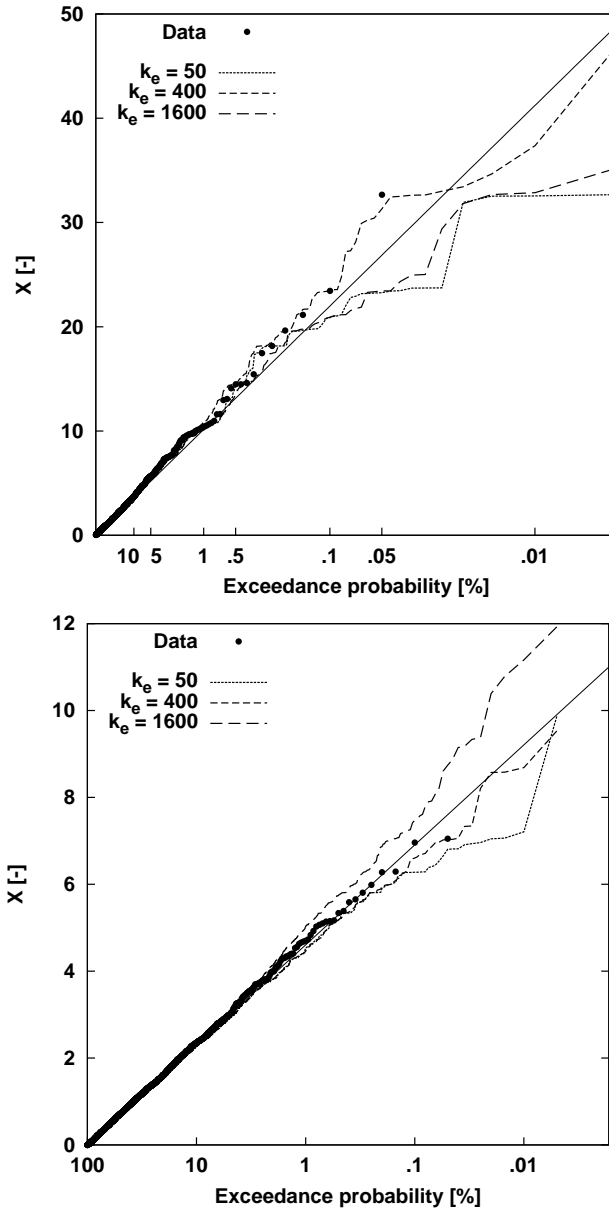
Figure 3.3: *Probability plots of the data (2000 values, dots) from the lognormal model (top) and the exponential model (bottom) and the values X^* resampled from these data with method L_1 (20 000 values, curves), using different values of k_e and $k_M = 400$. The straight lines represent the theoretical distributions of X.*

3.4 Simulation of precipitation and temperature for the Ourthe catchment

This section compares the performance of different resampling algorithms for the simulation of precipitation and temperature in the catchment of the river Ourthe upstream of Tabreux (1588 km^2), located in eastern Belgium (Ardennes) with altitudes varying between 200 and 650 meters above mean sea level. The Ourthe is an important tributary of the river Meuse (subbasin 12 in Fig. 2.1). Like most of the Belgian Ardennes, the catchment largely consists of steep terrain and a soil of hard, impermeable rock. The storage capacity of this area is therefore low and the response to precipitation relatively fast. Through its position close to the Netherlands border, the Ourthe catchment contributes significantly to the discharge of the river Meuse in the Netherlands during flood waves.

Daily areal average precipitation for this area (derived from station records by the Royal Meteorological Institute of Belgium by means of Thiessen interpolation) and daily temperature from the enclosed station St. Hubert for the 32-year period 1967-1998 were used. The average annual precipitation for this period amounts to 970 mm.

In Chapter 2 a nearest-neighbour resampling algorithm was used for the multi-site simulation of precipitation and temperature of the Meuse basin to assess the probability of flood extremes. The same resampling algorithm, from here on referred to as 'RG1', is also used in this chapter, with the modification that a five-day, instead of a four-day, memory was included in the feature vector and nearest-neighbours were searched within a moving window of 121 calendar days.

A method of simulating larger daily precipitation amounts than those observed was introduced by Buishand (2007). In that study, the two largest historical daily amounts in a 60-day season were replaced by a value sampled from a Generalized Pareto Distribution (GPD), whenever they occurred in the resampled sequence. The replacement values were conditioned to exceed the third largest historical value x_3 in the season. The same approach was followed here to perturb a sequence generated with RG1, except that the replacement values were sampled from an exponential distribution fitted to the ten largest historical amounts in the season of interest. Seasons were defined as bimonthly periods (January-February, March-April, etc.). The used exponential distribution is equivalent to Buishand's GPD with shape parameter $\theta = 0$. The choice of zero shape parameter was justified by a regional analysis of the daily precipitation from different catchments in the Meuse area (Appendix A.1). From here on, this way of perturbing resampled precipitation from RG1 is referred to as 'RG1p'.

The concept of nearest-neighbour regression discussed in Section 3.2 was implemented for the simulation of standardized precipitation and temperature (from here on referred

to as 'RG2'). For precipitation the multiplicative model, $X_{\mathrm{P}} = M_{\mathrm{P}} \, e_{\mathrm{P}}$, was used. The estimation of $M_{\mathrm{P}i}$ for day i was based on the zeroth-order LOESS smoother L_0 for $X_{\mathrm{P}i-1} < 2$ and on the first-order LOESS smoother L_1 otherwise. In the latter only the daily precipitation amounts for the nearest neighbours of day $i-1$ and their successors were considered. L_1 was used here in combination with L_0 because precipitation contains zeroes, in contrast with the data of the theoretical examples. Applying L_1 in cases where $X_{\mathrm{P}i-1}$ is small could then lead to a negative value of $M_{\mathrm{P}i}$. Besides, the linear regression in L_1 is primarily intended to achieve a better estimate of $M_{\mathrm{P}i}$ for large $X_{\mathrm{P}i-1}$. The standardized temperature was simulated additively, i.e. $X_{\mathrm{T}} = M_{\mathrm{T}} + e_{\mathrm{T}}$, where M_{T} was estimated with the zeroth-order LOESS smoother L_0. The nearest neighbours of the preceding day, needed to estimate M_{P} and M_{T}, were collected similarly to RG1. The residuals $e^{*}_{\mathrm{P}j}$ and $e^{*}_{\mathrm{T}j}$ for day j in the simulation correspond to the same historical day. In analogy to the algorithm described in Section 3.2, the selection of this day should be conditioned on $\widetilde{M}_{\mathrm{P}j}$ and $\widetilde{M}_{\mathrm{T}j}$. However, this resulted in an underestimation of the lag 1 autocorrelation r_1 of daily precipitation. In order to enhance the persistence of the simulated daily precipitation amounts, the last simulated residual $e^{*}_{\mathrm{P}j-1}$ and its five-day memory were also taken into account. At the end of each step, $X^{*}_{\mathrm{P}j}$ was evaluated as $\widetilde{M}_{\mathrm{P}j} \, e^{*}_{\mathrm{P}j}$ and the value of $X^{*}_{\mathrm{T}j}$ as $\widetilde{M}_{\mathrm{T}j} + e^{*}_{\mathrm{T}j}$. An important contrast between RG1 and RG2 is that in the latter there is no longer a one-to-one correspondence between the simulated values and historical dates.

To assess the sensitivity of RG2 to the neighbourhood sizes, several 320-year sequences of daily precipitation and temperature were simulated with different settings of k_M and k_e. For comparison, also a 320-year simulation was performed with RG1 and RG1p. Only the winter half-year (October-March) was considered, because most floods take place in that season. From all these simulations the mean, standard deviation s_d, lag 1 autocorrelation coefficient r_1 and maximum of the daily precipitation in the winter half-year were compared with those of the 32-year observed record. The results are listed in Table 3.3. For RG1 and RG1p the mean and s_d show an underestimation, whereas r_1 is close to that observed. There is little difference between both simulations, confirming that the mean, s_d and r_1 are not sensitive to the replacement of the largest values. In the simulations with RG2 the mean is better reproduced than in those with RG1 and RG1p, but most simulations slightly overestimate s_d and underestimate r_1. The latter is comparable to the underestimation of r_1 for the lognormal data in Table 3.2. In none of the simulations does the bias of the simulated mean exceed twice the standard error of the estimate from the historical record. However, in a few simulations the values of s_d and r_1 fall outside their $2 \times se$-intervals. In most of these cases either $k_M \leq 100$ or $k_e \geq 800$. The value of r_1 generally tends to increase with k_M, in line with the results for the theoretical models. In most RG2-simulations, the largest winter amount is notably larger than that observed.

Table 3.3: *Properties of the daily precipitation in the winter half-year (October-March) from 320-year simulations with RG1, RG1p and RG2, using various values of k_M and k_e, compared with those observed ($\pm 2 \times se$). The standard deviation s_d and the lag 1 autocorrelation coefficient r_1 and their standard errors se were estimated by means of the jackknife method of Buishand and Beersma (1993, 1996). Estimates for the simulations deviating more than 2×se from the historical value are printed in bold. In the last column the largest daily winter amount (Max) is listed.*

	k_M	k_e	Mean (mm)	s_d (mm)	r_1	Max (mm)
Obs.	-	-	2.79 ± 0.206	4.59 ± 0.144	0.375 ± 0.033	54.7
RG1	-	-	2.61	4.47	0.375	54.6
RG1p	-	-	2.61	4.48	0.373	66.8
RG2	50	200	2.78	**4.79**	**0.324**	136.5
	100	200	2.70	4.62	**0.330**	64.0
	200	200	2.68	4.62	0.346	62.3
	400	200	2.76	4.71	0.354	67.9
	800	200	2.73	4.69	0.364	62.4
	1600	200	2.76	4.70	0.372	60.1
	200	50	2.67	4.60	0.369	72.5
	200	100	2.72	4.71	0.354	61.5
	200	400	2.69	4.66	0.351	67.3
	200	800	2.77	**4.74**	**0.339**	60.7
	200	1600	2.93	**4.95**	**0.314**	64.3
	400	50	2.73	4.65	0.364	56.5
	400	100	2.71	4.56	0.363	68.5
	400	400	2.74	4.64	0.361	71.9
	400	800	2.76	4.70	0.362	65.3
	400	1600	2.79	**4.85**	**0.341**	76.7
	800	50	2.71	4.63	0.360	55.7
	800	100	2.79	**4.74**	0.365	55.4
	800	400	2.74	4.60	0.371	60.5
	800	800	2.76	**4.76**	0.354	54.8
	800	1600	2.72	**4.78**	0.346	69.4

The distributions of daily precipitation and temperature

With the algorithms RG1, RG1p and RG2 described above, simulations of 12 000 years were performed. For RG2 a value of 400 was selected for k_M and k_e, based on the performance in Table 3.3 and the experiments with the theoretical models. Setting $k_M{=}400$ leads to a satisfactory reproduction of the mean, s_d and r_1 of daily precipitation. Furthermore, it is assumed that $k_e = 400$ is sufficiently large to reasonably approximate the tail of the distribution, while avoiding effects of variance heterogeneity. Figure 3.4 compares the simulated distributions of the daily precipitation amounts in the winter half-year with the observed distribution. The simulations show a good agreement with the observations. The figure clearly shows the exponential tail of the distribution in the RG1p-simulation, extending beyond the historically largest amount which limits the values in the RG1-simulation. The plot of RG2 is found roughly in between the plots of RG1 and RG1p, which means that the two-stage resampling algorithm produces a distribution of daily precipitation with a shorter tail than the exponential distribution.

Figure 3.5 shows that the RG1- and RG2-simulations reproduce the distribution of the daily temperature in winter quite well. There is only a slight underestimation of the
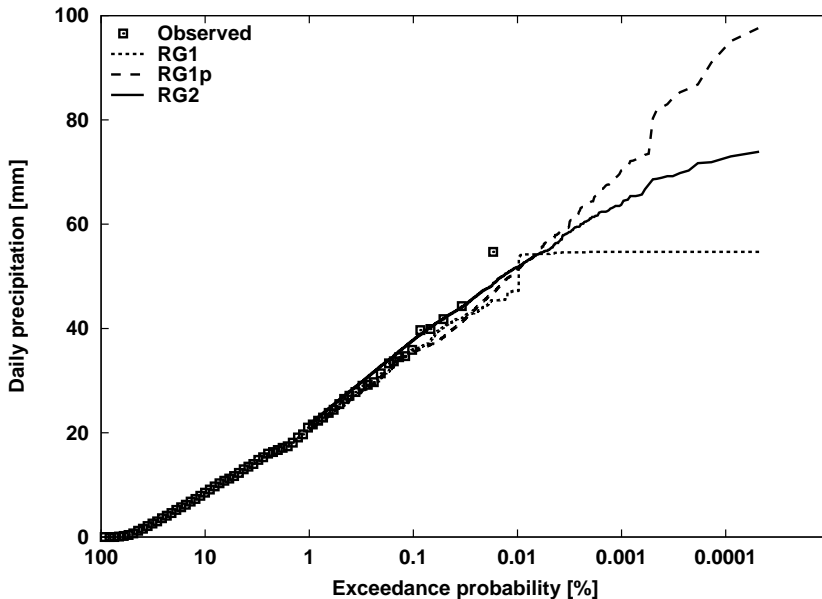

Figure 3.4: *Exponential probability plots of daily precipitation amounts in the winter half-year for the 12 000-year RG1-, RG1p- and RG2-simulations, compared with the plot of the observed daily precipitation.*

probability of very low temperatures. The highest simulated daily temperatures exceed the highest observed temperature. For the RG1-simulation this can be ascribed to two causes (Buishand and Brandsma, 2001). The values resampled for days in the winter half-year can originate from a historical date outside this season, due to the moving window. Furthermore, differences between the historical and simulated values can arise from the standardization and de-standardization.
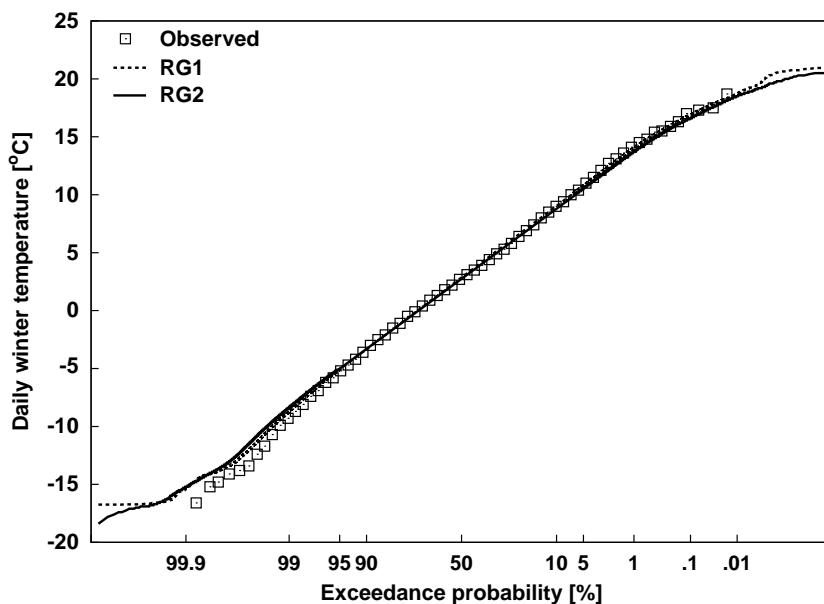

Figure 3.5: *Normal probability plots of the daily temperature in the winter half-year for the 12 000-year RG1- and RG2-simulations, compared with the plot of the observed daily temperature.*

The distribution of 4-day and 10-day precipitation maxima in winter

From the perspective of flood risks, the extremes of aggregated amounts of simulated precipitation in the winter half-year are of particular interest. The top panel of Fig. 3.6 compares the Gumbel plots of the 4-day precipitation maxima in the winter half-year for the different resampling algorithms. Up to a return period of 20 years the differences between the simulation methods are minor. The plots for RG1p and RG1 even coincide. For longer return periods, the plots diverge. The highest 4-day maxima are generated by RG2, followed by RG1p. For the Gumbel plots of the 10-day maxima, displayed in the bottom panel of Fig. 3.6, the differences between the three algorithms are negligible over the entire range of return periods. This is directly related to the exponential tail
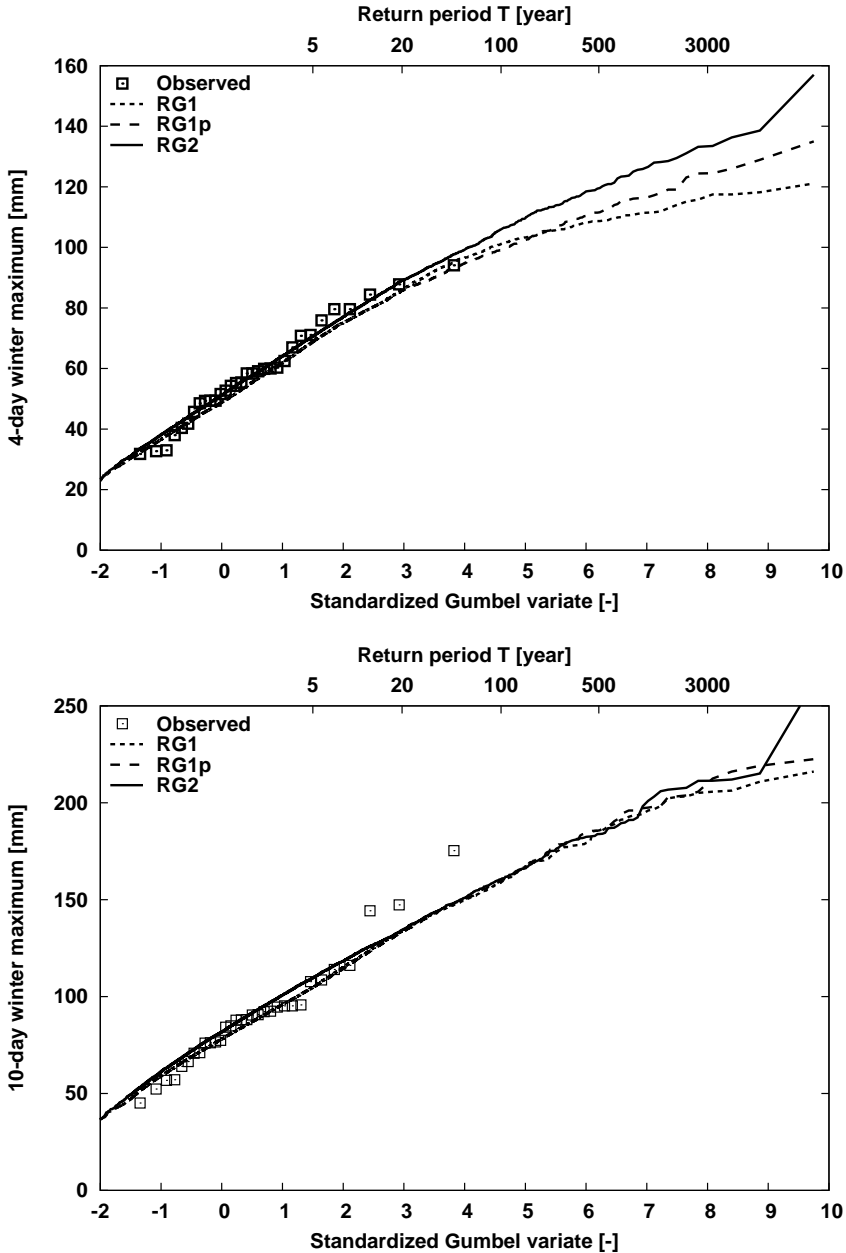
Figure 3.6: *Gumbel plots of the 4-day (top) and 10-day (bottom) precipitation maxima in the winter half-year for the 12 000-year RG1-, RG1p- and RG2-simulations, compared with those observed.*

of the distribution of daily precipitation in the winter half-year. For such a distribution extreme 10-day totals are mainly due to a cluster of moderately large daily amounts, rather than an isolated very large daily amount (Buishand, 2007). There is a good agreement between the Gumbel plots for the three resampling algorithms and the plot for the observed maxima. The main difference is that the three highest observed maxima are somewhat above the plots for the simulated data.

3.5 Extreme river discharges

To assess the effect of the different resampling algorithms on floods, the generated 12 000-year sequences of daily precipitation and temperature were used to drive the rainfall-runoff model HBV, already introduced in Section 2.4, for the river Ourthe at Tabreux in the same configuration and with the same model parameters.

Beside daily precipitation and temperature, the HBV model requires daily potential evapotranspiration (PET) values. These were derived from the daily temperature in the same way as in Chapter 2 (Eqn. 2.3), except that the proportionality constant α was de-
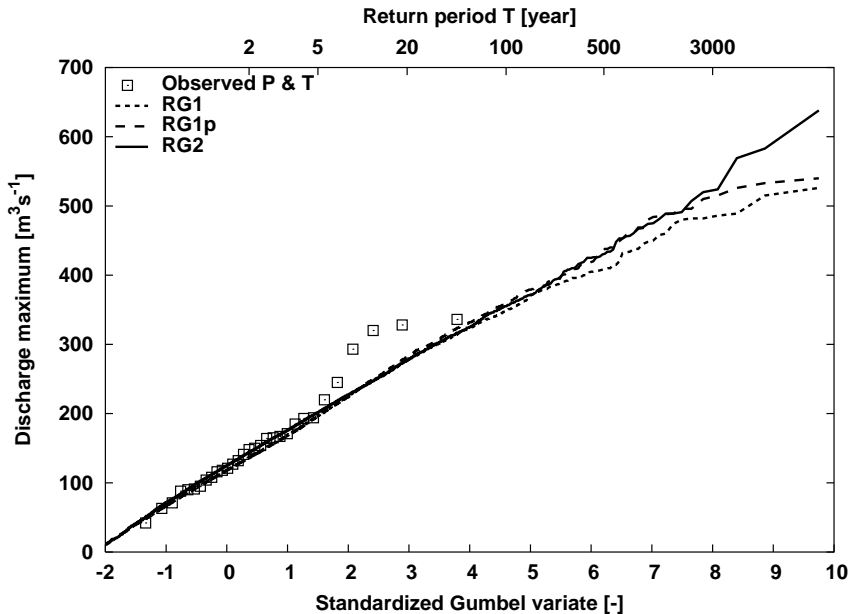

Figure 3.7: *Gumbel plots of the winter maxima of daily discharge for the river Ourthe at Tabreux from the 12 000-year RG1-, RG1p- and RG2-simulations compared with the plot based on observed daily precipitation and temperature.*

termined for each calendar month separately. This is explained in Section 4.4. From the simulated daily discharges the maxima of the winter half-years were extracted. Figure 3.7 compares the Gumbel plots of these maxima with the plot obtained by driving HBV with observed daily precipitation and temperature (and PET derived from these temperatures). The plots for the generated 12 000-year sequences show a good correspondence with the observed data. Up to a return period of about 200 years there is no distinction between the three simulations. For longer return periods the plot of RG1p and RG2 remain close together and are somewhat higher than that of RG1. This result points out that being able to simulating daily precipitation amounts beyond the observed range hardly influences the simulation of winter extremes of daily discharge for a tributary of the river Meuse, such as the river Ourthe.

3.6   Conclusion and discussion

A two-stage nearest-neighbour algorithm (RG2) is explored that allows for the simulation of daily precipitation amounts and temperatures beyond the range of observed values. The simulation of a new daily value in this algorithm proceeds by the subsequent estimation of the value that is expected to follow the preceding simulated values, and resampling a residual associated with one of the historical observations. Different implementations of this algorithm were tested on data from two AR1 processes. The best results were achieved with an algorithm which estimates the expected value by means of a local linear regression (first-order LOESS smoother). The influence of the neighbourhood size for the determination of the expected values, k_M, and that for the sampling of the residuals, k_e, was studied in detail. It was found that k_M should be chosen sufficiently large in order to achieve a satisfactory reproduction of the lag 1 autocorrelation. Furthermore, a small value of k_e limits the potential to simulate larger values than observed. On the other hand, a very large value of k_e may worsen the distribution of the simulated values due to variance heterogeneity.

The two-stage algorithm was further used to resample historical sequences of daily precipitation and temperature for the Ourthe catchment. Though an underestimation of the lag 1 autocorrelation and a slight overestimation of the standard deviation are found for most settings of the neighbourhood sizes, the bias was only significant in a few cases associated with a high value of k_e or a small value of k_M. With a suitable choice of k_M and k_e, a 12 000-year simulation was conducted with RG2. For comparison an additional simulation of the same length was conducted with the conventional single-stage algorithm RG1. A modified version RG1p of this simulation was created by perturbing the highest resampled values in each bimonthly season, in such a way that the distribution of the daily precipitation amounts was extended with an exponential tail. For all three simulations the distributions of the 4-day and 10-day winter maxima were in agreement with the observed data. At return periods longer than 100 years differences were seen between the Gumbel plots of the 4-day maxima, showing the influence of the

larger daily amounts. The plots of the 10-day maxima, however, barely differ. The simulated data were used to drive the HBV rainfall-runoff model for the Ourthe catchment. It was found that the larger daily precipitation amounts produced by RG1p and RG2 had no discernible effect on the distribution of the winter maxima of daily discharge.

A disadvantage of RG2 is that it is a very time-consuming algorithm, because a large number of nearest neighbours have to be sorted twice. A great saving in computer time can be achieved by using the same nearest neighbours for the estimation of the expected value and the resampling of residuals as in Prairie et al. (2006). However, for the Ourthe data this leads to a substantial positive bias in the standard deviation and a negative bias in the autocorrelation. A possible explanation is that conditioning on the expected precipitation and temperature of the new day yields a more homogeneous set of residuals than conditioning on the characteristics of the previously simulated day.

The RG1 algorithm has been extended to perform multi-site simulations (Buishand and Brandsma, 2001). A similar extension is possible for the RG2 algorithm. There is no need to generate from a multivariate normal distribution as in multi-site versions of the nonparametric weather generator based on kernel-density estimation techniques (Mehrotra and Sharma, 2006a, 2006b and 2007), which involves quite strong assumptions on the spatial dependence structure. A multi-site extension of the RG1p algorithm would also rely on assumptions on spatial dependence and is not straightforward. The extension of RG2 to multi-site generation is less complicated and requires less assumptions about the data.

Resampling of regional climate model output

Abstract

The objective of this chapter is to investigate whether resampling of the output from a regional climate model (RCM) can provide realistic long-duration sequences of precipitation and temperature for the simulation of extreme river flows. Resampling of RCM data is potentially be usefull to assess the impact of climate change on river flooding. Daily streamflows of the river Meuse in western Europe are considered. Resampling is performed with the nearest-neighbour algorithm that was applied to observed daily precipitation and temperature of the Meuse basin (Section 2.2). The HBV rainfall-runoff model of Chapter 2 was used to simulate streamflows. Two model runs of the KNMI regional climate model RACMO are considered. One of these model runs is driven by the global atmospheric model HadAM3H of the UK Meteorological Office for the period 1961-1990 and the other by ERA40 reanalysis data. Much attention is given to the bias correction of RCM precipitation. It is found that a relatively simple nonlinear correction adjusting both the biases in the mean and variability leads to a better reproduction of observed extreme daily and multi-day precipitation amounts than the commonly used linear scaling correction. This also results in more realistic discharge extremes, suggesting that a correct representation of the variability of precipitation is important for the simulation of extreme flood quantiles. For the Meuse basin it is further shown that it is advantageous to correct for the variability of the 10-day precipitation amounts rather than that of the daily amounts. Despite the remaining biases in the RCM data, the simulated extreme flood quantiles correspond quite well with those obtained using observed precipitation and temperature.

4.1   Introduction

General Circulation Models (GCMs) are considered to be the most advanced tools currently available for simulating the response of the global climate system to changing atmospheric composition (Mearns et al., 2001). There is a great interest in the impact of the climate changes projected by these models on river flooding (e.g. Prudhomme et al., 2002). It is well known that the magnitude of the climate-change impact depends partly on the characteristics of the river basin (e.g. Arnell and Reynard, 1996; Nijssen et al., 2001). Streamflow simulations are therefore needed to assess this impact. However, the precipitation produced by GCMs is generally not suitable to feed into hydrological models, partly because of the coarse spatial resolution of GCMs. A downscaling procedure is therefore needed to provide the required input. One approach is to use a high-resolution Regional Climate Model (RCM), driven by lateral boundary conditions from the GCM of interest. The popularity of this approach is growing, due to increased computer resources and the enhanced performance of RCMs and processing. Recent applications are presented by Kay et al. (2006a,b), who used a high-resolution RCM to assess changes in flood frequency for 15 catchments in the UK, and Lenderink et al. (2007), who investigated future discharges of the river Rhine.

A problem with the use of RCMs for hydrological purposes is that the simulated precipitation differs systematically from the observed precipitation (e.g. Frei et al., 2003). Lenderink et al. (2007) corrected for this bias by applying a (seasonally and spatially varying) correction factor, while Hay et al. (2002) made use of the gamma distribution to match the distribution of the modelled daily precipitation with that of observed daily precipitation. Arnell et al. (2003), on the other hand, did not use any bias correction.

Apart from the bias in the simulated precipitation, the estimation of flood quantiles suffers from the limited length of the RCM simulations (usually no longer than 30 years for present-day models). A strong extrapolation of the distribution of the simulated discharges is then needed to estimate the extreme flood quantiles if the hydrological model is run directly with the (bias-corrected) RCM output.

In this chapter both problems are tackled for the basin of the river Meuse upstream of Borgharen in the Netherlands (see Subsection 2.2.2). The weather generator of Chapter 2 is applied to RCM output instead of observed data. After bias correction the resampled data are used for streamflow simulations using the HBV rainfall-runoff model. The objective is to establish whether the use of RCM output in a hydrological model can yield extreme discharges (with return periods typically in the order of 1000 years) which are comparable to those based on observed meteorological data.

The remainder of the chapter is organized as follows. The use of RCM output and the applied bias corrections are discussed in Section 4.2. In Section 4.3 the resampling algorithm is briefly explained. Furthermore, the autocorrelation of daily precipitation

and the distribution of 10-day winter maxima of basin-average precipitation from the resampled sequences are presented. In Section 4.4 the hydrological simulations are described and results of extreme discharges are shown. Section 4.5 closes the chapter with a summary and a short discussion on the usefulness of the presented approach.

4.2 RCM output for the Meuse basin

4.2.1 The KNMI model RACMO

In this study the output of the KNMI regional climate model RACMO (Regional Atmospheric Climate MOdel) was used (Lenderink et al., 2003). This model has a resolution of about 50 km. Its domain roughly stretches from 40^oW to 50^oE and from 30^oN to 70^oN. The Meuse basin is located in the center of the domain and is almost covered by 15 grid boxes, as shown in Fig. 4.1. For the hydrological simulations described in Section 4.4, the Meuse basin is subdivided into 15 subbasins. The modelled area-average precipitation for each of the subbasins was obtained as a weighted average over the grid boxes covering the subbasin. The weights were determined as the fraction of the subbasin area falling within a specific grid box, using a 2.5km grid. The nearest grid box was assigned to those parts of the basin that were not covered by the 15 grid boxes.

Two multi-year RACMO runs were made available. In the framework of the EU-funded project PRUDENCE (Prediction of Regional scenarios and Uncertainties for Defining EuropeaN Climate change risks and Effects, see e.g. Christensen and Christensen, 2007), RACMO was driven by lateral boundaries from the atmospheric model HadAM3H of the Hadley Centre of the UK Meteorological Office. HadAM3H (short for Hadley Centre Atmospheric Model 3, High resolution) is operated at a resolution of 1.25^o in latitude and 1.875^o in longitude, corresponding to grid cells of about 150 km near the RACMO domain. For the control run of this configuration (reference period 1961-1990) the observed sea surface temperature and sea ice are used (Jones et al., 2001). This model run will from here be referred to as RACMO-HCCTL. The second RACMO run, from here denoted as RACMO-ERA40, was driven by 40 years of reanalysis data (ERA40) of the European Centre for Medium-Range Weather Forecasting (Uppala et al., 2005). A reanalysis is an estimate of the state of the atmosphere, based on observations and a numerical weather forecast. Its circulation is therefore expected to be more realistic than that of any GCM. Hence, the comparison between a GCM-driven RCM run and one driven by reanalysis data provides insight into the influence of the driving GCM on the considered RCM run. The forecast model used for the reanalysis is operated at a resolution of about 125 km. RACMO uses data from either the driving GCM (HadAM3H) or the reanalysis to set the boundary conditions of the horizontal velocity, heat and moisture (on all vertical levels) and the sea-level pressure. Details on the RACMO model can be found in Lenderink et al. (2003).

From the RACMO-ERA40 run the data for the 30-year period 1969-1998 were extracted in order to have two runs of the same length. The period 1969-1998 was preferred to 1961-1990, because streamflow simulations with observed data were available for that period (see Section 2.2). With the simulation driven by ERA40 boundaries it is possible to discriminate between the bias resulting from the driving HadAM3H GCM and the bias introduced by RACMO. For each of the subbasins the interpolated area-average precipitation was compared with the corresponding subbasin precipitation for the historical reference period 1969-1998 from the records used in Chapter 2.

The left panel of Fig. 4.2 shows an area-weighted average of the relative bias of the mean daily precipitation amount in each calendar month. The largest biases are found in the winter half-year (October-March), on average 26% in RACMO-HCCTL and 16% in the RACMO-ERA40. Except for a few months, RACMO-HCCTL shows a larger bias than
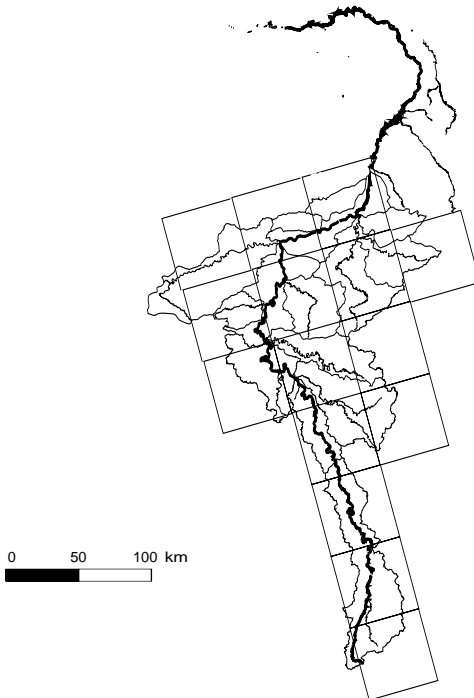

Figure 4.1: *Locations of the 15 RACMO grid boxes used in this study, relative to the Meuse subbasins (thick grey contours) and the river Meuse with tributaries. State boundaries (dashed) and the location of the gauging station Borgharen are also shown.*

RACMO-ERA40 The relative bias of the former is comparable with that found for the regional climate models HadRM2 (Shabalova et al., 2003) and HadRM3H (Lenderink et al., 2007) of the Hadley Centre for the adjacent Rhine basin. The wet bias is partly a result of the fact that the observed precipitation amounts were not corrected for the systematic undercatch inherent to rain gauges. Frei et al. (2003) report a systematic undercatch of about 8% for the lowland stations in the Alps (below 600 m). For the Meuse basin (almost entirely below 600 m), the undercatch may differ somewhat from this value, due to climatological differences and other types of rain gauges. It is unlikely that all precipitation biases found here are due to undercatch.

The right panel of Fig. 4.2 presents the basin-average temperature bias. This bias refers to the difference between the area-weighted average T_{area} of the subbasin temperatures obtained from RACMO and the Thiessen average T_{stns} of 11 stations, serving as a reference temperature. The bias in RACMO-HCCTL is similar to that in RACMO-ERA40, except for October, which is colder and the period December-February, which is warmer than in RACMO-ERA40.

Van Ulden et al. (2007) analyzed the circulation bias of HadAM3H for Europe. They report a positive bias in the strength of the westerlies in winter, leading to a wetter and milder climate. This is consistent with the relatively large positive bias in precipitation and temperature in RACMO-HCCTL during winter.

Table 4.1 compares several characteristics of daily precipitation from both RACMO runs with those of the observed precipitation. Results are presented for the winter half-year as well as the summer half-year (April-September). The coefficient of variation (CV)
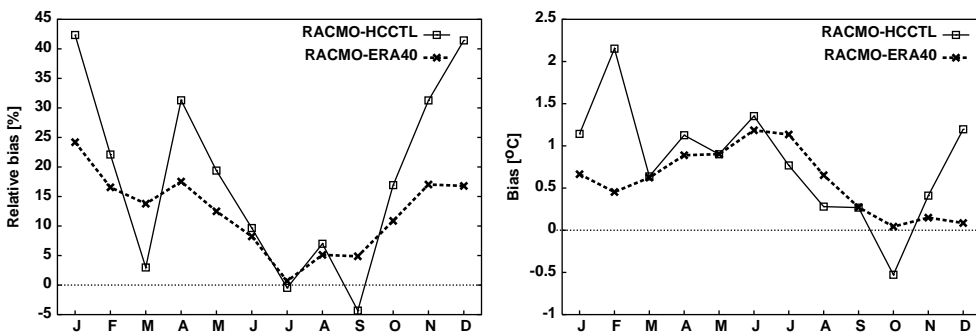

Figure 4.2: *Basin-average relative bias in the monthly precipitation (left) and the absolute bias in the mean monthly temperature (right). The data from RACMO-HCCTL for the period 1961-1990 and RACMO-ERA40 for the period 1969-1998 are compared with the observations for the period 1969-1998.*

Table 4.1: *Mean, Coefficient of Variation (CV) and lag 1 autocorrelation coefficient r_1 of daily precipitation, fraction f_{wet} of wet days (with 0.3 mm or more) and mean wet-day amount m_{wet}. These statistics are area-weighted averages over subbasins. The last row contains the mean correlation r_s between the daily precipitation amounts in different subbasins (averaged over all pairs of subbasins) for the observations and both RACMO runs. Results are given for the winter half-year (October-March) as well as the summer half-year (April-September).*

	Winter half-year			Summer half-year		
	Obs.	HadAM3H	ERA40	Obs.	HadAM3H	ERA40
Mean (mm/day)	2.78	3.49	3.20	2.40	2.64	2.59
CV	1.73	1.48	1.46	1.81	1.69	1.79
r_1	0.37	0.35	0.34	0.27	0.25	0.24
f_{wet} (%)	55.79	67.91	68.34	50.28	57.13	56.13
m_{wet} (mm/day)	4.94	5.10	4.65	4.75	4.58	4.57
r_s	0.85	0.90	0.90	0.73	0.81	0.82

displayed in this table is defined as the ratio between the sample standard deviation and the sample mean. Both RACMO runs show a considerable underestimation of the CV of the daily precipitation amounts in the winter half-year. The overestimation of the mean daily precipitation in winter is accompanied by an overestimation of the fraction of wet days in both the RACMO-HCCTL and RACMO-ERA40, whereas the mean wet-day amount is rather well preserved. There are also too many wet days in the summer half-year in both RACMO simulations. In the RACMO-HCCTL run the lag 1 autocorrelation coefficient r_1 of daily precipitation is slightly underestimated in both seasons. The bias in r_1 is even somewhat larger in RACMO-ERA40. This bias is mainly due to the inability of RACMO to reproduce the relatively large values of r_1 for the French part of the basin ($r_1 = 0.40$ in the winter half-year, compared to $r_1 = 0.35$ for the Belgian part in the winter half-year). The correlation r_s between the precipitation amounts in different subbasins is higher than observed in both runs, in the summer as well as the winter half-year. The differences between the HadAM3H-driven and ERA40-driven runs are small, suggesting that the bias is mainly an artefact of RACMO.

4.2.2   Bias correction

Because the bias in precipitation and temperature was found to vary spatially, bias corrections were carried out for each subbasin individually. For precipitation a simple linear correction using a scaling factor was compared with a slightly more advanced nonlinear correction. To reduce the effect of sampling variability, the scaling factor was determined for every five-day period of the year as the ratio between the average observed precipitation and that of the RACMO run in a window including the 30 days before and

after the considered five-day period.

The linear correction adjusts the mean precipitation, but leaves the CV unaffected, because both mean and standard deviation are multiplied by the same factor. As an alternative, a power transformation was studied, which corrects the CV as well as the mean. In this nonlinear correction each daily precipitation amount P is transformed into a corrected amount P^* using

$$P^* = a\, P^b \,. \tag{4.1}$$

Shabalova et al. (2003) used this expression to modify observed 10-day precipitation amounts in order to obtain a scenario of a future climate with a changed mean and CV. For the estimation of the parameters a and b they assumed that these 10-day precipitation amounts have a Weibull distribution. For the daily precipitation amounts in the Meuse basin this assumption is too restrictive. The parameters a and b were therefore obtained with a distribution-free approach. As in the case of the linear scaling factor, these parameters were estimated for each five-day period, using the same 65-day window. First, the value of b was determined such that the CV of the corrected daily precipitation matched that of the observed daily precipitation. This was done iteratively, using a root-finding algorithm. The factor a was then determined such that the mean of the transformed daily values corresponded with the observed mean. The resulting value of a depends on b. By contrast b depends only on the CV and its determination is independent of the value of a. The left panel of Fig. 4.3 displays the annual cycle of the exponent b for both RACMO runs.

A value greater than unity indicates that the CV of the precipitation is enhanced by the correction. In RACMO-HCCTL this is the case throughout the year. In RACMO-ERA40 the correction reduces the CV in the months June, July and August. The correspondence between the two curves suggests that the bias in the CV originates from RACMO itself rather than the driving GCM.

Alternatively, a and b can be chosen such that two different quantiles Q_{p1} and Q_{p2} of the corrected precipitation match those of the observations. Since the transformation in Eqn. 4.1 is monotone, the quantiles of the transformed daily precipitation amounts are simply obtained by applying the same transformation to the quantiles $Q_{p1,\mathrm{RCM}}$ and $Q_{p2,\mathrm{RCM}}$ of the uncorrected daily precipitation amounts from RACMO. From the requirement that

$$a Q_{p1,\mathrm{RCM}}^b = Q_{p1,\mathrm{OBS}} \qquad \text{and} \qquad a Q_{p2,\mathrm{RCM}}^b = Q_{p2,\mathrm{OBS}} \,, \tag{4.2}$$

where $Q_{p1,\mathrm{OBS}}$ and $Q_{p2,\mathrm{OBS}}$ are the corresponding observed quantiles, it follows by elimination of a and taking logarithms that

$$b = \frac{\log\left(Q_{p2,\mathrm{OBS}}/Q_{p1,\mathrm{OBS}}\right)}{\log\left(Q_{p2,\mathrm{RCM}}/Q_{p1,\mathrm{RCM}}\right)} \,. \tag{4.3}$$

For RACMO-HCCTL the values of b obtained from Eqn. 4.3 with $p1 = 65$, $p2 = 99$ or $p1 = 65$, $p2 = 95$ are compared with those fitted on the CV. The 65% quantile roughly

corresponds with the mean daily precipitation amount. The results are shown in the right panel of Fig. 4.3. The curve based on Q_{65} and Q_{99} closely follows that based on the CV, except for small deviations in summer. Taking Q_{95}, instead of Q_{99}, results in slightly larger values of b. In order to cope with bias in the variability of multi-day amounts, the use of the CV is preferred to determine the parameter b in Eqn. 4.1.

Figure 4.4 shows the basin-averaged exponential probability plots of daily precipitation for the winter half-year for both RACMO runs. The plots clearly illustrate the effect of both corrections. After applying the linear bias correction to the RACMO precipitation, the intermediate quantiles (exceedance probabilities > 0.1) agree better with the observed quantiles, but the more extreme quantiles (exceedance probabilities < 0.1) are too low and actually worse than those for the uncorrected data. This is consistent with the underestimation of the CV. With the nonlinear correction it is possible to adjust both the intermediate and the more extreme quantiles of the distribution, while keeping the number of parameters in the correction formula at a minimum. For the summer half-year, the effect of the nonlinear correction is smaller (not shown), because the bias in the CV is smaller in this season, as shown in Table 4.1.

Though the distribution of the nonlinearly corrected daily precipitation amounts resembles that of the observations quite satisfactorily, this is not necessarily true for the distribution of the multi-day precipitation amounts. Large multi-day events can be more important for the generation of floods than an extreme daily event. Extreme flows in the lower part of the Meuse basin are often associated with large multi-day precipitation totals in winter over periods of about 10 days, rather than extreme daily events
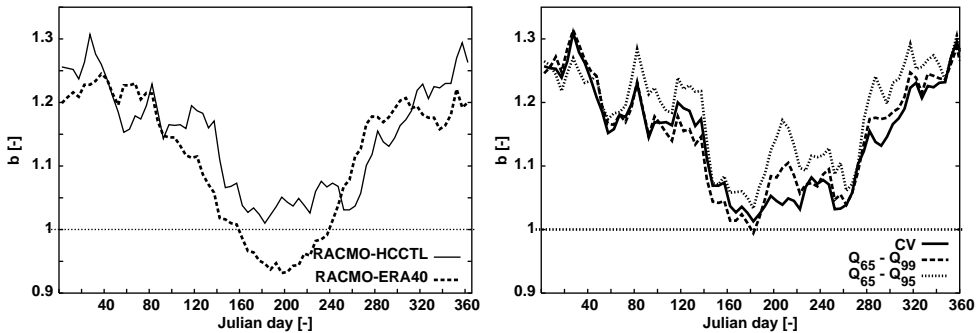

Figure 4.3: *Annual cycle of the area-averaged exponent b in Eqn. 4.1. On the left the exponents derived for RACMO-HCCTL and RACMO-ERA40 are shown. On the right the values of b based on the CV and those based on two different pairs of quantiles: $Q_{65} - Q_{99}$ and $Q_{65} - Q_{95}$ are given for RACMO-HCCTL.*

(Tu, 2006). Fig. 4.5 is similar to Fig 4.4, but now for the (non-overlapping) 10-day precipitation amounts. For RACMO-HCCTL the nonlinear correction leads to a better agreement with the observations than the linear correction. The same is found for RACMO-ERA40, but the larger quantiles of the distribution of the 10-day precipitation amounts (exceedance probabilities < 0.1) are still somewhat underestimated. This is partly due to an additional negative bias in the autocorrelation of the daily values, resulting from the nonlinear transformation of the data. The autocorrelation generally decreases if a value of $b > 1$ is needed to increase the CV, as is demonstrated in Section 3
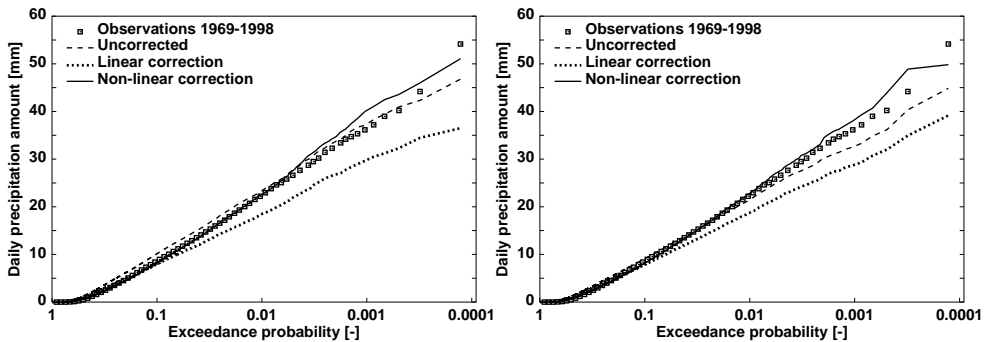
Figure 4.4: *Exponential probability plots of the daily precipitation in the winter half-year, averaged over individual subbasins for RACMO-HCCTL (left) and RACMO-ERA40 (right). The plots for the uncorrected, linearly-corrected and nonlinearly corrected precipitation are compared to the plot for the observed precipitation.*
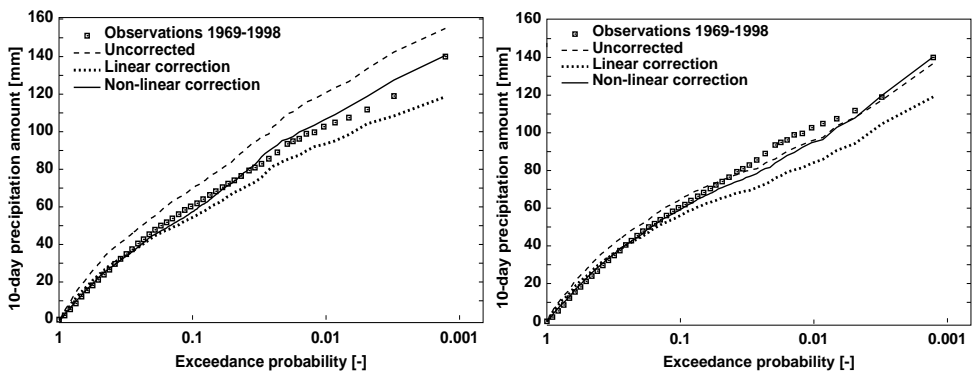

Figure 4.5: *Similar to Fig. 4.4, but now for the (non-overlapping) 10-day precipitation amounts.*

of this chapter. This decrease of the autocorrelation leads to a decrease of the standard deviation of the multi-day precipitation amounts, resulting in an underestimation of the large quantiles of these amounts. The most obvious and least complicated solution to this problem is to 'overcompensate', i.e. to use a larger value of b, such that the CV of the n-day totals, CV_n, of the transformed RACMO precipitation equals that of the n-day totals of the observations for some $n > 1$.

In Fig. 4.6 the observed values of CV_n for $n \leq 15$ are compared to those of uncorrected and corrected RACMO data for two different nonlinear corrections, one based on CV_1 and one based on CV_{10}. For the uncorrected RACMO data all CV_n are underestimated. With a nonlinear correction based on CV_1, the multi-day CVs improve, but they are still too low, in particular for RACMO-ERA40. With a nonlinear correction based on CV_{10} the underestimation of the multi-day CVs disappears, at the cost of an overestimation of CV_1 and CV_2.
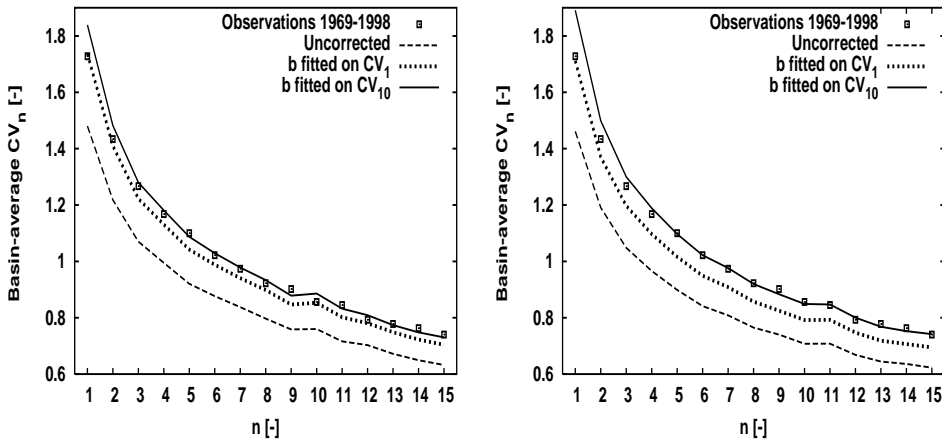

Figure 4.6:　*Basin-average coefficient of variation of n-day precipitation amounts CV_n for RACMO-HCCTL (left) and RACMO-ERA40 (right) for the winter half-year. The uncorrected runs and the nonlinearly corrected runs based on CV_1 and CV_{10} are compared with the observations.*
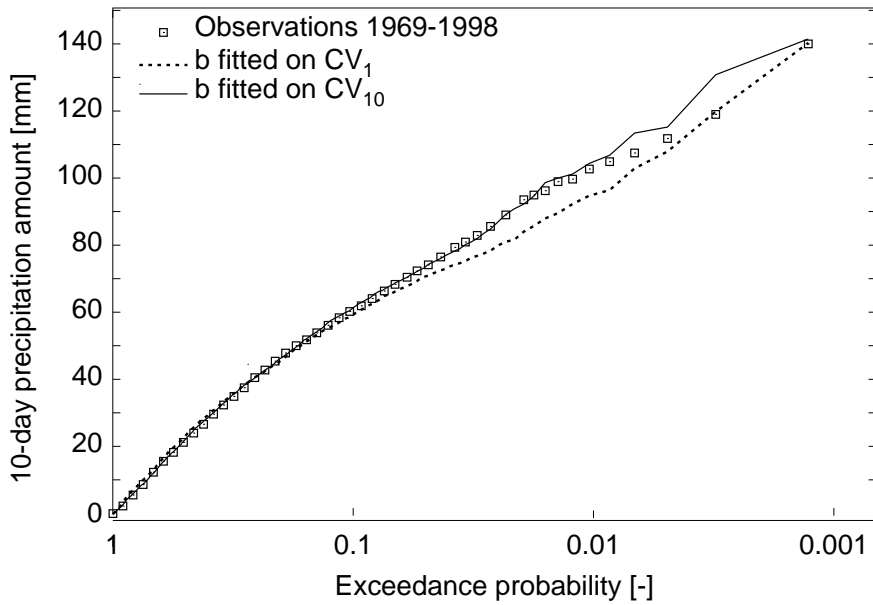
Figure 4.7: *Exponential probability plots of the 10-day precipitation amounts in the winter half-year for RACMO-ERA40, after a nonlinear correction of the daily precipitation amounts with b fitted on CV_1 and CV_{10} respectively.*

Figure 4.7 shows how the exponential probability plot of the 10-day precipitation amounts of RACMO-ERA40 changes due to fitting b on CV_{10} instead of CV_1. The correction based on CV_{10} results in a better correspondence with the observed 10-day precipitation amounts, due to a slightly larger value of b in the correction.

The bias correction of temperature is more straightforward than that of precipitation, involving shifting and scaling to adjust the mean and variance respectively. For each subbasin, the corrected daily temperature T^* is obtained as

$$T^* = \overline{T} + \frac{\sigma\left(T_{\text{stns}}\right)}{\sigma\left(T_{\text{area}}\right)}\left(T - \overline{T}\right) + \left(\overline{T}_{\text{stns}} - \overline{T}_{\text{area}}\right) , \qquad (4.4)$$

where T is the uncorrected daily temperature from RACMO, T_{stns} is the Thiessen average for the basin of observed temperatures from 11 stations, and T_{area} is the corresponding basin-average temperature obtained from RACMO. In this equation an overbar denotes the 30-year average and σ the standard deviation. Both statistics were determined for each 5-day period of the year separately, using the same 65-day window as for the bias correction of daily precipitation. A similar transformation was used by Shabalova et al. (2003) to perturb observed temperature with the changes of the mean and standard deviation projected by an RCM scenario run. Note that the temperature anomalies were scaled by the same factor for all subbasins and the temperature means were shifted by the same offset. The annual cycle of the scaling factor is shown in Fig. 4.8. The deviation from unity is within 0.15 for RACMO-HCCTL and nearly always less than 0.05 for RACMO-ERA40. Roughly the same factors were obtained for individual grid boxes containing one or more temperature stations.

4.3   Resampling of RCM output

In Chapter 2 nearest-neighbour resampling was based on station data. In this study resampling was driven by the uncorrected RACMO subbasin data instead. Furthermore, a five-day memory and a moving window of 121 days were used, instead of a four-day memory and a 61-day moving window in order to improve the simulation of extreme multi-day precipitation amounts. The bias corrections described in Section 4.2 were applied afterwards to the resampled 3000-year sequences.

It was shown in Chapter 2 that the resampling algorithm described above preserves the autocorrelation of its base material quite well. However, Table 4.1 shows that RACMO tends to underestimate the lag 1 autocorrelation of daily precipitation and a nonlinear bias correction influences the autocorrelation. Fig. 4.9 compares the basin-average autocorrelation coefficients of corrected and uncorrected resampled precipitation for both RACMO runs with those observed for the winter half-year. For the observations also the standard errors *se* were calculated, using the jackknife method of Buishand and
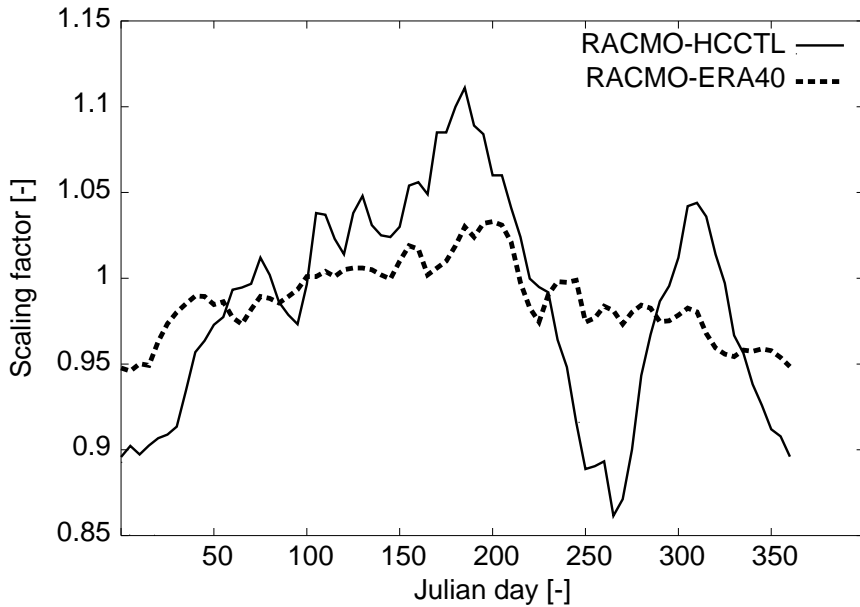
Figure 4.8: *Annual cycle of the scaling factors applied to correct the standard deviation of the daily temperature from RACMO-HCCTL and RACMO-ERA40 respectively.*
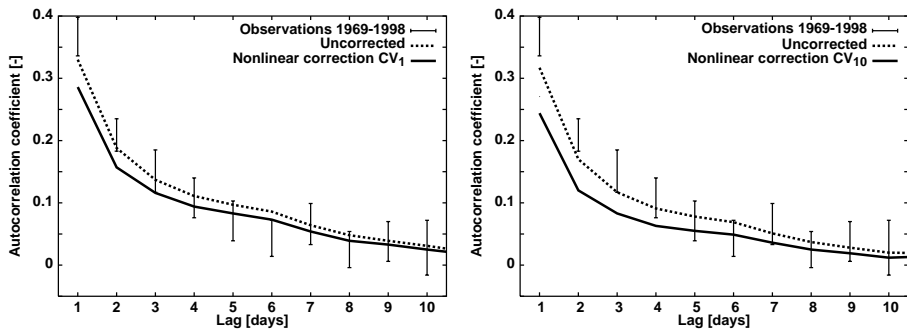

Figure 4.9: *The basin-average autocorrelation coefficients of the observed daily precipitation, the 3000-year resampled RACMO-HCCTL run (left) and the RACMO-ERA40 run (right) for the winter half-year, before and after the nonlinear correction. The autocorrelation coefficients of the observations are represented by error bars, which indicate the $2 \times se$-intervals of the coefficients.*
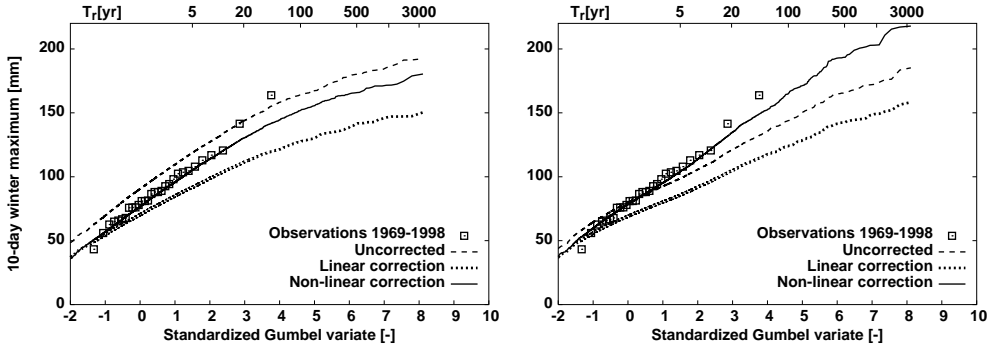
Figure 4.10:   *Winter maxima of basin-average 10-day precipitation amounts from re-sampled RCM data (9000 years), either uncorrected or after applying a linear correction or a nonlinear correction, compared with observed precipitation. The exponent b of the nonlinear correction was based on CV_1 for RACMO-HCCTL in the left panel and on CV_{10} for RACMO-ERA40 in the right panel. The upper horizontal axes indicate the mean recurrence time T_r (return period) in years.*

Beersma (1993). Apart from a significant negative bias in the lag 1 autocorrelation, the uncorrected resampled data from RACMO-HCCTL reproduce the autocorrelation coefficients quite well. The transformation in Eqn. 4.1, however, results in a decrease of the autocorrelation coefficients, in particular for shorter time lags in the winter half-year. The resampled data from RACMO-ERA40 show a larger bias in the autocorrelation coefficients than those from RACMO-HCCTL. Transformation based on CV_{10} leads to a further decrease of the autocorrelation coefficients. The effect of this decrease on the variability of the 10-day precipitation amounts is compensated by an overestimation of CV_1. The nonlinear correction also leads to a slight decrease of the spatial correlation r_s of the daily precipitation amounts (not shown). The spatial correlation of the nonlinearly corrected sequences remains, however, too high. This bias has little effect on the simulated floods for the Meuse, because these are more sensitive to the spatial correlation of the 10-day precipitation amounts. The latter is better reproduced by RACMO than r_s.

In Fig. 4.10 the 10-day winter maxima of basin-average precipitation from observations and those from the resampled 3000-year sequences for both RACMO runs are shown. Each plot displays the average ordered maxima of three independent sequences of 3000 years. The plot for the nonlinearly corrected data corresponds quite well with that of the observations. A linear correction appears to be worse than no correction at all.

4.4 Rainfall-runoff simulations

For the simulation of streamflow, the HBV rainfall-runoff model of Chapter 2 was used with the same schematization and parameters. For temperature areal averages of the subbasins were used instead of station data. Daily values of potential evapotranspiration (PET) for the Belgian subbasins were made available by RMIB. Since similar PET values for the French subbasins were not available, the average over the Belgian part of the basin was used for these subbasins. In the hydrological simulations with RACMO output, PET was derived for each of the subbasins from the daily temperature T using the relation:

$$\text{PET} = [1 + \alpha_m(T - \overline{T}_m)]\,\overline{\text{PET}}_m \tag{4.5}$$

with $\overline{T}_m$ the mean observed temperature (^{o}C) and $\overline{\text{PET}}_m$ the mean observed PET (mm day^{-1}) for calendar month m in the period 1967-1998. $\overline{T}_m$ was obtained from the average of the four nearest stations to the subbasin of interest using an altitude correction of -0.6^oC per 100 m. In the simulation with bias-corrected (resampled) RACMO output, the bias-corrected (resampled) temperature T^* was used for T in Eqn. 4.5. The proportionality constant α_m was determined for each calendar month by means of a regression of the observed values of PET for the Belgian part of the basin on the observed daily temperatures. The values of α_m range from approximately 0.08^oC^{-1} in the summer half-year to 0.13^oC^{-1} in the winter half-year. These values are considerably lower than the value of 0.17^oC^{-1} used in Chapter 2.
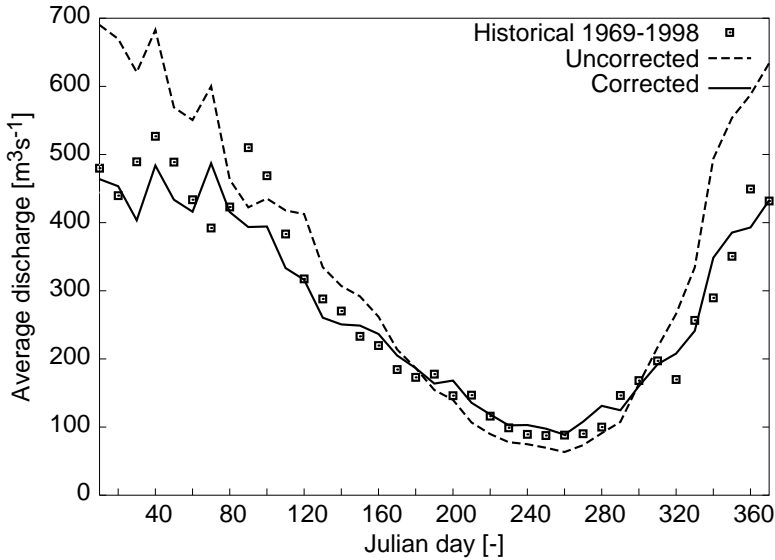
Figure 4.11: *Mean annual cycle of the 10-day average discharge simulated by HBV with observed precipitation and temperature (historical, squares) and with corrected and uncorrected data from RACMO-HCCTL.*

Figure 4.11 shows the mean annual cycle of the discharge as simulated by HBV with observed precipitation and temperature and with corrected and uncorrected data from RACMO-HCCTL. Although the annual cycle of the mean discharge from the RACMO data appears realistic, the mean discharge during December-February is overestimated if no bias correction is applied. This is a result of the bias in the mean winter precipitation, shown in the left panel of Fig. 4.2. Figure 4.12 compares the Gumbel plots of the discharge winter maxima as obtained from the bias-corrected 30-year RACMO runs (using the nonlinear correction) with those simulated using observed data. There is a close correspondence between the plots for the HBV simulation with bias-corrected RACMO data and the plot for the HBV simulation with observed data, except for the two highest maxima from RACMO-HCCTL. The two highest maxima in the simulation with observed data correspond with two known flood events in December 1993 and January 1995. In RACMO-ERA40 these two events are reproduced correctly, because they are related to large-scale weather features, which influence RACMO through the boundary conditions. Figure 4.12 further shows the average Gumbel plots of the discharge winter maxima resulting from the use of the resampled sequences from RACMO data. The plots are similar to those of the corresponding 10-day precipitation maxima in Fig. 4.10. There are marked differences between the plots for the HBV simulations with uncorrected resampled RACMO data and those for the simulations with observed

precipitation and temperature. The differences are even larger if a linear correction is applied to the precipitation input data. The quantiles of the distribution of the winter discharge maxima are then underestimated considerably as a result of the underestimation of the CVs of the multi-day precipitation amounts. For the nonlinearly corrected precipitation input data, the resulting Gumbel plots are much closer to those obtained with observed precipitation and temperature. The correction of the variability of multi-day precipitation is thus essential for a realistic simulation of the discharge maxima. A matter of concern is that the simulated maxima for December 1993 and January 1995 are clearly above the plots for the resampled data for both RACMO-HCCTL and RACMO-ERA40. This was also found when resampling from the observed daily precipitation and temperature in Chapter 2. The December 1993 and January 1995 maxima would have been plotted at a longer return period if longer discharge simulations were available. The 95-year discharge record at Borgharen contains only one other event (January 1926) that is comparable with the floods of December 1993 and January 1995.

For RACMO-ERA40, Fig. 4.13 shows the effect of using different CVs for fitting the exponent b in the nonlinear correction on the simulated winter discharge maxima. For return periods beyond five years the correction based on CV_1 results in rather low quantiles compared to those obtained with observed precipitation. A better agreement is achieved if b is fitted on CV_{10}. For RACMO-HCCTL the differences are small (not shown). Nevertheless, for the Meuse basin it is recommendable to base the value of b on CV_{10} rather than CV_1.
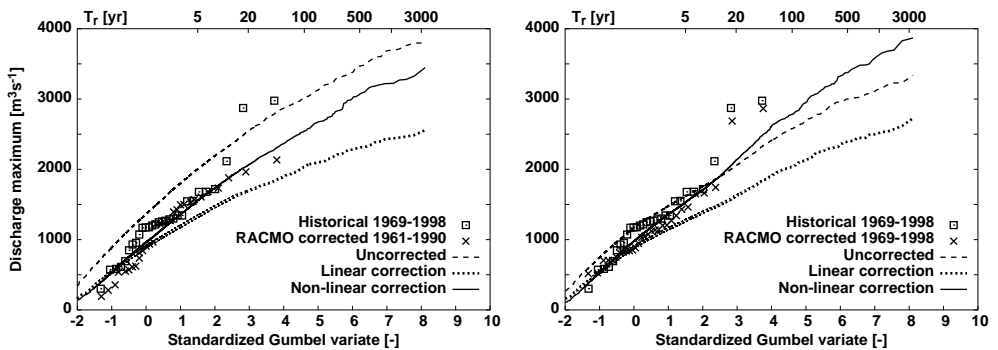

Figure 4.12: *Winter maxima of discharge as simulated by HBV with observed meteorological data (boxes), nonlinearly corrected RACMO data (crosses) and resampled 9000-year sequences of RACMO data, either uncorrected or with a linear or a nonlinear correction. The exponent b of the nonlinear correction was based on CV_1 for RACMO-HCCTL in the left panel and on CV_{10} for RACMO-ERA40 in the right panel.*
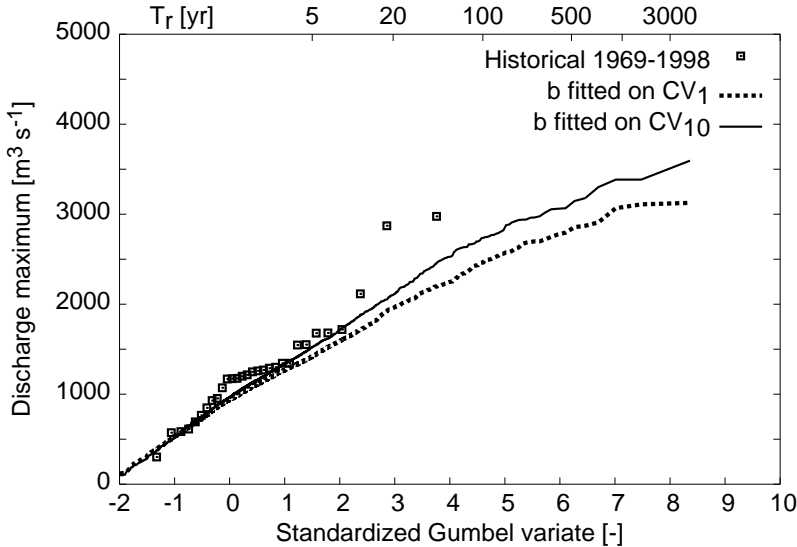
Figure 4.13: *Discharge winter maxima from two 3000-year HBV simulations based on the resampled RACMO-ERA40 run. Both simulations are based on the same resampled sequences, but with different values of the correction parameter b, based respectively on CV_1 and CV_{10}.*

4.5   Conclusion and summary

In this study output of the KNMI regional climate model RACMO was resampled with a nearest-neighbour technique to produce long-duration sequences of daily precipitation and temperature for the Belgian and French subbasins of the river Meuse. Bias corrections were applied to synthetic 3000-year sequences of precipitation and temperature to reproduce statistical properties of observed data. With the bias-corrected resampled sequences the daily discharge in Borgharen was simulated with the HBV rainfall-runoff model.

It was found that the correction for the bias in the mean precipitation by linear scaling of the daily precipitation amounts leads to an underestimation of large quantiles of their distribution. As a result, the occurrence of extreme river flows is underestimated considerably. This problem was encountered with both model runs in this study (either driven by HadAM3H or ERA40). A marked improvement was achieved with a nonlinear transformation, adjusting the mean as well as the CV of daily precipitation. For RACMO-ERA40 even better results for extreme river flows were obtained by fitting the exponent in the nonlinear correction on the CV of the 10-day precipitation amounts. De-

spite a slight overestimation of the variability and a negative bias in the autocorrelation coefficients of the daily precipitation amounts, the distribution of the 10-day precipitation maxima is reproduced adequately. In order to reproduce the distribution of extreme discharges for a relatively large river basin like that of the Meuse, it is generally more appropriate to correct for biases in statistical properties of the multi-day precipitation totals instead of daily precipitation.

The used correction does not adjust the frequency of wet days. Biases in the wet-day frequency, or more general, the left tail of the frequency distribution of daily precipitation have usually little influence on the distribution of extreme river flows. However, the CVs of both the daily and multi-day precipitation amounts depend on the wet-day frequency. As a result, the nonlinear transformation may do less well for RCM simulations having a larger bias in the wet-day frequency than the RACMO simulations considered in this study. The bias in the autocorrelation (and the spatial correlation) of the simulated daily precipitation amounts may also restrict the use of this transformation.

The flood quantiles simulated with the bias-corrected resampled RCM precipitation resemble those simulated with observed precipitation quite well. The next question is whether the presented approach can successfully be applied to the output of RCM scenario runs. This question will be addressed in a subsequent study.

Estimated changes in flood quantiles

Abstract

Precipitation and temperature data from three regional climate model (RCM) experiments are used to assess the effect of climatic change on the flood quantiles of the French-Belgian river Meuse. In two of these experiments the RCM is driven by the global atmospheric model HadAM3H of the Hadley Centre (HC), and in the other experiment the RCM is driven by the global coupled atmosphere-ocean model ECHAM4/OPYC3 of the Max-Planck Institute for Meteorology (MPI). RCM simulations for the control climate (1961-1990) and the SRES-scenario A2 (2071-2100) are available. The HBV rainfall-runoff model is used to simulate river discharges. Long synthetic sequences of precipitation and temperature are resampled from the RCM output using a nearest-neighbour technique to obtain the flood quantiles for long return periods. The maxima of 10-day precipitation and discharge for the winter half-year (flooding season) are analysed. It is found that the changes in the extreme quantiles of 10-day precipitation and discharge are highly sensitive to the driving GCM. In the runs driven by HC, there is little change in the most extreme quantiles, whereas the MPI-driven run projects a remarkable increase. It is shown that this difference between the HC- and MPI-driven runs is strongly related to the change in the coefficient of variation of the 10-day precipitation amounts, which decreases in the former and hardly changes in the latter. The relevance of bias correction of RCM output with regard to the estimated changes of flood quantiles is demonstrated.

5.1   Introduction

From the perspective of policy making the interest in the impacts of local climatic change on river flows is increasing. It is generally believed that climate change will lead to increased flooding in many areas (Kay et al., 2006b). For the Netherlands potential changes in the statistics of extreme flows are highly relevant, since the major part of the country is situated in the delta of the rivers Rhine and Meuse.

Most of the research on the impact of climate change on river discharges in the Netherlands relates to the river Rhine. To assess the impact of climate change on the monthly mean and peak discharges of the river Rhine, Kwadijk and Rotmans (1995) applied gridded patterns of changes in temperature and precipitation, obtained from seven equilibrium experiments with general circulation models (GCMs), to the observed monthly precipitation and temperature and used the perturbed data to drive a distributed hydrological model (RHINEFLOW) for the river basin. The same approach was followed in a study coordinated by the International Commision for the Hydrology of the Rhine Basin (CHR) using the output from one transient and two equilibrium GCM experiments (Grabs, 1997 and Middelkoop, 2001). As in Kwadijk and Rotmans (1995), the effect of climate change was calculated by applying the changes found in the GCM experiments to the baseline climate and RHINEFLOW was used at a monthly resolution for the rainfall-runoff modelling of the Rhine basin. The assessment of the changes in river discharges was limited to the mean annual cycle at different gauging stations. In a later study (Middelkoop, 2000) the RHINEFLOW model was operated at a temporal resolution of ten days, using data from the UKHI GCM of the Hadley Centre of the UK Met Office. Shabalova et al. (2003) were the first to use data from a regional climate model (RCM) to assess the impact of climate change on the discharges of the river Rhine in the Netherlands. They used HadRM2 of the Hadley Centre nested within the global coupled climate model HadCM2. The changes in 10-day precipitation and temperature were applied to the observed baseline series. Using RHINEFLOW, it was found that the changes in extreme 10-day flows were very sensitive to the type of transformation (linear or nonlinear) applied to the precipitation amounts. This sensitivity was also observed in a study of Prudhomme et al. (2002) for the Severn catchment (UK). Lenderink et al. (2007) investigated the direct use of bias-corrected 10-day HadRM3H regional climate model data (also from the Hadley Centre) as input to RHINEFLOW. They compared the changes in discharge with those obtained by perturbing the RCM control run. One of their findings was that direct use of RCM data should be preferred if other discharge characteristics than the mean (such as extremes) are of interest.

Several other studies have been performed for individual subbasins of the river Rhine upstream of the Netherlands. A number of relatively small subbasins were considered in the CHR study described by Grabs (1997) and Middelkoop (2000). Detailed hydrological models were used to estimate climate change impacts. As in the RHINEFLOW application to the entire river basin, scenarios for future climate were obtained by perturbing

the baseline climate with the changes from three GCM experiments. Bárdossy and Zehe (2002) studied the impact of climate change on floods and the runoff regime of the major German subbasins of the river Rhine, using a stochastic downscaling technique for generating daily precipitation and temperature, conditional on the circulation patterns of a control and a scenario run of the ECHAM4 GCM, and the semi-distributed HBV model (Lindström et al., 1997) for hydrological simulations. Kleinn et al. (2005) nested the distributed hydrological model WaSiM-ETH for the Rhine upstream of Cologne into a cascade of two versions of the Swiss/German regional climate model CHRM (with respective spatial resolutions of 14 km and 56 km). The 56-km model was driven by observed lateral boundary conditions from a 5-year ECMWF reanalysis. Future climate conditions were not considered in that study.

For the Meuse basin an extensive study has been carried out by Booij (2002, 2005). He used a first order Markov chain to generate a time series of daily basin-average precipitation and developed a discrete random cascade model for spatial disaggregation of precipitation. The parameters of the Markov chain for the current and the future climate were obtained from transient runs of three GCMs (CGCM1, HadCM3 and CSIRO9) and two RCMs (HadRM2 and HIRHAM4). The parameters for the cascade model were estimated from the two RCMs. HBV was used for the hydrological simulations. A subdivision of the Meuse basin into 15 subbasins was compared with a subdivision into 118 subbasins and no subdivision. De Wit (2007) analysed the impact of climate change on the occurrence of low flows in the river Meuse, using RCM simulations from the EU-funded PRUDENCE (Prediction of Regional scenarios and Uncertainties for Defining EuropeaN Climate change risks and Effects) project, see e.g. Christensen and Christensen (2007). Their study indicates that climate change will lead to a decrease in the average discharge of the Meuse during the low flow season. Considerable problems were, however, encountered with the simulation of critical low flow conditions of the Meuse. Bultot et al. (1988) and Gellens and Roulin (1998) investigated the impact of climate change for some Belgian subbasins of the river Meuse by perturbing the baseline climate.

In Chapter 4 a detailed study of bias correction of RCM output for the Meuse basin was presented. Also nearest-neighbour resampling was applied to obtain long sequences of daily precipitation and temperature required to simulate long-duration series of river flows. The study in that chapter was restricted to two experiments with the KNMI regional climate model RACMO under current climate conditions. The simulated series were successfully used to estimate flood quantiles for return periods far beyond the extent of the original RCM runs. Therefore, this approach offers a possibility to estimate extreme flood quantiles for a future climate using data from scenario runs.

In this chapter the methodology presented and tested in Chapter 4 is employed to assess the effects of RCM climate change projections on rare flood quantiles. The work in this chapter could also be regarded as an extension of the work done by Lenderink et al. (2007), because it demonstrates a new way to take advantage of RCM output for the

investigation of rare flood quantiles, by using a resampling method and a more sophisticated bias correction. Furthermore, the hydrological model is operated at a daily, rather than a 10-day timestep. Three RCM-GCM configurations are considered. Since for rivers like the Meuse the occurrence of extreme flows depends strongly on the variability and the extremes of multi-day precipitation amounts (Tu (2006) mentions durations between seven and ten days), the statistics of 10-day precipitation amounts receive much attention.

First, a description of the study area is given and the RCM-GCM configurations, the nearest-neighbour resampling scheme and the rainfall-runoff model are discussed. This is followed by an explanation of the bias correction of RCM output and its implications for the three RCM-GCM configurations. Then the changes in precipitation and temperature characteristics, found by comparing the control and scenario runs, are discussed with particular attention to the quantiles of extreme 10-day precipitation amounts. Subsequently, the simulated changes of flood quantiles resulting from the hydrological simulations are presented. Finally, the results are summarized and some concluding remarks are made.

5.2   Study area, models and methods used

The river Meuse is the second largest river in the Netherlands. It originates in the north-east of France and traverses the Belgian Ardennes, which is the source of a major portion of its discharge. The gauging station Borgharen, considered in this study, is located near the Belgian-Netherlands border (drainage area $\approx$ 21,000 km^2). The mean discharge at this gauging station ranges from 100 m^{3}s^{-1} in September to about 500 m^{3}s^{-1} in January. This strong seasonal cycle can mainly be ascribed to that of the evapotranspiration (de Wit et al., 2007).

For 15 subbasins the daily area-average precipitation was available for the historical period 1961-1998. These data were obtained from the Royal Meteorological Institute of Belgium for the Belgian subbasins and calculated from station data (63 stations) for the French subbasins. Daily potential evapotranspiration (PET) data were available for the Belgian subbasins for the period 1967-1998. The PET values for the French subbasins were set equal to the area-weighted average of the Belgian subbasins. This is justified by the fact that in the flood situations of interest PET only plays a minor role. Daily temperature was available for 11 stations in and around the Meuse basin.

Three RCM-GCM configurations are considered in this study. One consists of the regional climate model RACMO of KNMI (Lenderink et al., 2003), driven by the high-resolution global atmospheric model HadAM3H (Jones et al., 2001) of the Hadley Centre. In the other two configurations the regional climate model RCAO (Räisänen et al., 2004) of the Swedish Meteorological and Hydrological Institute (SMHI) was used, either coupled to HadAM3H or the global atmosphere-ocean model ECHAM4/OPYC3 of the

Max-Planck-Institute of Meteorology (MPI) in Hamburg, Germany (Roeckner et al., 1999), also used by Bárdossy and Zehe (2002). These model configurations are from here denoted as RACMO-HC, RCAO-HC and RCAO-MPI, respectively.

The specific choice of RCM runs and driving GCMs allows for a distinction between effects related to the driving GCM and those produced by the RCM itself. For each configuration two runs were considered, one for the control period 1961-1990 and one for the period 2071-2100, based on the SRES-scenario A2. These RCM runs were performed in the framework of the PRUDENCE project (Jacob et al., 2007). RCAO and RACMO have a resolution of ≈ 50 km over the Meuse basin, which is located near the centre of their domains. From both models 15 grid boxes were selected which almost entirely cover the basin (Fig. 5.1).

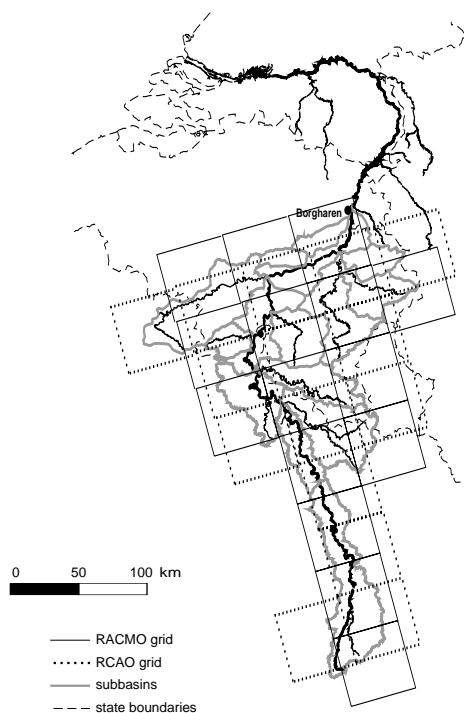The main goal of the current study is to investigate events with return periods in the

Figure 5.1: *Locations of the 15 used grid boxes of RACMO (solid) and those of RCAO (dotted), relative to the Meuse subbasins (grey).*

order of 1000 years, relevant to the design water levels of the embanked part of the river Meuse in the Netherlands. Since all model runs have a length of only 30 years, this requires strong extrapolation, introducing large uncertainties in precipitation and flood quantiles to be estimated. Therefore, a data-driven weather generator was used in this study to generate long-duration time series of precipitation and temperature. This weather generator is based on nearest-neighbour resampling and uses precipitation and temperature data from the RCM integrations. The algorithm implemented for this study essentially samples days from the model runs with replacement. The selection of a day being added to the synthetic sequences is conditioned on the spatially averaged standardized precipitation and temperature of the last added day and the precipitation total of its five predecessors. The general principles of nearest-neighbour resampling and the application to daily precipitation and temperature are described in Rajagopalan and Lall (1999). One of the features of the algorithm is that it is capable of reproducing the daily variability and persistence in the underlying data, and hence the variability of multi-day aggregates (Chapter 2). Besides, the spatial correlation of precipitation and temperature and the correlation between those two variables on a daily resolution are preserved by definition. Therefore, it is a particularly suitable tool in the study of extreme discharges. More on the specific implementation of the algorithm used in this study can be found in Chapter 2 and Chapter 4.

For rainfall-runoff modelling the semi-distributed HBV model, developed at SMHI, was used (Lindström et al., 1997). The Meuse basin upstream of Borgharen was divided into 15 subbasins, depicted in Fig. 5.1. Beside daily precipitation and temperature, the HBV model also requires daily PET for each subbasin. In the simulations with observed meteorological data the available observed PET values were used. For the simulations with RCM data, daily PET was derived from the (bias-corrected) daily temperature using Eqn. 4.5. An elaborate description of the HBV model and its application to the Meuse basin can be found in Booij (2005).

5.3   Bias correction of RCM data

In Chapter 4 the precipitation bias in the control simulation of RACMO-HC for the study area was discussed. Table 5.1 summarizes the performance of the used model configurations for the Meuse basin for the winter as well as the summer half-year. The observations for the 30-year period 1969-1998 were used as a reference. This period was also considered in Chapter 4. All three model runs show a positive bias in the mean precipitation, in particular RCAO-MPI. This bias is mainly related to that of the fraction f_{wet} of wet days (≥ 0.3 mm), because the mean wet-day amount m_{wet} is fairly well reproduced. The left panel of Fig. 5.2 shows the basin-average relative precipitation bias for each calendar month. RACMO-HC and RCAO-HC have similar biases, whereas RCAO-MPI has a much larger bias in the months July through October. The large positive bias in this part of the year is characteristic for control simulations driven by MPI
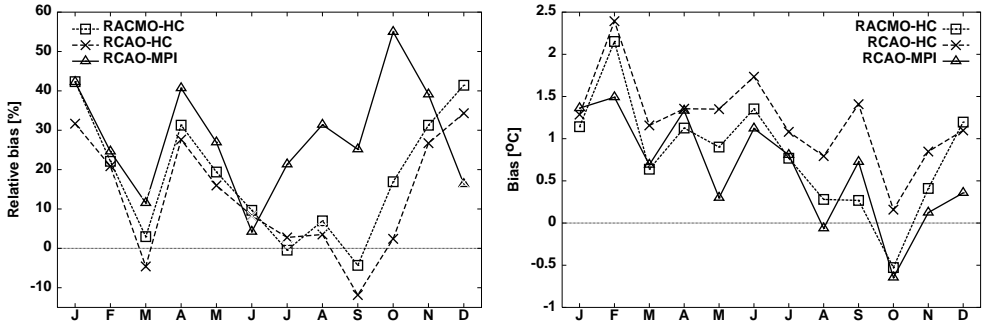
Figure 5.2: *Basin-average relative bias in the monthly precipitation (left) and the absolute bias in the mean monthly temperature (right) for the control simulations of RACMO-HC (squares), RCAO-HC (crosses) and RCAO-MPI (triangles) for the period 1961-1990. Biases are calculated with respect to the observed means for the period 1969-1998.*

Table 5.1: *Performance of the three model configurations for precipitation during the winter half-year (October-March) and the summer half-year (April-September). The mean daily amount, the coefficient of variation CV_1, the lag 1 autocorrelation coefficient r_1, the fraction f_{wet} of wet days and the mean wet-day amount m_{wet} are area-weighted averages over all subbasins.*

Winter	Observed	RACMO-HC	RCAO-HC	RCAO-MPI
Mean (mm/day)	2.77	3.49	3.25	3.58
CV_1	1.73	1.48	1.36	1.26
r_1	0.37	0.35	0.40	0.35
f_{wet} (%)	56	68	70	76
m_{wet} (mm/day)	4.94	5.10	4.60	4.72

Summer	Observed	RACMO-HC	RCAO-HC	RCAO-MPI
Mean (mm/day)	2.40	2.64	2.58	2.97
CV_1	1.81	1.69	1.69	1.54
r_1	0.27	0.25	0.31	0.22
f_{wet} (%)	50	57	56	63
m_{wet} (mm/day)	4.75	4.58	4.52	4.69

for western Europe and is possibly related to a positive bias in the westerlies (van Ulden et al., 2007). Furthermore, the coefficient of variation (CV) of daily precipitation (CV_1) is too low in all RCM runs. This is also the case for the CV of the 10-day precipitation amounts (not shown).

The lag 1 autocorrelation coefficient r_1 in winter is overestimated by RCAO-HC and slightly underestimated in the other two model configurations. In summer the same is found, though the differences between the models and the observations are somewhat larger.

A linear scaling of precipitation does not correct the underestimation of CV_1 or that of the multi-day CVs. It was shown in Chapter 4 that this can have undesirable effects on large quantiles of multi-day precipitation. Hence, such a correction is unsuited for any study of extreme precipitation and simulated discharge. A slightly more advanced nonlinear correction in the form

$$P^* = a\,P^b \tag{5.1}$$

was introduced in Chapter 4 to correct the variability as well as the mean precipitation. The seasonally and spatially varying (i.e. among subbasins) parameters a and b were determined for each interval of five calendar days in the year by considering days within a moving window of 65 days centred on the 5-day period of interest. For each window the values of a and b were chosen such that the mean precipitation and the CV of 10-day precipitation amounts (CV_{10}) matched those of the corresponding days from the observed precipitation. Figure 5.3 shows how the basin-average exponent b varies throughout the year for all three control simulations. As observed for the biases in the mean precipitation, there is a strong resemblance between the values of b for the two HC-driven simulations. For the RCAO-MPI simulation the values of b are considerably higher. In particular in the months September through November (roughly between day 240 and day 330) the values of the exponent are rather large. It was suspected that these large values were related to the positive bias in f_{wet}. To investigate this, the bias in f_{wet} was removed prior to the nonlinear correction. A small, seasonally varying reduction was applied to the wet-day precipitation amounts, such that the fraction of days with precipitation amounts above the wet-day threshold (of 0.3 mm) matched the observed f_{wet}. Negative precipitation amounts were set to zero. Though this adjustment resulted in smaller values of the exponent b, the reduction was only marginal.

The right panel of Fig. 5.2 shows the absolute monthly temperature biases. These were obtained by comparing the basin-average temperature calculated from the grid boxes with the reference temperature for the basin, obtained from data of 11 stations using Thiessen interpolation. For the three configurations the temperature biases are roughly of the same order, though the bias of RCAO-HC is on average larger than that of the other two model configurations. The daily temperatures of the subbasins were corrected

in the same way as in Chapter 4, involving a translation and a scaling which respectively adjust the mean and the variability. The same translation and scale factor were used for all subbasins, but these parameters were determined separately for each 5-day interval in the year, again using a moving window of 65 calendar days.

5.4 Changes of temperature and precipitation in the RCM runs

For each model configuration precipitation and temperature for the Meuse basin in the A2-scenario run were compared with those in the control run. The left panel of Fig. 5.4 displays the relative change of the mean precipitation. All model configurations show an increase in winter and a decrease in summer. The changes in RCAO-MPI are the largest in magnitude, ranging from a decrease of about 70% in August to an increase of 60% in December. The decrease in summer precipitation is accompanied by a strong decrease in the number of wet days (30% to 50% in the summer months June, July and August). In winter the change in precipitation frequency is small, but there is a clear increase in the mean wet-day amounts. For December, January and February, this increase ranges from 16% for the HC-driven runs up to 32% for RCAO-MPI.
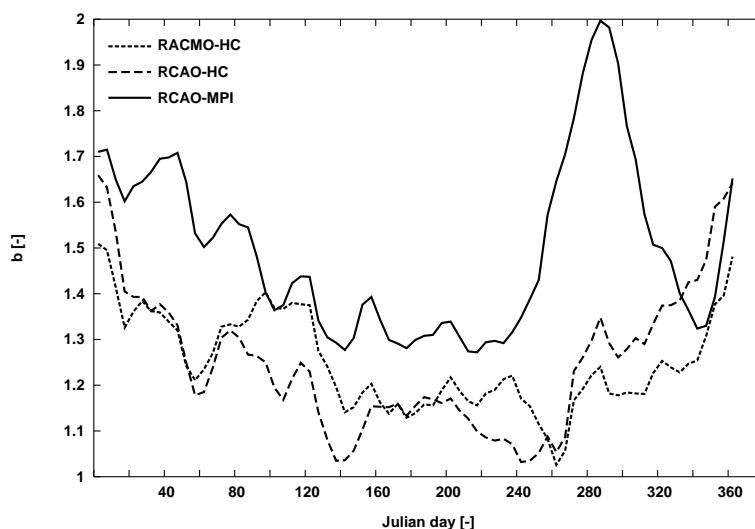

Figure 5.3: *Annual cycle of the area-averaged correction parameter b for RACMO-HC, RCAO-HC and RCAO-MPI.*
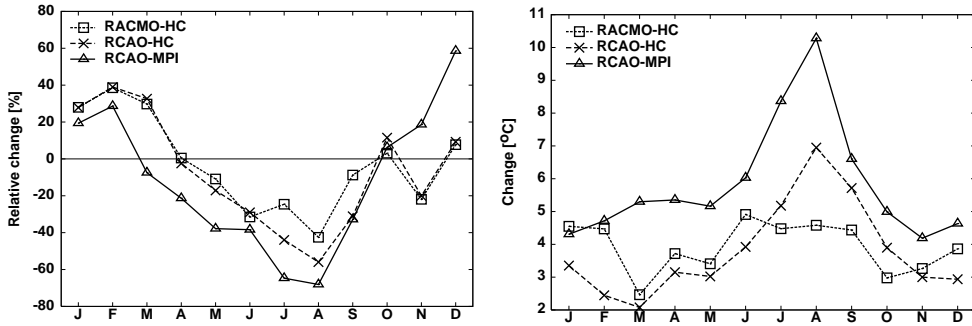
Figure 5.4: *Relative change in the monthly precipitation (left) and the absolute change in the monthly mean temperature (right), resulting from the A2 scenario, as projected by RACMO-HC, RCAO-HC and RCAO-MPI.*

The right panel of Fig. 5.4 displays the change of the mean monthly temperature. Throughout the entire year an increase is found in all model configurations. The changes in both HC-driven runs do not differ much, except for August and September, where RCAO-HC shows a considerably larger increase. This is probably related to the drying-out of the soil, the effects of which can also be seen in the precipitation in the summer months. In the RACMO model several modifications of the soil scheme were made to reduce the positive feedback between soil moisture and temperature. The soil depth was increased, the response of the evapotranspiration to the available soil moisture was modified and the percolation of soil water to deeper layers was reduced. Furthermore, the cloud scheme was altered to increase the cloud cover in summer (Lenderink et al., 2003). In RCAO-MPI the change of the temperature in the summer months is even larger than in RCAO-HC, especially in August, which shows an increase of more than 10 degrees.

In Fig. 5.5 the relative change of CV_{10} is shown for all model configurations. The close correspondence between both HC-driven runs (except for May and June) suggests a strong influence of the driving GCM. For RACMO-HC and RCAO-HC the change in winter is comparable to that found by Buishand and Lenderink (2004) for the Rhine basin, using an RCM from the Hadley Centre also driven by HadAM3H boundaries. They observed a decrease of 16% for the months December, January and February. In summer the relative change shown in Fig. 5.5 is larger than the relative change found by Buishand and Lenderink (2004).

The change in CV_{10} can be understood from the changes in certain basic statistical properties of the daily precipitation amounts. For a stationary daily sequence the variance of 10-day totals, V_{10}, and the variance of daily amounts, V_1, are related through (Cox

and Lewis (1966), page 72):

$$V_{10} = 10V_1 \left(1 + 2\sum_{i=1}^{9} r_i \frac{10-i}{10}\right) , \qquad (5.2)$$

where r_i denotes the lag i autocorrelation coefficient. Dividing both sides by the squared mean 10-day amount leads to the following expression for CV_{10}:

$$CV_{10}^2 = \frac{CV_1^2}{10} \left(1 + 2\sum_{i=1}^{9} r_i \frac{10-i}{10}\right) \qquad (5.3)$$

For CV_1 Räisänen (2002) derived

$$CV_1^2 = \frac{CV_{wet}^2 + 1}{f_{wet}} - 1 \qquad (5.4)$$

where CV_{wet} is the CV of the wet-day precipitation amounts. From the last two equations it can be seen that CV_{10} decreases with the number of wet days and increases with CV_{wet} and the autocorrelation coefficients. Figure 5.6 shows the relative change of f_{wet} and CV_{wet} (left panel) and the relative change of CV_1, CV_{10} and $r_{123} = r_1 + r_2 + r_3$ (right panel) for the RACMO-HC run. From the latter it is seen that the direction of change of the autocorrelation coefficients determines whether or not the change of CV_{10} exceeds that of CV_1 (in accordance with Eqn. 5.3). In January, February and
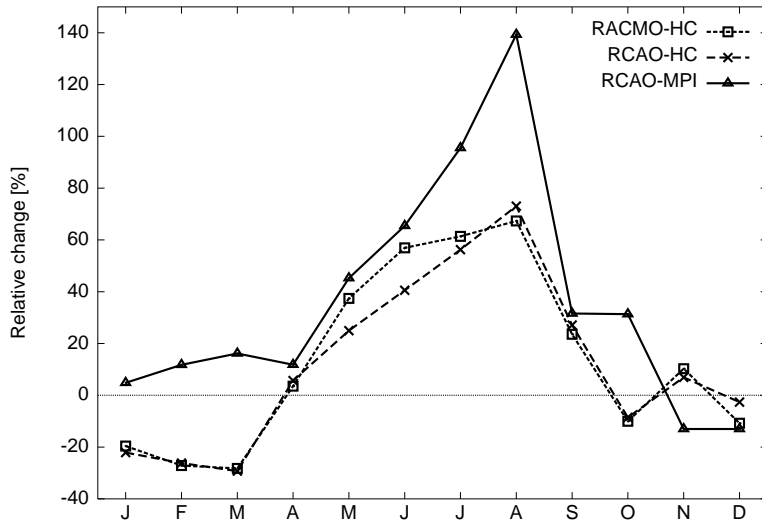

Figure 5.5: *Relative change of* CV_{10} *for each calendar month.*

March f_{wet} increases and CV_{wet} decreases, resulting in a decrease of CV_1. This effect is accompanied by a decrease of the autocorrelation, leading to a larger decrease for CV_{10} than for CV_1. The rather large increase of CV_{10} for the months June, August and September ($\approx 60\%$) can be attributed to an increase of CV_{wet} and the strength of the autocorrelation in combination with a decrease of f_{wet}. The seasonal changes of f_{wet}, CV_{wet} and the autocorrelation in RCAO-HC are similar to those in RACMO-HC. The results for RCAO-MPI for the winter half-year are, however, quite different. There is a slight increase in CV_{10} ($\approx 5\%$), mainly due to an increase in CV_{wet}.

Figure 5.7 shows the spatial pattern of the change of CV_{10} over a part of western Europe, derived from the (overlapping) 10-day totals of grid-box precipitation for each of the three model configurations. There is a striking resemblance between RACMO-HC and RCAO-HC, which confirms the strong influence of the driving GCM on these properties mentioned earlier. Both model configurations show a decrease of CV_{10} over a large part of the North Sea, southern Norway, The Netherlands, Belgium and western France, in contrast with an increase over central Europe. In the model configuration RCAO-MPI, on the other hand, CV_{10} only decreases in southern Scandinavia and an increase is seen over larger areas. The resemblance between the two HC-driven configurations and their difference from RCAO-MPI confirms the strong influence of the driving GCM on the relative variability of multi-day precipitation in these months.

The changes in CV_{10} in the three RCM simulations are comparable to those in the CV of monthly precipitation found in an extensive study by Räisänen (2002). In that study 19 atmosphere-ocean GCMs were considered, all forced with an increase in the atmospheric CO_2 concentration of 1% yr^{-1}. For most areas of the world an increase in the CV of monthly precipitation was found. However, for the high northern latitudes (50^oN and
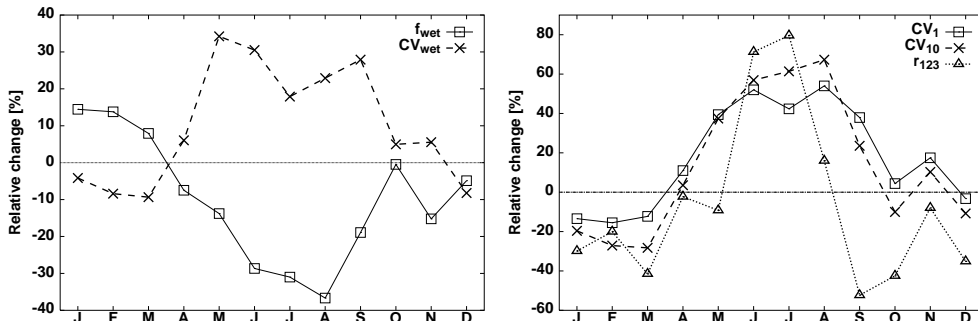
Figure 5.6:   *Relative change of f_{wet} and CV_{wet} for RACMO-HC (left panel) and the corresponding relative change of CV_1, CV_{10} and the sum of the first three autocorrelation coefficients r_{123} (right panel).*

Figure 5.7: *Relative change (%) of* CV_{10} *over western Europe in the months December through February in the three model configurations RACMO-HC (upper left), RCAO-HC (upper right) and RCAO-MPI (lower) as determined from the daily grid-box precipitation.*
(This figure was not included in the original article)

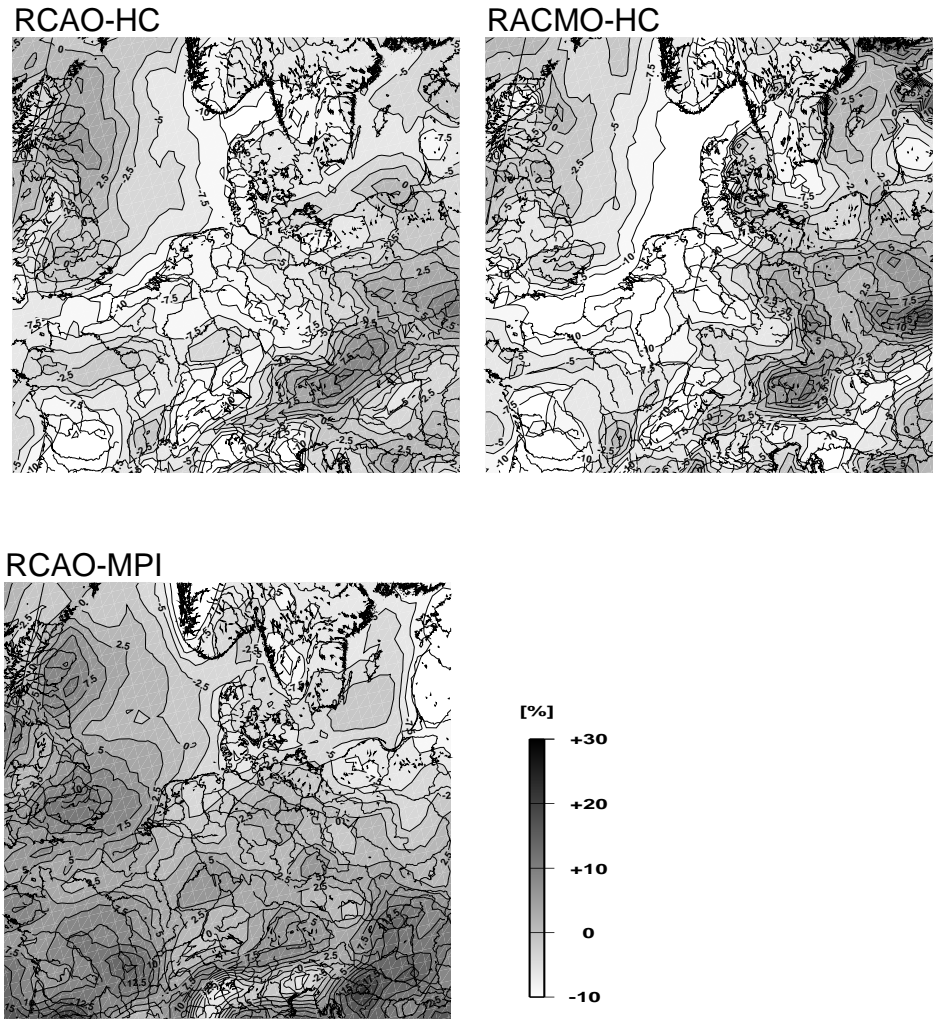higher) a decrease was observed for autumn and winter. This decrease was associated with a relatively large increase in the mean monthly precipitation. Similar results have been found for the response of the CV of seasonal amounts in GCM climate change simulations (Rowell, 2005; Giorgi and Bi, 2005).

5.5   Simulated changes in precipitation extremes

The nearest-neighbour resampling algorithm explained earlier was applied to the RCM control runs to generate daily sequences of precipitation and temperature for the 15 sub-
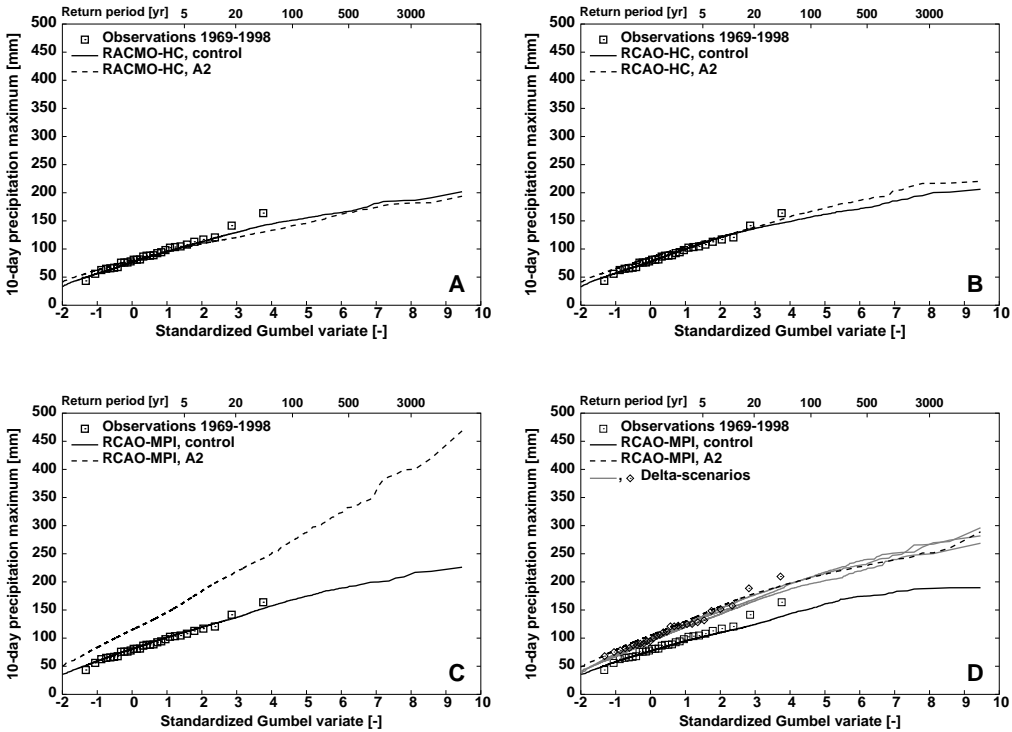
Figure 5.8:   *Gumbel plots for the 10-day winter maxima of basin-average precipitation obtained after resampling and bias correction. Panels A, B and C show the results for the three model configurations: RACMO-HC, RCAO-HC and RCAO-MPI. Panel D shows the effect of limiting the bias correction on the resampled A2-scenario run from RCAO-MPI (dashed) and the 'delta' scenarios, obtained by applying the relative changes found in RCAO-MPI to the control runs of the three model configurations (dotted) and the observations (triangles).*

basins simultaneously, each with a length of 9000 years. The corrections discussed earlier were used to adjust the mean and CV_{10} of modelled precipitation amounts and the mean and standard deviation of the daily temperatures. This procedure was repeated for the A2-scenario runs, using the same corrections. In this section the distribution of the simulated 10-day maxima of basin-average precipitation for the winter half-year (flooding season) are discussed. The three panels A, B and C in Fig. 5.8 compare the Gumbel plots of these maxima in the control run and the A2-scenario run for each model configuration.

For RACMO-HC (panel A) a slight decrease is seen for return periods longer than five years. The change of the highest quantiles of the distribution is less than 10 mm. The effect of the increase in the mean precipitation is counterbalanced here by the decrease of CV_{10}, shown in Fig. 5.5. Describing the distributions of the 10-day precipitation amounts by a square-root-normal distribution, it is demonstrated in Appendix A.2 that the changes in the mean and CV_{10} can account for the changes in the extreme value distribution. Although a slight increase in the most extreme quantiles of 10-day precipitation is seen for RCAO-HC (panel B), the magnitude of the changes is comparable to that of RACMO-HC.

The results found for RCAO-MPI (panel C) are, however, strikingly different. The most extreme quantiles are roughly doubled. This large increase is most likely related to the nonlinear bias correction. Figure 5.9 presents the ratios between the corrected and uncorrected daily precipitation amounts in the months of October and December for the Ourthe subbasin. From the left panel it can be seen that in October the highest values

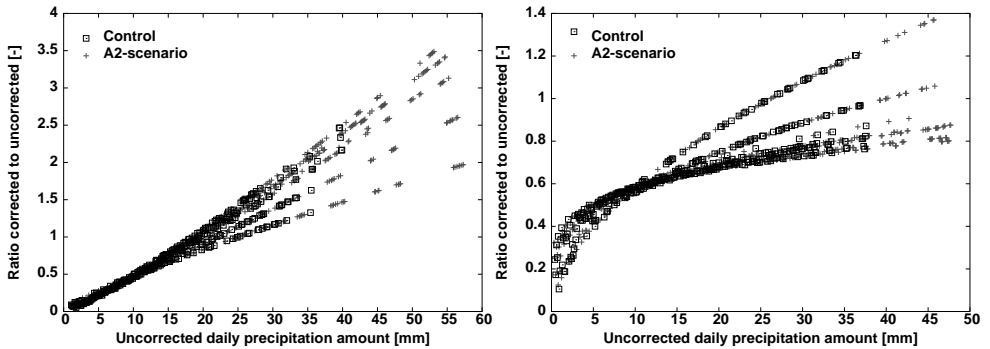Figure 5.9: *Ratio between the corrected and uncorrected precipitation amounts for individual wet days in October (left) and December (right) in RCAO-MPI for the Ourthe subbasin (1588 km^2). The results for both the A2-scenario run and control run are shown. The days falling within the same 5-day period in the year (and thus having the same bias-correction parameters) seem to fall along a curve in the plot.*
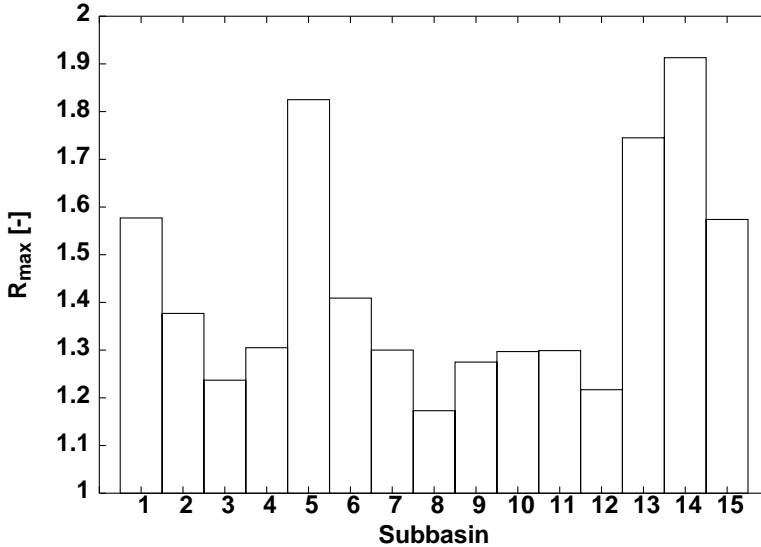
Figure 5.10: *The upper bound of the ratio between the corrected and uncorrected daily precipitation amount $R_{\max}$ for each subbasin (the numbers correspond with those in Fig. 2.1).*

in the A2-scenario run are multiplied by more than a factor of three, due to the large correction exponent b in Eqn. 5.1 for that month (see Fig. 5.3). This results in daily precipitation amounts exceeding 160 mm. In some occasions, two such values occurred within a short time span, leading to extremely large 10-day amounts. For December (right panel) the correction ratios are all below 1.5.

To restrict the effect of the nonlinearity of the bias correction on large daily precipitation amounts, a modification was made to limit the ratio of corrected to uncorrected daily precipitation amounts. Using the same moving window of calendar days as for the determination of the coefficients a and b in Eqn. 5.1, the averages $M_{20,\mathrm{RCM}}(i)$, $i = 1 \ldots 73$ of the 20 largest daily precipitation amounts from the control run data were calculated for all 73 consecutive 5-day periods of the year. In the same way the values of $M_{20,\mathrm{OBS}}$ were calculated for the observations. Then the ratios $R_{20}(i) = M_{20,\mathrm{OBS}}(i)/M_{20,\mathrm{RCM}}(i)$, $i = 1 \ldots 73$ were determined and the largest value $R_{\max} = \max_{1 \leq i \leq 73} R_{20}(i)$ was used as an upper bound for the ratio of corrected to uncorrected rainfall amounts. This procedure was carried out for each subbasin separately. From Fig. 5.9 it can be seen that $R_{\max}$ varies between 1.2 and 1.9.

The effect of the limited correction is shown in panel D of Fig. 5.8. For the control run, the quantiles of the 10-day winter maxima are somewhat lower than if no restriction would have been applied (Panel C). The agreement with the observed quantiles is, however,

still satisfactory. Limiting the bias correction has a substantial effect on the extreme quantiles of the A2-scenario run. Because for the RCAO-MPI runs the average change in CV_{10} was found to be small in winter (see Fig. 5.5), it was expected that a 'delta' scenario, i.e. scaling the daily precipitation amounts of the control run by a seasonally varying factor (which represents the relative changes in the mean precipitation) may sufficiently describe the changes of the winter extremes. Therefore, the changes in the mean precipitation in RCAO-MPI were applied to the observations and the control runs from all three model configurations. Panel D of Fig. 5.8 shows that the 10-day winter maxima in the resulting delta scenarios resemble those from the A2-scenario run with a limited nonlinear bias correction. Thus, the change of the extreme quantiles obtained by applying the limited nonlinear bias correction to the resampled RCM runs is consistent with that expected in the case of a little change of the CV_{10} of winter precipitation. This makes the limited correction much more plausible than the original correction.

5.6   Estimation of changes in flood quantiles

The bias-corrected resampled series of daily precipitation and temperature discussed earlier, were used to drive hydrological simulations with the HBV rainfall-runoff model. Figure 5.11 shows the Gumbel plots of the simulated winter maxima of daily discharge at Borgharen.

The flood quantiles obtained from RACMO-HC (panel A) and RCAO-HC (panel B) show roughly the same response to the A2 scenario. For both model configurations a slight decrease is seen for intermediate return periods, whereas the quantiles for the longest return periods tend to increase, in particular for RACMO-HC. For RCAO-MPI (panel C) the response of flood quantiles to the A2 scenario is much larger than for the HC-driven simulations. This is consistent with the change of the 10-day precipitation maxima. These results suggest that, at least for the winter half-year, the change of flood quantiles is more sensitive to the change of large-scale characteristics produced by the GCM, than to local effects produced by the RCM. The plots for the annual maxima (not shown) are almost identical to those shown in Fig. 5.11, in particular for the RCAO simulations. For RACMO there is a slight difference due to a number of large April events in the A2-scenario run.

Figure 5.12 displays the relative change of the flood quantiles as a function of the standardized Gumbel variate, showing the different responses of the three model configurations to the A2 scenario more clearly. The changes for the RACMO-HC and RCAO-HC simulations are slightly different from those found by Buishand and Lenderink (2004) and Lenderink et al. (2007) for the flood quantiles of the river Rhine. They found a rise of 10% in the 100-year flood. This increase is, however, less than the increase of the mean winter discharge, which is most likely related to the decrease of the CV of 10-day precipitation amounts in winter in the HC-driven runs mentioned earlier. For RCAO-
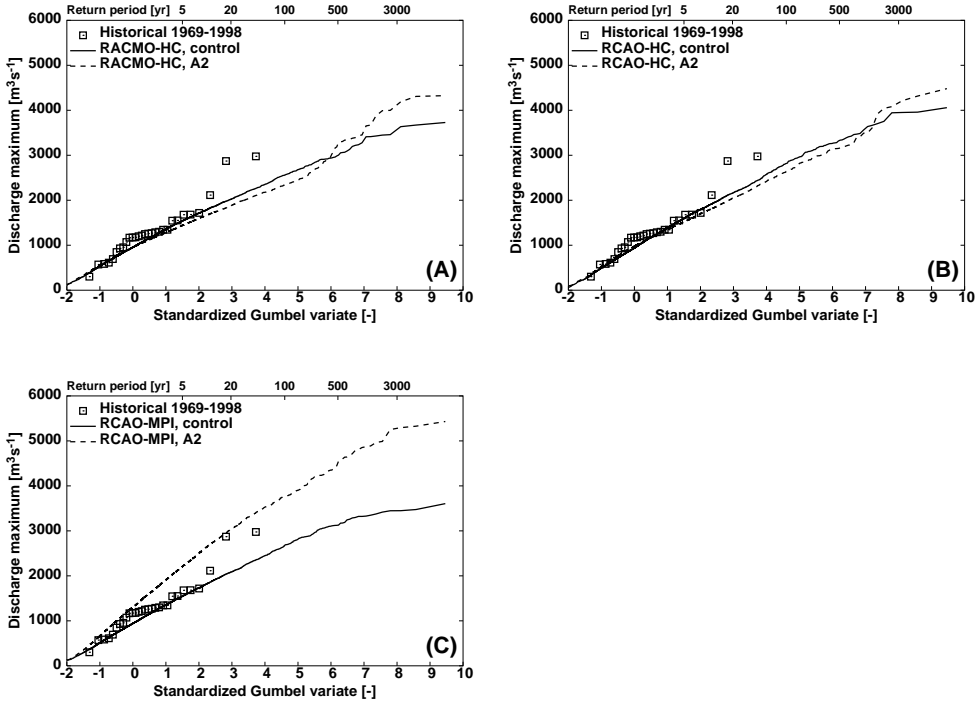
Figure 5.11:   *Gumbel plots for the maxima of daily discharge in the winter half-year for the three model configurations RACMO-HC, RCAO-HC and RCAO-MPI, the latter with the limited bias correction.*

MPI the relative change is between 35% and 55% over virtually the entire range of return periods. This is roughly comparable to the relative changes in the flood quantiles of the river Rhine from the delta scenario based on the UKHI experiment by Middelkoop (2000).

In order to explore the influence of the bias correction on the changes of the flood quantiles, the HBV simulations were repeated with the uncorrected resampled data from RACMO-HC and RCAO-MPI. For the control runs of these model configurations considerable biases were found in the flood quantiles (29% for RACMO-HC and 15% for RCAO-MPI for the 5-year event). The relative changes of the flood quantiles are compared in Fig. 5.13. For the RACMO-HC simulations (left panel) the relative change of flood quantiles is only slightly affected by the bias correction up to a return period of 100 years. For return periods beyond 500 years, the flood quantiles from the corrected data increase by about 15%, whereas those from the uncorrected data decrease by approximately the same amount. For the RCAO-MPI simulations the relative change obtained from uncorrected data is systematically lower than that obtained *with* the nonlinear

bias correction. Thus, biases in the mean and variability of precipitation not only affect the absolute values of flood quantiles, but also their relative changes for future climate conditions. Bias correction is recommended, as it leads to realistic flood quantiles for current climate conditions.
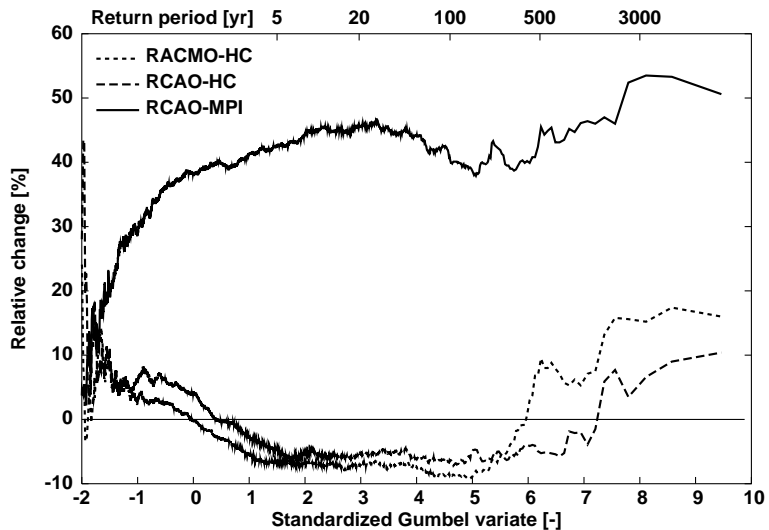

Figure 5.12: *Relative change of the flood quantiles as a function of the standardized Gumbel variate for the three model configurations.*
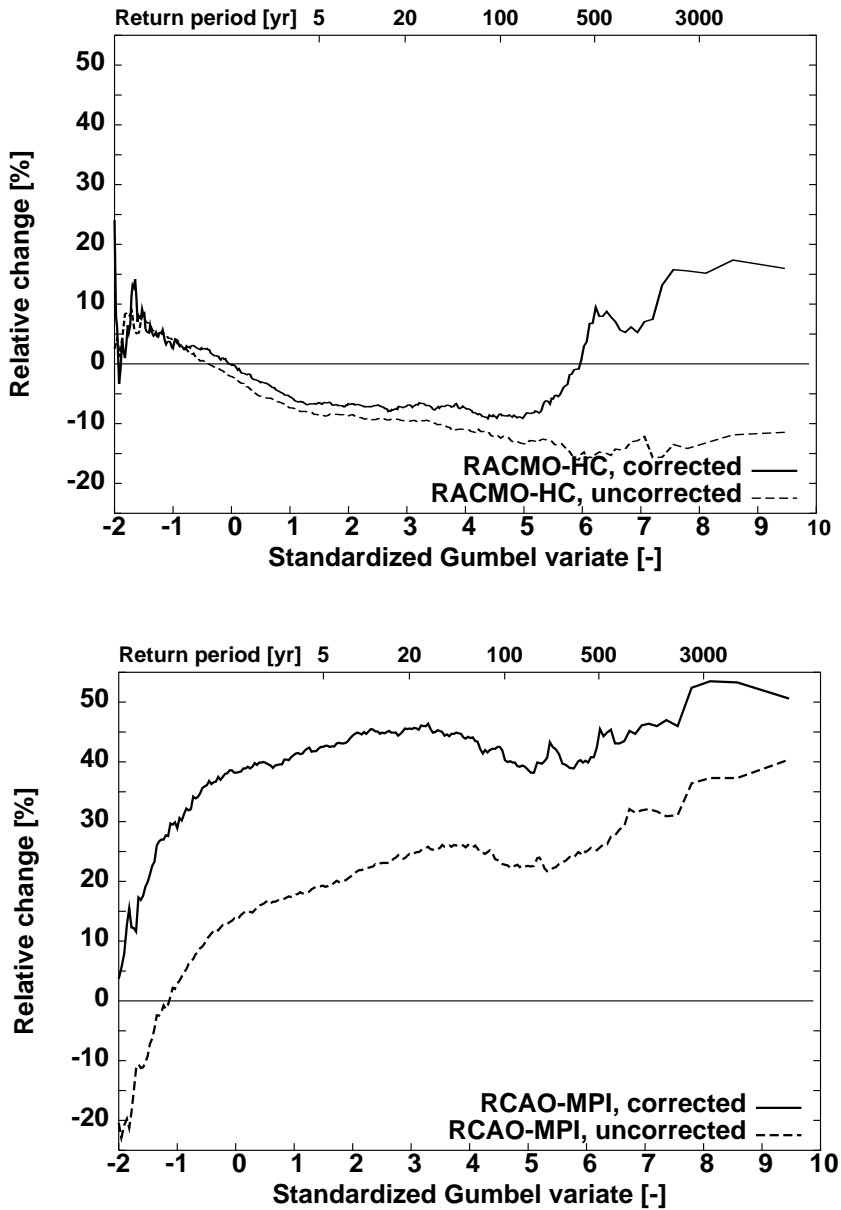
Figure 5.13:   *Influence of the nonlinear bias correction on the relative change of the simulated flood quantiles for RACMO-HC (top) and RCAO-MPI (bottom).*

5.7 Discussion and conclusion

Daily precipitation and temperature from three RCM simulations (RACMO-HC, RCAO-HC and RCAO-MPI) were used to estimate the changes in flood quantiles of the river Meuse. For each model configuration, two 9000-year sequences were generated by re-sampling from the control run (1961-1990) and the A2-scenario run (2071-2100). These sequences were corrected for differences in the mean and variability between the control run and observed climate. The HBV rainfall-runoff model was used to simulate the daily discharges at the gauging station Borgharen. The changes in the flood quantiles for the winter half-year were studied.

A substantial difference was found between the changes in flood quantiles from the two HC-driven simulations and those obtained from the RCAO-MPI simulations. In the HC-driven simulations there was little change in both the quantiles of extreme 10-day precipitation and the flood quantiles, despite a clear increase in the mean winter precipitation (Fig. 5.4). This could be explained by the fact that the increase in the mean precipitation was counteracted by a decrease in CV_{10}. By contrast, in the RCAO-MPI simulations there was little change in the CV_{10}. Mainly due to the increase in the mean precipitation amounts the quantiles of the 10-day precipitation maxima and the daily discharges increase by about 50%. The results confirm the relevance of the CV of multi-day winter precipitation as an indicator of the changes in flood quantiles, beside the change in the mean.

The change in the CV of multi-day precipitation is entirely determined by the changes in the frequency of wet days, the CV of the wet-day precipitation and the autocorrelation of daily precipitation. For the decrease of CV_{10} in the HC-driven simulations, all these factors had some influence. This decrease is consistent with that of the CV of monthly precipitation for high northern latitudes, averaged over an ensemble of GCM simulations as discussed by Räisänen (2002). However, he also reports substantial variation among the changes predicted by individual GCMs. An ensemble of RCM runs nested in different GCM runs is needed to complete the picture of the potential changes in CV_{10} and flood quantiles of the river Meuse.

It was observed that the relative change of simulated flood quantiles depends on whether or not a bias correction was used, in particular for the RCAO-MPI simulation. In Chapter 4 it was stated that a nonlinear bias correction, adjusting the relative variability of multi-day precipitation amounts, is essential for a realistic simulation of extreme flood quantiles. However, for the RCAO-MPI simulation the correction had to be restricted to avoid the occurrence of unrealistically large daily precipitation amounts.

The bias correction used in this study does not take the physical causes of the precipitation bias into account. It was noted that the precipitation bias is likely to be related to biases in the atmospheric circulation. A natural alternative would be to correct for

the bias in the circulation first. Nearest-neighbour methods conditioned on circulation indices might then be useful. Though such a correction has a more physical basis, its practical value is not clear. Furthermore, it is not certain whether the same correction should be applied to the circulation of the SRES A2-scenario run.

Possible trends in precipitation and temperature are disregarded in the resampling procedure. A trend could bias the selection of a new day towards the years surrounding the previous selection. For daily precipitation the trend is small compared to its variability. Daily temperature has a smaller variability and shows a considerable trend in the A2 scenario. Though the temperature in itself hardly influences the simulated extreme flows directly, the basin-averaged temperature has an influence on the resampling algorithm. The effect of the temperature trend was investigated for the A2-scenario run of RCAO-MPI. Two additional 9000-year resampling simulations were performed: one driven by the detrended temperatures and one by temperatures of which the trend had been doubled. No systematic influence of the temperature trend was found on the distribution of the maximum 10-day precipitation in winter.

It should be noted that the uncertainty in the change of the flood quantiles increases with the return period. Part of the uncertainty can be reduced by prolonging the meteorological sequences in the resampling stage. However, the uncertainty related to the limited length of the RCM runs remains. Since there is only one 30-year realization for each model experiment, this uncertainty is difficult to quantify. Furthermore, it is not clear whether the linear relation between PET and temperature derived for the current climate, is still valid in a changed climate or should be modified. However, it was shown by Lenderink et al. (2007) that the influence of assumptions regarding the potential evapotranspiration on extreme discharges are very small compared to other sources of uncertainty.

Summarizing, this study has shown that meaningful estimates of changes in extreme flood quantiles can be obtained from the daily output of RCM experiments. Apart from the change in the mean precipitation, the change in the CV of 10-day precipitation amounts emerged to be important for the Meuse basin. These changes are controlled strongly by the driving GCM. It is therefore recommended to use a comprehensive set of GCM simulations for future evaluations of the change in flood quantiles. Finally, it should be noted that bias corrections of precipitation can have a strong influence on the estimated changes of flood quantiles, but should be applied with care.

Conclusions and discussion

6.1   Summary and conclusions

In this thesis the applicability of time-series resampling was studied within the context of simulating extreme flows for the river Meuse. Time-series resampling should be seen as a non-parametric means to generate realistic stationary sequences of arbitrary length based on a sequence of limited length (e.g., a historical record). As demonstrated by Beersma (2007), time-series resampling is useful to simulate very rare extreme hydrometeorological events that are not present in the original short sequence and that result from a rearrangement of the individual values. Resampling of areal precipitation and temperature for a river basin in combination with rainfall-runoff modelling offers a powerful tool to study unprecedented extreme discharge events.

How large are floodquantiles at long return periods (in particular the design discharge) under current climate conditions?

To answer this question, a nearest-neighbour resampling technique was applied to observational data to generate long-duration (order 1000 years) sequences of daily precipitation and temperature for 15 subbasins of the river Meuse upstream of the Belgian-Netherlands border. The used algorithm was basically the same as that of Buishand and Brandsma (2001) for the Rhine basin, though a few modifications were required to make it suitable for the Meuse basin. A four-day memory element was included in the feature vector for the search of nearest neighbours to improve the reproduction of the autocorrelation of daily precipitation. Furthermore, a method was devised for passive (i.e. indirect) resampling from short or incomplete records of areal precipitation for the 15 subbasins, whilst the selection of nearest neighbours was driven by station records for

a longer historical period. The resampled sequences were used as input to the rainfall-runoff model HBV for the Meuse basin, resulting in a long-duration daily series of river discharge. From the latter the extremes in the winter half-year have been investigated, which follow the same distribution as the annual discharge maxima (except at very short return periods), since the largest flood events mainly occur in winter.

Gumbel plots of the simulated extremes agree fairly well with the Gumbel plot of the observed discharge extremes for the 38-year period 1961-1998. The historical 1993 and 1995 floods deviate noticably from the plots for the simulations. This deviation is mainly due to the large variability of the highest values in a 38-year record. There is furthermore a systematic difference between the quantiles of the observed discharges and those of the simulations at short and moderate return periods due to a systematic underestimation of flood peaks in this regime by the HBV model. The difference vanishes when 10-day average discharges are considered, which indicates that extreme flood volumes are well represented by the simulations.

During this study, four 3000-year simulations of precipitation and temperature based on the historical period 1961-1998 were performed, 'Sim61' in Chapter 2 being one of them. These simulations only differed in the random-number seed used, which makes them comparable but independent. The generated sequences were used by Aalders et al. (2004) to simulate extreme discharges. The simulations were chained to form a $12\,000$-year simulation (de Wit and Buishand, 2007). Due to the length of the simulated discharge series, the 1250-year discharge level can be obtained as an empirical quantile from the simulated maxima without the need to fit a parametric distribution. This resulted in a 1250-year discharge level of approximately $3750\,\mathrm{m}^3\mathrm{s}^{-1}$. The same procedure was followed with four 3000-year simulations based on the period 1930-1998 ('Sim30' in Chapter 2), resulting in a 1250-year level of about $3400\,\mathrm{m}^3\mathrm{s}^{-1}$. To translate these levels to maxima of hourly discharge, a relative increase of 1% should be applied in combination with an absolute increase of $80\,\mathrm{m}^3\mathrm{s}^{-1}$ (Kramer and Schroevers, 2008). This leads to a value of $3867\,\mathrm{m}^3\mathrm{s}^{-1}$ for Sim61 and $3514\,\mathrm{m}^3\mathrm{s}^{-1}$ for Sim30. The value based on Sim30 comes in the order of the design discharge of the Becht Committee in 1977 ($3600\,\mathrm{m}^3\mathrm{s}^{-1}$), but is still considerably lower than the currently used value of $3800\,\mathrm{m}^3\mathrm{s}^{-1}$. The value from Sim61 is higher, due to a more pronounced influence of the wet years in the period 1961-1998. It is possible that the underestimation of the flood peaks by the HBV model also influences these estimates. Recently, the calibration of the HBV model for the meuse has been reinvestigated (Kramer and Schroevers, 2008). A large ensemble of parameter sets has been considered. For five of these sets a number of historical floods have been hindcasted. It was concluded that, in terms of the Nash-Sutcliffe efficiency and the reproduction of the flood peaks, the new parameter sets outperform the original parameter set used in this study. This at least illustrates that there is room for improvement in the tuning of the HBV model.

How should the output of regional climate models be processed to be useful for the determination of flood quantiles?

This question was dealt with in Chapter 4. The performance of the regional climate model RACMO of the Royal Netherlands Meteorological Institute (KNMI) under current climate conditions was studied in detail. One 30-year run of this model driven at its lateral boundaries by the Hadley Centre's global atmospheric model HadAM3H (HC) and one run driven by the ERA40 reanalysis were used for resampling and rainfall-runoff simulation. In both runs the mean winter precipitation was overestimated, whereas the relative variability (coefficient of variation) was generally underestimated. The correction of the mean and the relative variability of 10-day precipitation, CV_{10}, turned out to be essential for a realistic simulation of flood events. To achieve this, a nonlinear bias correction, capable of simultaneously adjusting the mean daily precipitation and CV_{10}, was applied to the daily precipitation of the resampled sequences. The parameters in the correction formula were fitted using the precipitation from the model runs and the observations. With the correction a satisfactory agreement was seen between the simulated flood quantiles and those obtained by driving the HBV model with observational data. A minor drawback of this nonlinear correction is that it slightly changes the autocorrelation of daily precipitation. Furthermore, in a climate-change scenario unrealistically large precipitation amounts may arise. To avoid this side effect, the ratio between the corrected and uncorrected precipitation amounts was restricted.

How do rare flood quantiles change in a climate-change scenario represented by a regional climate model?

This is the topic of Chapter 5. For the study to the effects of climate change, three different RCM-GCM configurations were considered: RACMO-HC, RCAO-HC and RCAO-MPI, where RCAO is the regional climate model of the Swedish Meteorological and Hydrological Institute (SMHI) and MPI refers to the coupled atmosphere-ocean model ECHAM4/OPYC3 of the Max-Planck-Institute for Meteorology. All these model experiments are part of the EU-funded integrated project PRUDENCE (Christensen and Christensen, 2007). For each configuration the control simulation (1961-1990) and a simulation for the SRES-scenario A2 (2071-2100) were used. Bias-corrected precipitation and temperature data were fed into the HBV model. The changes in the mean and variability of precipitation for the winter half-year are more similar in model simulations driven by the same GCM than in those of the same RCM, driven by different GCMs. This is not surprising, since the weather in this season is dominated by large scale features that control the RCM boundary conditions. At least for the mid-western part of Europe, the pattern of changes in the mean and CV_{10} indirectly induced by the respective GCMs was fairly different. The model experiments driven by HadAM3H project a moderate increase in the mean precipitation, accompanied by a decrease of the relative variability of 10-day precipitation in a region covering the Netherlands, Belgium and

northern France. Hence, the increase of the absolute variability is less than proportional to that of the mean and the increase of the flood quantiles is small. At a return period of 1250 years, the increase shown by both RCM experiments is below the 10% per degree of de Wit et al. (2008). The increase in annual mean temperature is, however, larger than 2°C. In the ECHAM4-driven experiment the mean precipitation in the area of interest increases considerably and the change of the relative variability is small. As a result, the flood quantiles roughly increase in proportion with the mean precipitation. The 1250-year discharge level rises by approximately 45%. Given a rise of 3°C of the mean global temperature in the A2 scenario (Fig. 9.6 of Boer et al., 2001) for ECHAM3/OPYC4, this is about 15% per ^{o}C. The relative changes in the quantiles of extreme discharge can be sensitive to the application of the nonlinear bias correction. Conversely, these changes may be sensitive to an underestimation in the relative variability of precipitation. Thus, it might not be sound to base conclusions concerning the change in flood extremes on uncorrected model runs.

Modification of the resampling algorithm

By definition the resampled time series can only contain individual values that are present in the original series, which also limits the highest resampled value. To investigate whether this limitation puts an unnatural restriction to the simulation of extreme river discharges, a two-stage resampling algorithm, capable of generating daily precipitation amounts beyond the highest value in the observations (or climate model run), was developed. In this algorithm the principle of nearest neighbours is used to estimate the expected value conditioned on the previously simulated amounts and to sample residuals. A first-order LOESS smoother (a locally weighted regression line) was found to a be suitable estimator. Before applying the algorithm to meteorological data, it was tested with data from two theoretical AR1-processes with known distributions. The two-stage algorithm was then tested for the basin of the river Ourthe, one of the Meuse's tributaries. The resulting synthetic precipitation and temperature sequences were used to drive the HBV model for the Ourthe basin in order to simulate the daily discharge. The experiments with the two-stage algorithm show that it produces higher values than those in the original data. The estimation of the expected values and the number of nearest neighbours for selecting the residuals strongly influenced the tail of the distribution of the simulated values. In contrast to the single-stage algorithm, the number of neighbours involved in the determination of the expected values and the selection of residuals in the two-stage algorithm was rather large. Though the algorithm produces daily precipitation amounts beyond the observed range, this hardly had any effect on the simulated discharge maxima. This indicates that at least for the Ourthe, the single-stage resampling of historical daily precipitation amounts does not put an unrealistic restriction to the simulated discharge extremes.

6.2 Other developments and prospects

Regarding the estimated 1250-year discharge, it is important to identify the sources of uncertainty inherent to the presented resampling approach. Firstly, a rather long simulation is required to obtain an accurate estimate of the 1250-year discharge. The variance of the empirical quantile $\widehat{x}_T$ with return period T determined from the annual (or seasonal) maxima of an N-year resampling simulation, is approximated by (e.g., David, 1981):

$$\mathrm{Var}\left(\widehat{x}_T\right) \approx \frac{1}{N+2} \frac{1/T(1-1/T)}{f^2\left(\widehat{x}_T\right)} \approx \frac{1}{NTf^2\left(\widehat{x}_T\right)} \;, \tag{6.1}$$

for T and N large. Here, f denotes the probability density function of the maxima, evaluated at the estimated quantile. Several methods have been proposed to estimate f or $1/f$, see for instance Bloch and Gastwirth (1968) and McKean and Schrader (1984). Here, a Gumbel distribution was fitted (censored, only using the upper 2% of the maxima). For the 12 000-year simulation of Sim61 a standard deviation of 136 m^{3}s^{-1} was derived for the 1250-year event. For Sim30 a standard deviation of 88 m^{3}s^{-1} was found (see also de Wit and Buishand, 2007).

The original meteorological sequences used for resampling form another source of uncertainty. In Chapter 2 it was already found that resampling from the relatively wet period 1961-1998 resulted in higher quantiles of the winter maxima of 10-day precipitation than resampling from the entire period 1930-1998. To investigate the sensitivity of the simulations to the selection of historical years, 20 000-year simulations were conducted with different subsets of 33 years taken from the interval 1930-1998 (Leander and Buishand, 2008). The length of the simulations guarantees that the aforementioned uncertainty of the resampling itself can be neglected. The Gumbel plots of the simulated 10-day precipitation maxima are presented in Fig. 6.1. A reference simulation using data from the entire historical period is also shown. Furthermore, a distinction is made between the simulations from subperiods that either include or exclude the year 1995. The 1250-year level of the 10-day precipitation maximum roughly ranges from 165 mm upto 210 mm, about 25% of the value from the reference simulation ($\approx$180 mm). Furthermore, the influence of 1995 is seen. The plots of the simulations including 1995 are above, whereas those of the simulations without 1995 are below that of the reference simulation. It was noticed that some days of the winter of 1995 occurred relatively frequently in the simulation, due to the resampling algorithm being trapped within certain sequences of historical days. This is more likely to happen when the historical sequence is short.

The foregoing also applies to resampling from short RCM runs introducing uncertainty in the outcome. A long model run or an ensemble of model runs is therefore desirable. Because of the computational expenses of models, it might be necessary to reconsider the tradeoff between the length of simulations and the spatial (and temporal) resolution. For the river Meuse it is concluded that increasing the spatial resolution of the RCMs contributes little to the accuracy of the estimated changes of flood quantiles, due to

the strong influence of large scale features from the driving GCMs. Instead, it is more worthwhile to prolong the model runs.

The two-stage resampling algorithm of Chapter 3 is a more general algorithm than the single-stage algorithm introduced in Chapter 2 and has more advantages than just the ability of generating larger daily precipitation amounts than observed. It may also mitigate the aforementioned trapping of the simulation. An extension to a multi-site version could therefore be valuable. In multi-site simulations the two-stage algorithm would facilitate the generation of unprecedented spatial patterns of daily precipitation.

Although the results in this study demonstrate the feasibility of using RCM output for the assessment of extreme discharges in a future climate, the bias in the variability of precipitation from RCMs should be considered with care, as well as the bias in the mean precipitation. However, it is anticipated that the performance of GCMs and RCMs improves with each new generation of models and the required bias correction will gradually decrease. More important, the signals of change emerging from different GCMs (influ-
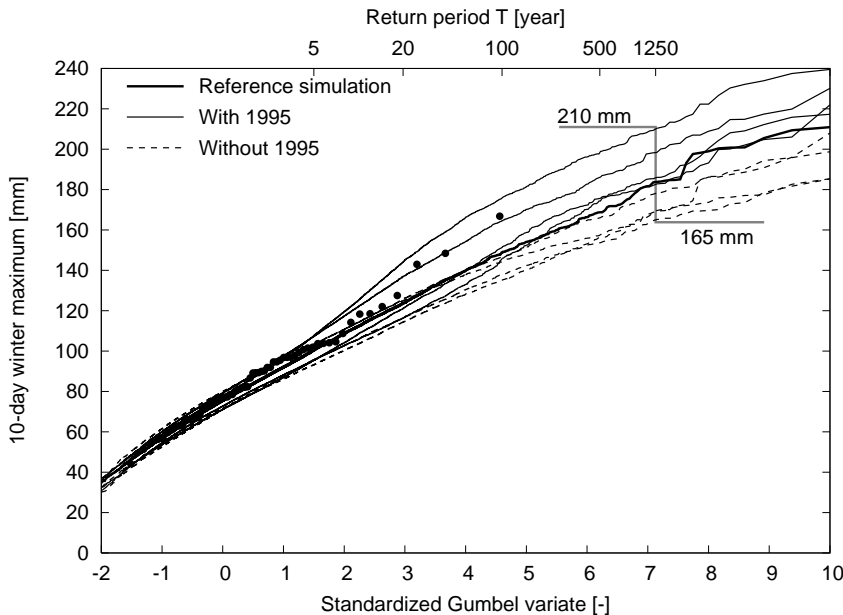

Figure 6.1:   *Gumbel plots of the winter maxima of 10-day basin-average precipitation in 20 000-year simulations using different subsets of years from the historical period 1930-1998. The historical maxima (dots) and the reference simulation (thick curve) using the entire historical period, are also shown.*

ential to precipitation in winter) diverge. The lack of consensus among different models regarding this point is illustrated in Fig. 6.2. Here the change of the relative variability of 10-day precipitation, CV_{10}, in the months December through February is plotted against the change of the mean precipitation for the three RCM experiments in this study and four GCMs. For the latter, the precipitation is used from the grid box closest to the Meuse basin. For all GCMs in the plot the mean precipitation increases. However, two of the GCMs (GFDL-CM2 and CCCMA-CGCM) show only a minor change in CV_{10}, while in the other two CV_{10} either increases (MIROC3) or decreases (ECHAM5) in the order of 10%. RCMs driven by these four GCMs are bound to show a similar spread. To represent the uncertainty of models, it is recommended to consider experiments with an ensemble of driving GCMs, rather than an ensemble of RCMs driven by the same GCM. This is the objective of the EU-funded integrated project ENSEMBLES, aimed at providing policy-relevant information on climate and climate change and with an emphasis on probablistic methods. A large number of model experiments from state-of-the-art climate models participating in this project will shortly become available. The application of the presented resampling methodology within this context is currently in preparation.
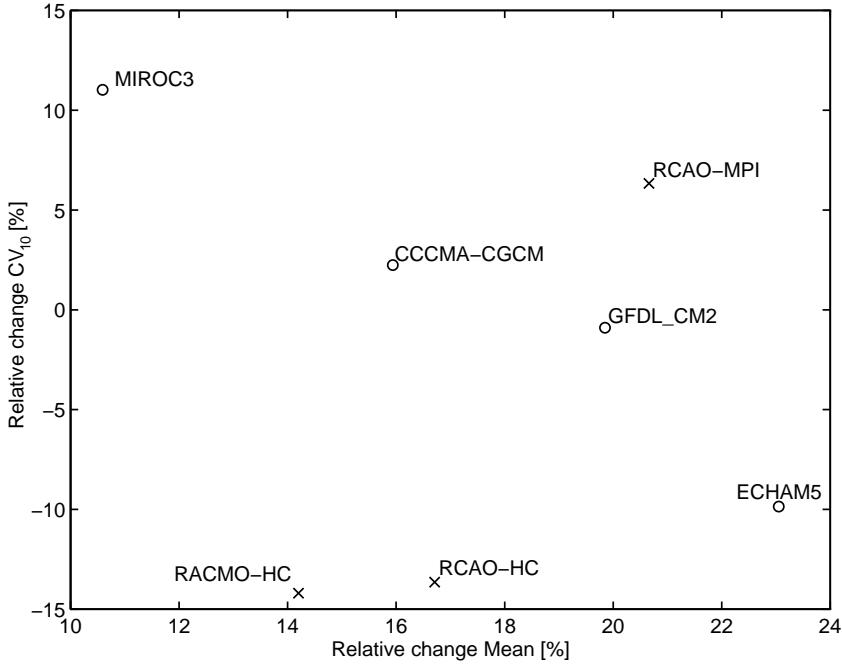
Figure 6.2: *Relative change of the coefficient of variation of 10-day precipitation* (CV$_{10}$) *versus that of the mean precipitation in the months December-February, as obtained from various GCM experiments and the RCM experiments used in this study. For the RCM experiments (crosses) the mean and coefficient of variation of overlapping 10-day basin-average precipitation amounts were determined in the control climate (1961-1990) and the A2 scenario (2071-2100). The relative differences between the scenario and the control climate were determined for each month separately and then averaged. For the GCMs the same procedure was followed for the daily data from the nearest grid point, using the control simulations for the control climate and the A1B scenario . These data were obtained from the Climate Explorer website (*`http://climexp.knmi.nl`*)*

The GEV distribution

A.1 Regional estimation of the shape parameter

The perturbation of the RG1-simulation (RG1p) requires that the shape of the upper tail of the distribution of daily precipitation is known. To find a suitable representation for the tail, the bimonthly maxima of the daily precipitation amounts for 15 subcatchments of the river Meuse (upstream of the Netherlands) were analysed. It is assumed that the largest amount X in a bimonthly period follows a Generalized Extreme Value (GEV) distribution:

$$\Pr(X \leq x) = \exp\left[-\left(1 - \theta\frac{x - \mu}{\sigma}\right)^{1/\theta}\right] . \tag{A.1}$$

The location parameter μ and the scale parameter σ vary over the year and over the subcatchments. A common shape parameter θ is assumed for all subcatchments, which varies over the year. The regional L-moments approach (Hosking and Wallis, 1997) was followed to estimate the common θ.

First, the probability weighted moments b_0, b_1 and b_2 were determined from the ordered maxima $x_1 \leq x_2 \leq \ldots \leq x_n$ as (Landwehr et al., 1979)

$$b_0 = \sum_{j=1}^{n} \frac{x_j}{n} , \quad b_1 = \sum_{j=2}^{n} \frac{(j-1)x_j}{n(n-1)} , \quad b_2 = \sum_{j=3}^{n} \frac{(j-1)(j-2)x_j}{n(n-1)(n-2)} . \tag{A.2}$$

The sample L-moments ℓ_2 and ℓ_3 were derived using (Hosking and Wallis (1997), page 26)

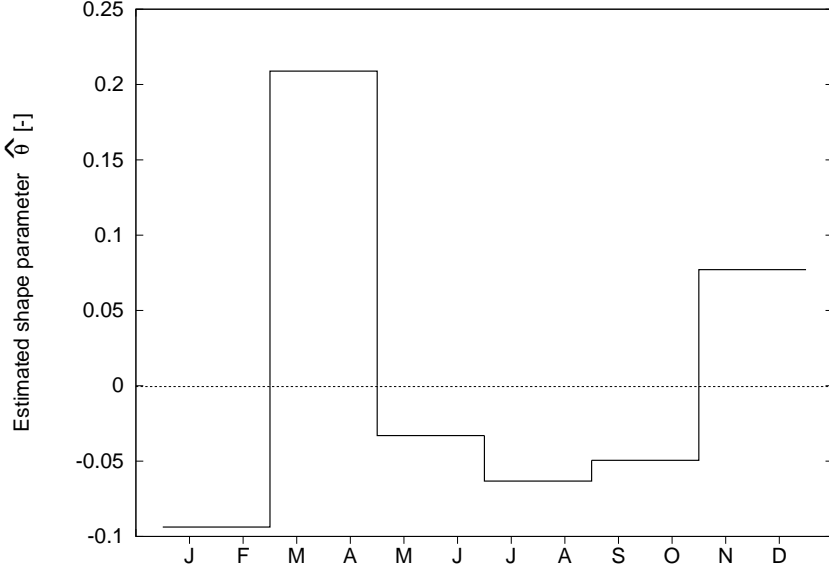$$\ell_2 = 2b_1 - b_0 , \qquad \ell_3 = 6b_2 - 6b_1 + b_0 . \tag{A.3}$$

Figure A.1: *Regional estimates of the GEV shape parameter θ of bimonthly maxima of daily precipitation for 15 subcatchments of the river Meuse.*

For each subcatchment, the sample L-skewness $t_3 = \ell_3/\ell_2$ was determined and then averaged over the catchment. The estimated shape parameter $\hat{\theta}$ of the GEV distribution then follows from the average sample skewness t_3^R as (Hosking and Wallis (1997), page 196).

$$\hat{\theta} = 2.9554 \ c^2 + 7.8590 \ c \qquad \text{with} \qquad c = \frac{2}{3 + t_3^R} - \frac{\log 2}{\log 3} \ . \qquad (A.4)$$

Figure A.1 shows the values of $\hat{\theta}$ calculated from the data for the 15 subcatchments. In November-December a positive $\hat{\theta}$ is found, whereas in January-February the value is negative. In March-April, again, a positive value of 0.21 is seen. Averaging $\hat{\theta}$ over the winter half-year results in a value of about 0.02. Given the fact that this is close to zero, the distribution of the bimonthly maxima of daily precipitation is close to the Gumbel distribution:

$$\Pr(X \le x) = \exp\left[-\exp\left(-\frac{x - \mu}{\sigma} \right) \right] \qquad (A.5)$$

in this season, which implies that the exceedances of a high threshold are approximately exponentially distributed. For the summer half-year there is a tendency towards a neg-

ative shape parameter. Thence, for this season the exponential distribution underestimates the tail of the distributions. This is, however, not relevant for the simulation of extreme discharges in winter.

A.2 Penultimate approximation of the extreme value distribution

This appendix investigates whether the change in the quantiles of the extreme 10-day precipitation amounts in the RACMO-HC simulations can be explained by the changes in the mean and CV alone. The distribution of the 10-day precipitation amounts P_{10} can satisfactorily be described by the square-root-normal distribution, i.e. $X = \sqrt{P_{10}}$ is normally distributed with mean μ_X and standard deviation σ_X. These two parameters determine the mean μ_P and standard deviation σ_P of P_{10} (Katz, 1999):

$$\mu_P = \mu_X^2 + \sigma_X^2 \qquad \text{and} \qquad \sigma_P^2 = 2\sigma_X^2 \left(\sigma_X^2 + 2\mu_X^2 \right) . \tag{A.6}$$

Here these relations are used to derive μ_X and σ_X from μ_P and σ_P:

$$\sigma_X^2 = \mu_P - \sqrt{\mu_P^2 - \frac{1}{2}\sigma_P^2} \qquad \text{and} \qquad \mu_X^2 = \sqrt{\mu_P^2 - \frac{1}{2}\sigma_P^2} . \tag{A.7}$$

The distribution of the 10-day winter maxima can be derived from the distribution of P_{10}, $F(x) = \text{Prob}\,(P_{10} \leq x)$, using extreme-value theory. Let M_n be the maximum of the 10-day precipitation amounts in n subsequent, non-overlapping 10-day periods. Assuming independence between these precipitation amounts, the distribution of M_n is given by (Leadbetter et al., 1983):

$$H(x) = \text{Prob}\,(M_n \leq x) = \{F(x)\}^n \sim \exp\{-n[1 - F(x)]\} . \tag{A.8}$$

This distribution can be approximated by a GEV distribution (Smith, 1990):

$$H(x) \approx \exp\left\{ -[1 - \theta(x - \mu)/\sigma]^{1/\theta} \right\} . \tag{A.9}$$

The parameters μ, σ and θ of H depend on n. The location parameter μ is obtained as the $1/n$ upper quantile of F, i.e.

$$1 - F(\mu) = 1/n . \tag{A.10}$$

Subsequently, the scale parameter σ and the shape parameter θ are calculated using the first and second derivatives F' and F'' of F in μ:

$$\sigma = \frac{1}{n} \frac{1}{F'(\mu)} \qquad \text{and} \qquad \theta = \sigma \frac{F''(\mu)}{F'(\mu)} + 1 . \tag{A.11}$$
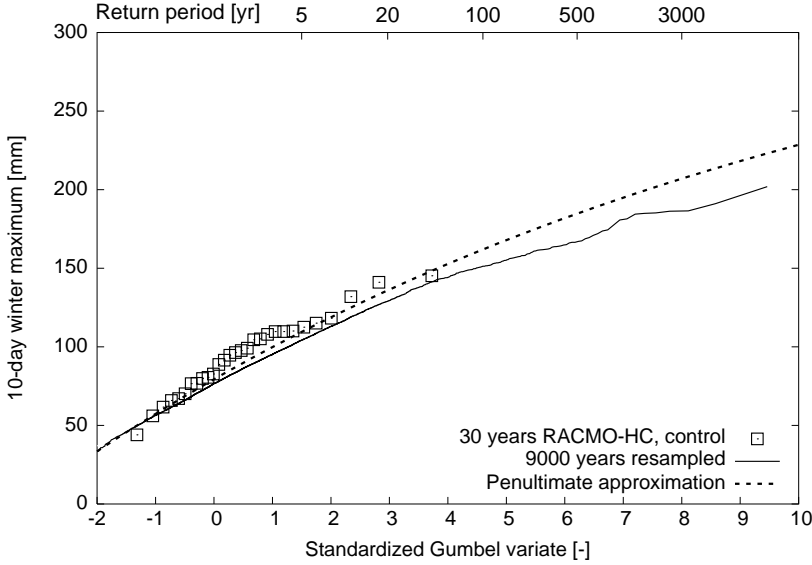
Figure A.2: *Penultimate approximation of the distributions of extreme 10-day basin-average precipitation totals for the winter half-year (dashed), compared with the empirical quantiles from a 9000-year resampled series (solid) and those of the 30-year RCM control run (squares).*

This approximation is known as the penultimate distribution. Since the winter half-year is considered here, a value of 18.5 was chosen for n. Because $\left(\sqrt{P_{10}} - \mu_X\right)/\sigma_X$ is assumed to be standard normally distributed, the solution of Eqn. A.10 is given by

$$\mu = \left[\mu_X + \sigma_X \Phi^{-1}\left(1 - \frac{1}{n}\right)\right]^2 \; , \tag{A.12}$$

where Φ^{-1} is the inverse of the standard normal distribution function. The probability density F' and its derivative F'' in μ, which are required to calculate the scale parameter σ and the shape parameter θ, are given by

$$F'(\mu) = \frac{1}{2\sigma_X\sqrt{\mu}} \; \varphi(z) \tag{A.13}$$

and

$$F''(\mu) = -\frac{1}{4\mu\sigma_X} \; \varphi(z)\left(\frac{1}{\sqrt{\mu}} + \frac{z}{\sigma_X}\right) \; , \tag{A.14}$$

where φ denotes the standard normal density and $z = \left(\sqrt{\mu} - \mu_X\right)/\sigma_X$.

The 10-day precipitation maxima considered in this thesis refer to overlapping 10-day periods. These maxima are generally larger than those for consecutive 10-day periods. To account for this decrepancy, the location parameter μ and the scale parameter σ were multiplied by 1.13, which implies that the quantiles of the distribution of M_n change with the same factor. The factor 1.13 is due to Hershfield (1961). It has been used to adjust the quantiles of clock-hour and 1-day maxima to the corresponding quantiles of sliding 60-minute and 24-hour maxima, respectively.

Figure A.2 compares the Gumbel plots for the 10-day precipitation maxima in winter from the 30-year run and the 9000-year resampled series with the penultimate approximation. For the latter, $\mu = 79.4$ mm, $\sigma = 21.2$ mm and $\theta = 0.0755$. It is seen that this GEV distribution slightly overestimates the quantiles of the resampled maxima, though there is a good agreement with those of the 30-year RCM run. Figure A.3 shows the relative change of the quantiles of the derived from the penultimate approximation roughly agrees with that found from the resampled sequences. This indicates that the changes of the mean and CV_{10} indeed can account for the change of the quantiles of the maxima in winter.
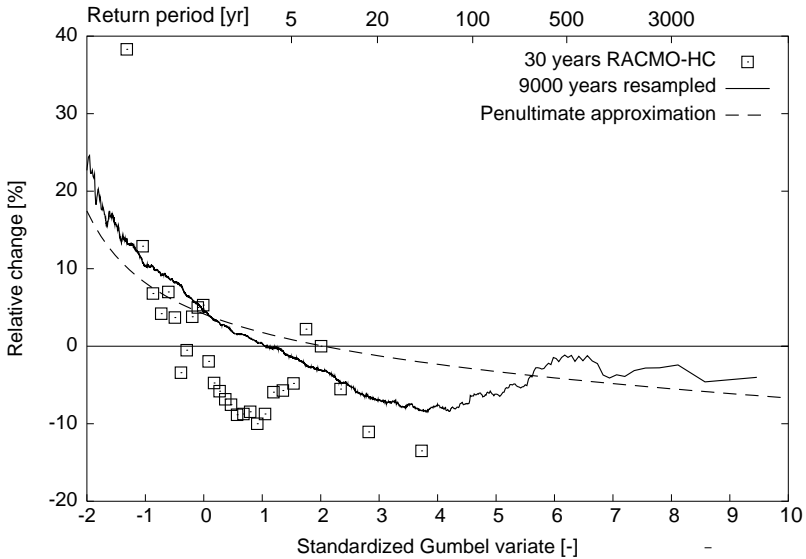

Figure A.3: *Change in the quantiles of the 10-day winter maxima of basin-average precipitation, extracted from the bias-corrected 30-year control run and A2-scenario run of RACMO-HC (squares) and from the corresponding 9000-year resampled sequences (solid) and penultimate approximations (dashed) derived from these runs.*

Bibliography

Aalders, P., P.M.M. Warmerdam, and P.J.J.F. Torfs, 2004. Rainfall generator for the Meuse basin: 3000 year discharge simulations in the Meuse basin. Report 124, Wageningen University, Wageningen.

Arnell, N.W., D.A. Hudson, and R.G. Jones, 2003. Climate change scenarios from a regional climate model: Estimating change in runoff in southern Africa. *Journal of Geophysical Research*, **108(D16),** 4519, doi:10.1029/2002JD002782.

Arnell, N.W. and N.S. Reynard, 1996. The effects of climate change due to global warming on river flows in Great Britain. *Journal of Hydrology*, **183,** 397–424.

Bárdossy, A. and E. J. Plate, 1992. Space-time model for daily rainfall using atmospheric circulation patterns. *Water Resources Research*, **28,** 1247–1259.

Bárdossy, A. and E. Zehe, 2002. Hydrological impact of climate change on the river Rhine. Report of the irma-sponge project "Development of flood management strategies for the Rhine and Meuse basins in the context of integrated river management", Institute of Hydraulic Engineering (IWS), University of Stuttgart, Stuttgart, Germany.

Bartlett, M. S., 1946. On the theoretical specification and sampling properties of autocorrelated time series. *Journal of the Royal Statistical Society, Series B*, **8,** 27–41.

Beersma, J.J., 2002. Rainfall generator for the Rhine basin: Description of 1000-year simulations. KNMI-publication 186-V, Royal Netherlands Meteorological Institute (KNMI), De Bilt.

Beersma, J.J., 2007. Extreme hydro-meteorological events and their probabilities. PhD thesis, Wageningen University, Wageningen.

Bloch, D.A. and J.L. Gastwirth, 1968. On a simple estimate of the reciprocal of the probability density function. *Annals of Mathematical Statistics*, **39,** 1083–1085.

Boer, G.J., R.J. Stouffer, M. Dix, A. Noda, C.A. Senior, S. Raper, and K.S. Yap, 2001. *Projections of future climate change*. In: *Climate Change 2001: The Scientific Basis. Contribution of Working Group I to the Third Assessment Report of the Intergovernmental Panel on Climate Change*, J.T. Houghton, Y. Ding, D.J. Griggs, M. Noguer, P.J. van der Linden, X. Dai, K. Maskell and C.A. Johnson (eds.), pp. 527-582. Cambridge University Press, Cambridge, UK and New York, NY, USA.

Booij, M.J., 2002. Appropriate modelling of climate change impacts on river flooding. PhD thesis, University of Twente, Enschede.

Booij, M.J., 2005. Impact of climate change on river flooding assessed with different spatial model resolutions. *Journal of Hydrology*, **303,** 176–198.

Buishand, T. A. and G. Lenderink, 2004. Estimation of future discharges of the river Rhine in the SWURVE project. Technical report TR-273, Royal Netherlands Meteorological Institute (KNMI), De Bilt.

Buishand, T.A., 2007. Estimation of a large quantile of the distribution of multi-day seasonal maximum rainfall: the value of stochastic simulation of long duration sequences. *Climate Research*, **34,** 185–194.

Buishand, T.A. and J.J. Beersma, 1993. Jackknife tests for differences in autocorrelation between climate time series. *Journal of Climate*, **6,** 2490–2495.

Buishand, T.A. and J.J. Beersma, 1996. Statistical tests for comparison of daily variability in observed and simulated climates. *Journal of Climate*, **9,** 2538–2550.

Buishand, T.A. and T. Brandsma, 1996. Rainfall generator for the Rhine catchment: a feasibility study. Technical Report TR-183, Royal Netherlands Meteorological Institute (KNMI), De Bilt.

Buishand, T.A. and T. Brandsma, 2001. Multi-site simulation of daily precipitation and temperature in the Rhine basin by nearest-neighbour resampling. *Water Resources Research*, **37,** 2761–2776.

Bultot, F., A. Coppens, G.L. Dupriez, D. Gellens, and F. Meulenberghs, 1988. Repercussions of a CO_2 doubling on the water cycle and on the water balance - a case study for Belgium. *Journal of Hydrology*, **99,** 319–347.

Charles, S.P., B.C. Bates, and J.P. Hughes, 1999. A spatiotemporal model for downscaling precipitation occurrence and amounts. *Journal of Geophysical Research*, **104(D24),** 31,657–669.

Christensen, J.H. and O.B. Christensen, 2007. A summary of the PRUDENCE model projections of changes in the European climate by the end of this century. *Climatic Change*, **81,** 7–30, doi:10.1007/s10584–006–9210–7.

Cleveland, W.S., 1979. Robust locally weighted regression and smoothing scatterplots. *Journal of the American Statistical Association*, **74,** 829–836.

Commissie Becht, 1977. Rapport Commissie Rivierdijken. Ministerie van Verkeer en Waterstaat, Den Haag.

Commissie Boertien I, 1993. Toetsing uitgangspunten rivierdijkversterkingen, deelrapport 2: Maatgevende belastingen. Ministerie van Verkeer en Waterstaat, Den Haag.

Commissie Boertien II, 1994. Onderzoek Watersnood Maas, deelrapport 4: Hydrologische aspecten. Ministerie van Verkeer en Waterstaat, Den Haag.

Cox, D.R. and P.A.W. Lewis, 1966. *The statistical analysis of series of events*. Chapman and Hall, London, UK.

David, H.A., 1981. *Order statistics*. John Wiley & Sons, New York.

de Wit, M.J.M. and T.A. Buishand, 2007. Generator of Rainfall And Discharge Extremes (GRADE) for the Rhine and Meuse basins. Rijkswaterstaat RIZA report 2007.027/KNMI publication 218, Lelystad, The Netherlands.

de Wit, M.J.M., H. Buiteveld, and W. van Deursen, 2008. *Extreme rivierafvoeren van Rijn en Maas*. In: *Extreme klimaatverandering en waterveiligheid in Nederland*, J. Bessembinder (ed.), pp. 28-32. KNMI-publication 221, Royal Netherlands Meteorological Institute (KNMI), De Bilt.

de Wit, M.J.M., H.A. Peeters, P. Dewil, K. Maeghe, and J. Baumgart, 2007. Floods in the Meuse basin: Event descriptions and an international view on ongoing measures. *International Journal of River Basin Management*, **5,** 279–292.

de Wit, M.J.M., B.J.J.M. van den Hurk, P.M.M. Warmerdam, P.J.J.F. Torfs, E. Roulin, and W.P.A. van Deursen, 2007. Impact of climate change on low-flows in the river Meuse. *Climatic Change*, doi:10.1007/s10584–006–9195–2.

Diermanse, F.L.M., 2004. HR2006 herberekening werklijn Maas. WL report Q3623, Waterloopkundig Laboratorium, Delft.

Eberle, M., H. Buiteveld, J.J. Beersma, P. Krahe, and K. Wilke, 2002. *Estimation of extreme floods in the River Rhine basin by combining precipitation-runoff modelling and a rainfall generator*. In: *Proceedings of the International Conference on Flood Estimation (Berne, Switzerland, 6-8 March 2002)*, M. Spreafico and R. Weingartner (eds.), pp. 459–467. CHR Report II-17, CHR Secretariat, Lelystad, The Netherlands.

Fernandez, B. and J.D. Salas, 1986. Periodic gamma autoregressive processes for operational hydrology. *Water Resources Research*, **22,** 1385–1396.

Frei, C., J.H. Christensen, M. Déqué, D. Jacob, R.G. Jones, and P.L. Vidale, 2003. Daily precipitation statistics in regional climate models: Evaluation and intercomparison for the European Alps. *Journal of Geophysical Research*, **108(D3),** 4124, doi:10.1029/2002JD002287.

Gaver, D.P. and P.A.W. Lewis, 1980. First-order autoregressive gamma sequences and point processes. *Advances in Applied Probability*, **12,** 727–745.

Gellens, D. and E. Roulin, 1998. Streamflow response of belgian catchments to IPCC climate change scenarios. *Journal of Hydrology*, **210,** 242–258.

Giorgi, F and X Bi, 2005. Regional changes in surface climate interannual variability for the 21st century from ensembles of global model simulations. *Geophysical Research Letters*, **32,** L13701, doi:10.1029/2005GL023002.

Grabs, W. (ed), 1997. Impact of climate change on hydrological regimes and water resources management in the Rhine basin. CHR Report I-16, Secretariat of the International Commision for the Rhine basin (CHR), Lelystad.

Harrold, T.I., A. Sharma, and S.J. Sheater, 2003a. A nonparametric model for stochastic generation of daily rainfall occurrence. *Water Resources Research*, **39,** doi:10.1029/2003WR002182.

Harrold, T.I., A. Sharma, and S.J. Sheater, 2003b. A nonparametric model for stochastic generation of daily rainfall amounts. *Water Resources Research*, **39,** doi:10.1029/2003WR002570.

Hay, L.E., M.P. Clark, R.L. Wilby, W.J. Gutowski Jr., G.H. Leavesley, Z Pan, R.W. Arrit, and E.S. Takle, 2002. Use of regional climate model output for hydrologic simulations. *Journal of Hydrometeorology*, **3,** 571–590.

Hershfield, D.M., 1961. Rainfall Frequency Atlas of the United States. Technical Paper 40, U.S. Department of Commerce, Weather Bureau.

Heylen, J., 1998. De hoogwaters op de grensmaas in december 1993 en 13 maanden later in januari-februari 1995. *Water*, **99,** 67–76.

Hosking, J.R.M. and J.R. Wallis, 1997. *Regional frequency analysis: An approach based on L-moments*. Cambridge University Press, Cambridge, UK.

Hughes, J.P. and P. Guttorp, 1994. A class of stochastic models for relating synoptic atmospheric patterns to regional hydrologic phenomena. *Water Resources Research*, **30,** 1535–1546.

Jacob, D. and Co-authors, 2007. An inter-comparison of regional climate models for Europe: Design of the experiments and model performance. *Climatic Change*, **81,** doi:10.1007/s10584–006–9195–2.

Jones, R., J. Murphy, D. Hassel, and R. Taylor, 2001. Ensemble mean changes in the simulation of the European climate of 2071-2100 using the new Hadley Centre regional modelling system HadAM3H/HadRM3H. Hadley Centre Report March 2001, p 19, Hadley Centre of the UK Met Office.

Katz, R.W., 1999. Power transformed time series. *Environmetrics*, **10,** 301–307.

Kay, A.L., R.G. Jones, and N.S. Reynard, 2006a. RCM rainfall for UK flood frequency estimation. I Method and validation. *Journal of Hydrology*, **318,** 151–162.

Kay, A.L., R.G. Jones, and N.S. Reynard, 2006b. RCM rainfall for UK flood frequency estimation. II Climate change results. *Journal of Hydrology*, **318,** 163–172.

Kleinn, J., C. Frei, J. Gurtz, D. Lüthi, P.L. Vidale, and C. Schär, 2005. Hydrologic simulations in the Rhine basin driven by a regional climate model. *J. Geophys. Res.*, **110,** D04102, doi:10.1029/2004JD005143.

Kors, A.G., F.A.M. Claessen, J.W. Wesseling, and G.P. Können, 2000. Scenario's externe krachten voor WB21. Unpublished document, Delft Hydraulics (WL); Royal Netherlands Meteorological Institute (KNMI); Institute for Inland Water Management and Waste Water Treatment (RIZA).

Kramer, N. and R. Schroevers, 2008. Generator of rainfall and discharge extremes (GRADE) - partF. Deltares report Q4424, Deltares, Delft.

Kwadijk, J. and J. Rotmans, 1995. The impact of climate change on the river Rhine: A scenario study. *Climatic Change*, **30,** 397–426.

Lall, U. and A. Sharma, 1996. A nearest neighbor bootstrap for resampling hydrologic time series. *Water Resources Research*, **32,** 679–693.

Lammersen, R., 2004. Effects of extreme floods along the Niederrhein (LowerRhein). final report, Landwirtschaft und Verbraucherschutz des Landes Nordrhein-Westfalen, Düsseldorf, Germany; Provincie Gelderland, Arnhem, The Netherlands; Rijkswaterstaat Directie-Oost, Arnhem, The Netherlands.

Landwehr, J.M., N.C. Matalas, and J.R. Wallis, 1979. Probability weighted moments compared with some traditional techniques in estimating Gumbel parameters and quantiles. *Water Resources Research*, **15,** 1055–1064.

Lawrance, A.J., 1980. *Some autoregressive models for point processes*. In: *Proceedings Colloquia Mathematica Societatis János Bolyai*, P. Bartfai and J. Tomko (eds.). Elsevier, Amsterdam.

Leadbetter, M.R., G. Lindgren, and H. Rootzén, 1983. *Extremes and related properties of random sequences and processes*. Springer-Verlag, New York.

Leander, R. and T. A. Buishand, 2008. Rainfall Generator for the Meuse Basin: Description of 20 000-year simulations. KNMI-publication 196-IV, in press, Royal Netherlands Meteorological Institute (KNMI), De Bilt.

Lenderink, G., T.A. Buishand, and W. van Deursen, 2007. Estimates of future discharges of the river Rhine using two scenario methodologies: direct versus delta approach. *Hydrology and Earth System Sciences*, **11,** 1145–1159.

Lenderink, G., B.J.J.M. van den Hurk, E. van Meijgaard, A.P. van Ulden, and H. Cuijpers, 2003. Simulation of present-day climate in RACMO2: first results and model developments. Technical Report TR-252, Royal Netherlands Meteorological Institute (KNMI), De Bilt.

Lindström, G., B. Johansson, M. Persson, M. Gardelin, and S. Bergström, 1997. Development and test of the distributed HBV-96 hydrological model. *Journal of Hydrology*, **201,** 272–288.

McKean, J.W. and R.M. Schrader, 1984. A comparison of methods for Studentizing the sample median. *Communications in Statistics, Simulation and Computation*, **13,** 751–773.

McKenzie, E., 1982. Product autoregression: A time-series characterization of the gamma distribution. *Journal of Applied Probability*, **19,** 463–468.

Mearns, L.O., M. Hulme, T.R. Carter, R. Leemans, M. Lal, and P. Whetton, 2001. *Climate scenario development*. In: *Climate Change 2001: The Scientific Basis. Contribution of Working Group I to the Third Assessment Report of the Intergovernmental Panel on Climate Change*. J.T. Houghton, Y. Ding, D.J. Griggs, M. Noguer, P.J. van der Linden, X. Dai, K. Maskell and C.A. Johnson (eds.), pp. 739-768. Cambridge University Press, Cambridge, UK and New York, NY, USA.

Mehrotra, R. and A. Sharma, 2006a. A nonparametric stochastic downscaling framework for daily rainfall at multiple locations. *Journal of Geophysical Research*, **111,** D15101, doi:10.1029/2005JD006637.

Mehrotra, R. and A. Sharma, 2006b. A semi-parametric model for stochastic generation of multi-site daily rainfall exhibiting low frequency variability. *Journal of Hydrology*, **335,** 180–193.

Mehrotra, R. and A. Sharma, 2007. Preserving low-frequency variability in generated daily rainfall sequences. *Journal of Hydrology*, **345,** 102–120.

Mejía, J.M. and I. Rodríguez-Iturbe, 1974. Correlation links between normal and lognormal processes. *Water Resources Research*, **10,** 689–691.

Middelkoop, H., K. Daamen, D. Gellens, W. Grabs, J.C.J. Kwadijk, H. Lang, B.W.A.H. Parmet, B. Schädler, and J. Schulla, 2001. Impact of Climate Change on Hydrological Regimes and Water Resources Management in the Rhine Basin. *Climatic Change*, **49,** 105–128, doi: 10.1023/A:1010784727448.

Middelkoop, H. (ed), 2000. The impact of climate change on the river Rhine and the implications for water management in the Netherlands. Summary of the NRP project 952210. RIZA Report 2000.010, Institute for Inland Water Management and Waste Water Treatment (RIZA), Lelystad.

Ministerie van Verkeer en Waterstaat, 2001. Hydraulische randvoorwaarden 2001 voor het toetsen van primaire waterkeringen. Den Haag.

Ministerie van Verkeer en Waterstaat, 2007. Hydraulische randvoorwaarden primaire waterkeringen voor de derde toetsronde 2006-2011 (HR 2006). Den Haag.

Nijssen, B., G.M. O'Donnel, A.F. Hamlet, and D.P. Lettenmaier, 2001. Hydrologic sensitivity of global rivers to climate change. *Climatic Change*, **183,** 397–424.

Parmet, B.W.A.H. and M. Burgdorfer, 1995. Extreme discharges of the Meuse in the Netherlands: 1993, 1995 and 2100 – Operational forecasting and long-term expectations. *Physics and Chemistry of the Earth*, **20,** 485–489.

Parmet, B.W.A.H., W. van de Langemheen, E.H. Chbab, J.C.J. Kwadijk, N.N. Lorenz, and D. Klopstra, 2001. Analyse van de maatgevende afvoer van de Maas te Borgharen. RIZA Report 2002.013, RIZA, Arnhem.

Prairie, J.R., B. Rajagopalan, T.J. Fulp, and E.A. Zagona, 2006. Modified k-nn model for stochastic streamflow simulation. *Journal of Hydrologic Engineering*, **11,** 371–378.

Prudhomme, C., N. Reynard, and S. Crooks, 2002. Downscaling of global climate models for flood frequency analysis: where are we now? *Hydrological Processes*, **16,** 1137–1150.

Räisänen, J., 2002. CO_2-induced changes in interannual temperature and precipitation variability in 19 CMIP experiments. *Jounal of Climate*, **15,** 2395–2411.

Räisänen, J., U. Hansson, A. Ullerstig, R. Döscher, L.P. Graham, C. Jones, H.E.M. Meier, P. Samuelsson, and U. Willén, 2004. European climate in the late twenty-first century: regional simulations with two driving global models and two forcing scenarios. *Climate Dynamics*, **22,** 13–31.

Rajagopalan, B. and U. Lall, 1999. A k-nearest-neighbor simulator for daily precipitation and other variables. *Water Resources Research*, **35,** 3089–3101.

Richardson, C.W., 1977. A model of stochastic structure of daily precipitation over an area. Hydrology Paper 91, Colorado State University, Fort Collins, Colorado.

Roeckner, E., L. Bengtsson, J. Feichter, J. Lelieveld, and H. Rodhe, 1999. Transient climate change simulations with a coupled atmosphere-ocean GCM including the tropospheric sulfur cycle. *Journal of Climate*, **12,** 3004–3032.

Rowell, D.P., 2005. A scenario of European climate change for the late twenty-first century: seasonal means and interannual variability. *Climate Dynamics*, **25,** 837–849.

Shabalova, M.V., W.P.A. van Deursen, and T.A. Buishand, 2003. Assessing future discharge of the river Rhine using regional climate model integrations and a hydrological model. *Climate Research*, **23,** 233–246.

Smith, R.L., 1990. *Extreme value theory*. In: *Handbook of Applicable Mathematics, Supplement*, W. Ledermann, et al. (eds.), pp. 437–472. Wiley, Chichester.

Tu, M., 2006. Assessment of the effects of climate variability and land use change on the hydrology of the Meuse river basin. PhD thesis, UNESCO-IHE, Delft.

Uppala, S. M. and Co-authors, 2005. The ERA-40 re-analysis. *Quarterly Journal of the Royal Meteorological Society*, **131,** 2961–3012.

van Bennekom, A.R. and B.W.A.H. Parmet, 1998. *Bemessungsabfluss in den Niederlände; Menschliche einflüsse und andere unsicherheiten*, 125–131. In: Zukunft der Hydrologie in Deutschland. BfG Mitteilung 16, Bundesanstalt für Gewässerkunde, Koblenz.

van de Langemheen, W. and H.E.J. Berger, 2001. Hydraulische randvoorwaarden 2001: maatgevende afvoeren Rijn en Maas. RIZA report no. 2002.014, RIZA, Arnhem.

van den Hurk, B J J M and Co-authors, 2006. KNMI climate change scenarios 2006 for the Netherlands. Scientific Report 2006-01, Royal Netherlands Meteorological Institute (KNMI), De Bilt.

van der Wal, K., 2002. Neerslag-afvoermodellering met gegenereerde neerslagdata in het HBV-model (Rainfall-runoff modelling with generated precipitation data in the HBV model). Civil Engineering & Management research report 2002W-002/WMW-005, University of Twente, Enschede.

van Meijgaard, E., 1995. Excessive rainfall over the Belgian Ardennes in December 1993: Evaluation of model predictions. *Meteorological Applications*, **2,** 39–52.

van Meijgaard, E and R Jilderda, 1996. The Meuse flood in January 1995. *Weather*, **51,** 39–45.

van Noortwijk, J.M., H.J. Kalk, and E.H. Chbab, 2004. Bayesian estimation of design loads. *HERON*, **49,** 189–205.

van Ulden, A.P., G. Lenderink, B.J.J.M. van den Hurk, and E. van Meijgaard, 2007. Circulation statistics and climate change in Central Europe: PRUDENCE simulations and observations. *Climatic Change*, **81,** 179–192.

Weiss, G., 1977. Shot noise models for the generation of synthetic streamflow data. *Water Resources Research*, **13,** 101–108.

Wilks, D.S., 1998. Multisite generalization of a daily stochastic precipitation generation model. *Journal of Hydrology*, **210,** 178–191.

Woolhiser, D.A., 1992. *Modeling daily precipitation - progress and problems.* In: *Statistics in the environmental & earth sciences*, A.T. Walden and P. Guttorp (eds.), pp. 71-86. Edward Arnold, London.

Young, K.C., 1994. A multivariate chain model for simulating climatic parameters from daily data. *Journal of Applied Meteorology*, **33,** 661–671.

Samenvatting

Tijdreeksresampling is een methodiek om uit tijdreeksen van een beperkte lengte willekeurig lange tijdreeksen te produceren met vergelijkbare statistische eigenschappen, zónder expliciet aannamen over die eigenschappen te doen. Hoewel de gegenereerde reeksen bestaan uit de individuele waarden van de oorspronkelijke reeks, bevatten zij sequenties die in de korte reeksen niet voorkomen. In dit proefschrift is de techniek van tijdreeksresampling benut voor de simulatie van extreme rivierafvoeren van de Maas ter hoogte van Borgharen. Extreme rivierafvoeren ontstaan vaak door aanhoudende neerslag in het stroomgebied over meerdere dagen, iets dat bij uitstek gesimuleerd kan worden door middel van resampling van neerslag dagsommen voor het stroomgebied. In combinatie met neerslag-afvoer modellering is resampling daarom een bruikbaar instrument als men de statistiek van nog niet eerder voorgekomen extreme rivierafvoeren wil bestuderen. Voor neerslag-afvoer modellering is gebruik gemaakt van een conceptueel model van de Maas, waarin het stroomgebied bovenstrooms Borgharen is opgedeeld in 15 deelstroomgebieden. Als invoer vereist dit model neerslag, temperatuur en potentiële verdamping voor elk deelstroomgebied op dagbasis. Deze laatste variable wordt uit de dagelijkse temperatuur afgeleid. De lange reeks van gesimuleerde dagafvoer die uit deze aanpak voortvloeit, biedt de mogelijkheid de kwantielen van extreme afvoer voor zeer lange herhalingstijden (vele malen groter dan de lengte van de meetreeksen) te schatten met een grotere nauwkeurigheid dan mogelijk zou zijn enkel op basis van de gemeten extreme afvoeren. Deze schatting is bovendien ongevoelig voor veranderingen in het stroomgebied, die wel effect hebben op de meetreeks. Een bijkomend voordeel is dat de gevolgde aanpak ook geschikt is te maken om de effecten van klimaatverandering te onderzoeken. Dit is gedaan door, in plaats van historische neerslag en temperatuur data, uitvoer van regionale klimaatmodellen (RCMs) te resamplen. Die RCMs zijn elk aangedreven door simulaties van globale klimaatmodellen (GCMs) voor het huidige klimaat en een mogelijk toekomstig klimaat. Het doorrekenen van de geresamplede modeluitvoer met het neerslag-afvoer model leidt tot inzicht in de effecten van dit toekomstig klimaat op de statistiek van extreme rivierafvoer.

Hoofdstuk 1 schetst de historische achtergrond en de motivatie van dit onderzoek. Vanwege de Wet op de Waterkering is het nodig dat eens per vijf jaar de maatgevende afvoer opnieuw bepaald wordt. Deze is gedefinieerd als de extreme rivierafvoer met een herhalingstijd van 1250 jaar. De methodiek die men daar tegenwoordig voor gebruikt, wordt in dit hoofdstuk ruw geschetst. Ook wordt toegelicht dat de informatie uit RCM simulaties op meer dan één manier aangewend kan worden om een uitspraak te doen over extreme neerslag en rivierafvoer in een toekomstig klimaat en dat die niet noodzakelijk naar dezelfde uitkomsten leiden. Tot slot wordt kort aangegeven wat de rode draad is die de rest van de hoofdstukken verbindt.

In hoofdstuk 2 wordt het gebruikte resampling algoritme toegelicht en getest in combinatie met het neerslag-afvoermodel. Het resampling algoritme is gebaseerd op het principe van 'nearest neighbours'. Als invoer worden historische neerslag- en temperatuurreeksen gebruikt voor lokaties in en om het Maasstroomgebied uit de 38-jarige periode 1961-1998. De verdeling van de 10-daags neerslagmaxima voor het stroomgebied wordt realistisch gesimuleerd. Ook is er een redelijke overeenstemming tussen de verdeling van de gesimuleerde afvoermaxima en die gemeten in de 38-jarige basisperiode. De afvoerpieken van de historische 1993- en 1995-hoogwaters wijken echter opmerkelijk af van de curve van de verdeling van gesimuleerde extreme afvoeren. Deze afwijking kan echter worden toegeschreven aan de grote variabiliteit van de grootste extremen uit een 38-jarige afvoerreeks. Voorts is er een systematisch verschil te zien bij de kleinere en middelgrote extremen die verband houdt met de onderschatting van afvoerpieken door het neerslag-afvoer model in dit regime van afvoeren. Dit verschil verdwijnt nagenoeg als de extreme 10-daags gemiddelde afvoer beschouwd wordt, hetgeen aantoont dat extreme afvoervolumes wel goed in de simulatie worden gerepresenteerd. Naast deze simulatie is er ook een simulatie uitgevoerd met data uit de periode 1930-1998 (met uitzondering van 1940). Hiervoor is het resampling algoritme uitgerust met een extra stap, waarin het nearest-neighbour principe nogmaals wordt toegepast. Deze stap dient om uit een simulatie op basis van een beperkte set van lange stationsreeksen en korte reeksen van gebiedsneerslag, een simulatie te krijgen die het stroomgebied dekt. Deze simulatie levert extreme afvoeren op die lager liggen dan die uit de eerste simulatie (ongeveer 5%), doordat de gehele periode 1930-1998 droger is dan de deelperiode 1961-1998.

Hoofdstuk 3 bespreekt een aanpassing van het resampling algoritme om dagwaarden (neerslag en temperatuur) te kunnen simuleren buiten het interval van waarden waaruit geresampled wordt. Het principe van 'nearest-neighbours' wordt gebruikt om verwachtingswaarden van neerslag en temperatuur op de te simuleren dag te schatten, conditioneel op neerslag en temperatuur van eerder gesimuleerde dagen. Vervolgens wordt bij het random trekken van een residu dit principe nogmaals toegepast. Voor neerslag worden de verwachtingswaarde en het residu met elkaar vermenigvuldigd en voor temperatuur bij elkaar opgeteld om aan de gesimuleerde waarden te komen. Het aangepaste algoritme is getest op de gebiedsgemiddelde neerslag voor het stroomgebied van de Ourthe, een

zijrivier van de Maas, en de temperatuur van een representatief station (St. Hubert). De lange gegenereerde reeksen worden vervolgens gebruikt om een neerslag-afvoer model voor de Ourthe (onderdeel van dat voor de Maas) aan te drijven. Het nieuwe algoritme leidt ertoe dat de waarschijnlijkheidsverdeling van gesimuleerde neerslag dagsommen voorbij de hoogst waargenomen dagsom op een aannemelijke wijze wordt voortgezet en dat ook het gemiddelde, de variantie, de autocorrelatie en meerdaagse extremen goed worden gereproduceerd. De aanwezigheid van grotere dagsommen in de simulatie geeft echter in het winterhalfjaar geen aanleiding tot een noemenswaardige verhoging van de afvoerextremen van de Ourthe.

In hoofdstuk 4 is onderzocht of de verdeling van extreme rivierafvoeren ook met geresampelde neerslag- en temperatuurreeksen van het regionale klimaatmodel RACMO (KNMI) realistisch gesimuleerd kunnen worden, zoals dat in de voorgaande twee hoofdstukken voor historische data is beschreven. Twee verschillende 30-jarige simulaties van RACMO worden hierin gebruikt, één aangedreven door (randen uit) het globale atmosferische model HadAM3H (Hadley Centre, UK Meteorological Office) voor de periode 1961-1990 en één door de ERA40 reanalysis voor de periode 1969-1998. Beide 30-jarige perioden worden geassocieerd met het huidige klimaat en historische data voor de periode 1961-1990. Voor beide zijn voor de deelstroomgebieden reeksen van gebiedsneerslag en -temperatuur met een lengte van 9000 jaar simultaan gegenereerd en doorgerekend met het neerslag-afvoer model. In beide modelruns wordt de gemiddelde winterneerslag over het stroomgebied overschat, terwijl anderzijds de relatieve variabiliteit wordt onderschat. Uit de gesimuleerde extreme meerdaagse neerslag en extreme afvoeren blijkt dat het niet alleen nodig is de afwijking in het gemiddelde te corrigeren, maar dat ook de relatieve variabiliteit van belang is. Een correctie van de gemiddelde neerslag alléén leidt tot een sterke onderschatting van gesimuleerde extremen. Om beide aspecten onafhankelijk van elkaar te kunnen corrigeren, wordt een niet-lineaire correctie geïntroduceerd. Deze correctie, afgeleid van de 30-jarige modelruns en toegepast op de gegenereerde neerslagreeksen, blijkt toereikend om de verdeling van geobserveerde meerdaagse neerslagextremen te reproduceren, en ook de afvoerextremen die met geobserveerde neerslag gesimuleerd zijn.

In hoofdstuk 5 worden resampling, samen met de correctie van hoofdstuk 4, toegepast op zowel de model runs voor het controle klimaat (1961-1990) als die voor het SRES-scenario A2 (2071-2100). Drie modelconfiguraties worden hierin bekeken: het regionale model RACMO aangedreven door HadAM3H (zoals besproken in het vorige hoofdstuk) en het regionale model RCAO (Swedish Meteorological and Hydrological Institute), zowel in combinatie met HadAM3H als ECHAM4/OPYC (Max Planck Institute, Hamburg). Hoewel de methodiek hetzelfde is als in het voorgaande hoofdstuk (interpolatie van neerslag en temperatuur uit modelruns, resampling, biascorrectie en hydrologische modellering), is de stuatie gecompliceerder bij de RCAO-run aangedreven door ECHAM4. De onderschatting van de relatieve variabiliteit is hier zo groot dat de correctie ervan leidt tot onrealistisch grote neerslaghoeveelheden en verandering van de extremen. Om dit op te lossen, wordt een aannemelijke bovengrens voor de correctiefactor geïntroduceerd.

Uit de modelexperimenten blijkt dat de verandering van het gemiddelde en de relatieve variabiliteit van de meerdaagse neerslagsommen een sleutelrol spelen als het gaat om de verandering van extreme meerdaagse neerslag en extreme afvoeren. In het winterhalfjaar worden deze karakteristieken sterk bepaald door het drijvende globale model, zodat de verandering van de extremen in de twee HadAM3H-aangedreven configuraties hetzelfde beeld geeft, terwijl die uit de ECHAM4-aangedreven configuratie daar sterk van afwijkt. De HadAM3H randen geven aanleiding tot een afname in de relatieve variabiliteit van meerdaagse neerslag, die de toename van het gemiddelde compenseert, terwijl met ECHAM4 de relatieve variabiliteit nauwelijks verandert en de toename in de extremen parallel loopt met die in het gemiddelde. Verder wordt nog gedemonstreerd dat het weglaten van de biascorrectie tot afwijkende relatieve veranderingen van de afvoerextremen leidt, wat impliceert dat de bias in modeldata niet zomaar genegeerd kan worden.

In hoofdstuk 6, tenslotte, worden kort de belangrijkste conclusies van dit onderzoek op een rij gezet. De waarden van de maatgevende afvoer die volgen uit de verschillende simulaties in hoofdstuk 2 worden hier nader besproken en de nauwkeurigheid ervan wordt afgeschat. Simulaties van 12 000 jaar gebaseerd op de basis periode 1961-1998 leveren een maatgevende afvoer van ruwweg 3870 ± 136 m^{3}s^{-1} op, terwijl dat 3515 ± 88 m^{3}s^{-1} is voor simulaties uit de periode 1961-1998. Het verschil tussen deze twee uitkomsten demonstreert dat de historische basisperiode voor de simulatie ook onzekerheid in het eindantwoord introduceert. Deze onzekerheid wordt kleiner naarmate de historische periode langer wordt. Dit geldt ook voor het resamplen uit modelruns, waardoor het aan te bevelen is lange modelruns te gebruiken. Dit is belangrijker dan het verhogen van de ruimtelijke resolutie van de RCMs, temeer omdat grootschalige aspecten de doorslag geven als het om de verandering van afvoerextremen in de winter gaat. Een punt van zorg is wel dat modelruns uit verschillende GCM-RCM configuraties (met name die van verschillende GCMs) sterk uiteenlopende resultaten opleveren. Dit manifesteert de onzekerheid die momenteel nog in klimaatmodellen zit. Het is te verwachten dat deze onzekerheid kleiner wordt als de modellen verbeteren, waardoor ook de noodzaak van biascorrecties vermindert.

Curriculum Vitae

Robert Leander werd geboren op 1 november, 1973 te Woerden. Hij volgde het atheneum aan de Kalsbeek Scholengemeenschap te Woerden, waarvan hij in 1992 het diploma behaalde. In het najaar van 1992 begon hij aan de studie Technische Natuurkunde aan de Technische Universiteit Delft. Zijn afstudeeronderzoek vond plaats bij de vakgroep Stromingsleer, toen nog onder leiding van Prof. Frans Nieuwstadt. Na zijn afstuderen in 2001 werkte hij tijdelijk als freelance programmeur, o.a. binnen de vakgroep Stromingsleer. Op 16 september 2002 begon hij aan een betrekking als projectmedewerker aan het KNMI, in de afdeling die toen nog Klimaat Analyse heette en onder de bezielende leiding stond van dr. G.P. Können. Het project betrof de ontwikkeling van een stochastische neerslaggenerator voor het Maasstroomgebied, naast de al bestaande neerslaggenerator voor de Rijn. Dat project is in de loop der jaren uitgegroeid tot een promotieonderzoek, waarvan dit proefschrift het eindresultaat is.

Sinds oktober 2008 heeft Robert een nieuw dienstverband binnen dezelfde afdeling (inmiddels opgegaan in de grotere afdeling Klimaatdienstverlening en -Advies), waarin hij zich bezighoudt met de toesnijden van klimaatscenarios op de praktijk van professionele eindgebruikers ('Tailoring', oftewel 'Maatwerk' in goed nederlands).

Dankwoord

Op 16 september van het jaar 2002 begon ik mijn KNMI-carriere als medewerker in het project "Neerslaggenerator Rijn-Maas". Aanvankelijk zou het een kort dienstverband van anderhalf jaar worden en mijn taak zou zijn om de al bestaande neerslaggenerator voor het stroomgebied voor de Ourthe uit te breiden tot het gehele Maasstroomgebied. In dat eerste jaar had ik zelfs niet kunnen vermoeden dat die eerste stappen uiteindelijk zouden uitmonden in een proefschrift. Mijn toenmalige afdelingshoofd Günther Können stond altijd erg positief tegenover mijn werk en heeft mij er toe aangezet om aan een publicatie te werken over de eerste resultaten van het project, met als argument dat het voor mijn verdere carriere wel goed zou zijn als er tenminste één serieus artikel op mijn publicatielijst stond. Er zou echter nog behoorlijk wat water door de Maas stromen eer uit dat prille begin een proefschrift zou groeien. Dat het uiteindelijk toch zover gekomen is, heb voornamelijk te danken aan mijn co-promotor Adri Buishand, die, naar later bleek, mijn promotie traject al heel lang voor ogen had. Beste Adri, ik besef dat dingen niet altijd liepen zoals ze hadden moeten lopen. Ik waardeer het daarom des te meer dat je ondanks alles zo veel inspanning in dit proefschrift hebt gestoken. Niet zelden heb je daarvoor kostbare vrije tijd opgeofferd. Het lijdt geen enkele twijfel dat ik zonder jou nooit gepromoveerd zou zijn. Mijn (overigens bescheiden) kennis van statistiek heb ik ook geheel aan jou te danken. In de eerste jaren, toen alles nog nieuw voor me was, heb ik ontzettend veel hulp gehad van mijn kamergenoot Jules Beersma, die niet alleen verstand heeft van klimaatonderzoek maar van eigenlijk alles: van fietsreparaties tot het kopen van een huis. Jules, het was me een eer en genoegen om bij jou op de kamer te zitten. Ook mijn promotor Bart van den Hurk ben ik veel dank verschuldigd. Hoewel pas in een laat stadium als promotor, was hij inhoudelijk al vroeg bij dit onderzoek betrokken en heeft veel bijdragen door met ons mee te denken over het gebruik van klimaatmodellen. Bart, ik waardeer vooral je positieve insteek, enthousiasme en optimisme. Uiteraard was dit onderzoek onmogelijk geweest zonder de medewerking van Marcel de Wit van het (toenmalige) RIZA, en Rita Lammersen en Hendrik Buiteveld van de (tegenwoordige) Waterdienst. Ik ben hen zeer "GRADEful" voor de vele vruchtbare gesprekken die we

123

hebben gevoerd en, niet in de laatste plaats, de mogelijkheid om van het HBV-model gebruik te maken. Ook wil ik Günther Können, Albert Klein Tank en Arnout Feijt bedanken voor de ondersteuning die zij als afdelingshoofden aan mijn onderzoek hebben gegeven. Verder bedank ik iedereen van de afdeling KA (vroeger Klimaat Analyse en tegenwoordig Klimaatdienstverlening en -Advies) voor de leuke tijd die niet alleen achter me ligt, maar nog steeds voort duurt. Dankzij de goede onderlinge sfeer heb ik me van het begin af aan in de groep thuisgevoeld. Als laatste wil ik zeker niet vergeten mijn ouders te bedanken, die altijd klaar staan om mij te helpen en bij wie ik altijd mijn verhaal kwijt kan. Rest mij nog om de twee volgende promovendi van deze afdeling, Alexander Bakker en Aart Overeem (toch zo'n beetje half in onze groep) alle succes te wensen in hun promotieonderzoek en de afronding van hun proefschrift.